UNIVERSITY OF BELGRADE

FACULTY OF MECHANICAL ENGINEERING

MOHAMED ALKATEB

"Experimental and numerical investigation of corrosion crack growth in mild structural steel"

DOCTORAL DISSERTATION

BELGRADE 2021

УНИВЕРЗИТЕТ У БЕОГРАДУ

МАШИНСКИ ФАКУЛТЕТ

МОХАМЕД АЛКАТЕБ

Експериментално и нумеричко испитивање раста прслине у условима напонске корозије конструкционих челика

Докторска дисертација

БЕОГРАД, 2021

Mentor of Doctoral Dissertation

Prof. Dr. Aleksandar Sedmak

University of Belgrade, Faculty of Mechanical Engineering

Members of Committee

Prof. Dr. Aleksandar Sedmak

Faculty of Mechanical Engineering, University of Belgrade

Assoc. Prof. Dr. Gordana Bakić

Faculty of Mechanical Engineering, University of Belgrade

Assoc. Prof. Dr. Miloš Đukić

Faculty of Mechanical Engineering, University of Belgrade

Dr Srđan Tadić, research associate,

Innovation Center of the Faculty of Mechanical Engineering, Belgrade

Dr. Ivana Vasović, research associate,

Lola Institute, Belgrade

Date of Defense:

Ментор

Др Александар Седмак, ред. проф.

Машински факултет Универзитета у Београду

Чланови Комисије

Др Александар Седмак, ред. проф.

Машински факултет Универзитета у Београду

Др Гордана Бакић, ванр. проф.

Машински факултет Универзитета у Београду

Др Милош Ђукић, ванр. проф.

Машински факултет Универзитета у Београду

Др Срђан Тадић, научни сарадник,

Иновациони центар Машинског факултета, Београд

Др Ивана Васовић, научни сарадник,

Институт Лола, Београд

Date of Defense:

To my parents … Mabrouk and Sharefa

To my wife … Safia

To my children … Sharefa, Abdulramam and Hajer

ACKNOWLEDGEMENTS

Alhamdulillah, first and foremost who helped me finish this work. I express to him my sincere thanks and gratitude to him Almighty for his divine help and guidance that gave me the ability to succeed. I thank you for the life, health and energy you have given me without limits.

I would like to express my sincere thanks and great appreciation to Prof. Dr. Aleksandar Sedmak for his generous support and assistance. He was always available and ready to help and guide. I will never forget your care and patience. Without him, I wouldn't have been able to finish this goal.

I would also like to extend special thanks and deep appreciation to Dr Srđan Tadić, who did not hesitate to extend a helping hand. I found his door open and he did not hesitate for a moment to advise and advise to finish this work.

I would also like to thank all the faculty, staff, and administrators of the Faculty of Mechanical Engineering of the University of Belgrade whose extensive knowledge of the field helped me move forward and finish my studies.

I would also like to thank all my friends and colleagues who accompanied me and provided many useful opinions, instructions and relevant information for completing this research.

I always extend my last gratitude to my beloved wife and three beloved children for their patience and for keeping me cheerful during my studies.

Abstract

The phenomenon of SCC is one of the most important problems that different metals are exposed to, according to the causative environment and the influencing stresses. SCC is the type of subcritical cracking, occurring in a corrosive environment. Metal fracture may occur due to SCC at a lower permissible stress level, causing problems that are difficult to solve. The sensitive materials, the applied stresses and the corrosive environment are the basic requirements that cause this phenomenon. It is difficult to predict the complexity of the interactions that occur within a crack and how they will grow and spread. The basic mechanisms of SCC remain fundamentally unclear despite numerous studies and research conducted on the topic.

In this thesis, attention was focused on investigating crack growth behaviors in mild steel, computationally by the numerical method and by using the finite element simulation method. A model simulating crack growth was placed on the metal surface by applying tensile stress to the sample under normal conditions. The mechanical analysis of tensile stress was performed using the Code _Aster method to verify the effect of crack growth.

The calculations in this study were carried out according to equations relating to linking the main influencing variables to obtain the best results. Three related variables significantly influencing crack growth and propagation were simulated. K, dk/da and max stress, are the variables that were simulated compared to crack length and growth, according to basic conditions, and that was by applying a constant tensile load to the sample, completely affecting the growth of the crack. Values of these variables were recorded every 2 mm for the crack growth.

The results showed an increase in the values of K and max stress, while there was a decrease in the values of dK/da as the crack length increased. There was a great agreement between the results obtained mathematically according to equations and when applying simulations using finite elements. These results obtained are largely consistent with what has been obtained in most of the studies that have been conducted in this regard.

Keywords:

Electrochemical principles, environment conditions, crack tip, tensile stress, structural steel, cathodic reaction, stress intensity factor, finite element method, maximum stress.

РЕЗИМЕ

Појава напонске корозије је један од најважнијих проблема који се јављају у металним материјалима у неповољном окружењу и под дејством напона. Напонска корозија је врста поткритичне расата прслине, који се јавља у корзивној околини. Лом метала који настаје од последице напонске корозије при напону мањем од дозвољеног, је проблем који није лако решити, посебно код материјла осетљивих на корозију. Основна тешкоћа је да се утврди и предивди сложено међудејство наопна и корозије у присуству прслине, односно истраже механизми њеног настанка и раста. Основни механизми ове појаве су и даље недовољно разјашњени и поред великог броја истрживања која су спроведене последњих деценија.

У овој дисертацији пажња је усмерена на нумеричко истраживање понашања конструкционог угљеничног челика у условима напонске корозије, а у присутву прслине. У том циљу примењена је метода коначних елемената, односно њена проширена варијанта када је у питању симулација раста прслине насталој на металној површини, а под дејством затезног напона и корозионе средине. За израчунавање напонско-деформационог стања коришћен је софтвер Code _Aster који је отворен за допуне и модификације у скалду са конкретним проблемом који се решава.

Прорачуни и нумеричке симулације су изведени у складу са једначинама које повезују главне утицајне промељиве дља би се добили најбољи резултати. Три повезане променљиве које битно утичу на раст прслине су симулиране, фактор интензитета напона K, његова брзина, односно промена у односу на дужину прслине, dK/da, и максимални напон. Ове величина су одређиване за две врсте епрувета под дејтвом затезног напона, тако што су израчунате на свака 2 мм раста прслине. Резултати су показали раст K и максималног напона, док је брзина dK/da опадала при расту дужине прслине. Добијено је добро слагање нумериких и аналитичких резултата, као и добро слагање са експерименталним резултатима преузетим из литературе.

.

Кључне речи:

Електрохемисјки принципи, услови средине, врх прслине, затезни напон, контрукциони челик, катодна реакција, фактор интензитета напона, метода коначних елемената, максимални напон.

CONTENTS

LIST OF FIGURES

LIST OF TABLES

CHAPTER 1 - Introduction

1.1 Background

Stress corrosion cracking is a kind of environmentally assisted failure of engineering materials. Gradual crack propagation, and eventual final failure, is a result of simultaneous response of chemical reactions and mechanical forces at the crack tip [1]. Historically, the phenomenon was observed in 19th century as a spontaneous cracking of military brass cartridges during a monsoon periods in India, when it was named 'seasonal cracking', the term which has retained till the modern period. Later, it was appeared that SCC was a cause of some severe industrial and urban accidents, some of them with serious losses [2]. The SCC is caused by three main factors: i) material susceptibility, ii) environmental corrosive conditions, iii) low level tensile stresses, applied or even only residual. When the applied loading is cyclical, 'corrosion fatigue' (CF) is considered as a particular case of SCC. Figure 1.1 shows the relationship between these factors. When the applied loading is cyclical, 'corrosion fatigue' (CF) is considered as a special case of SCC. Also, depending on the rate of chemical reactions in the crack tip, 'hydrogen induced cracking' (HIC) is considered as a specific mechanism of SCC [3].

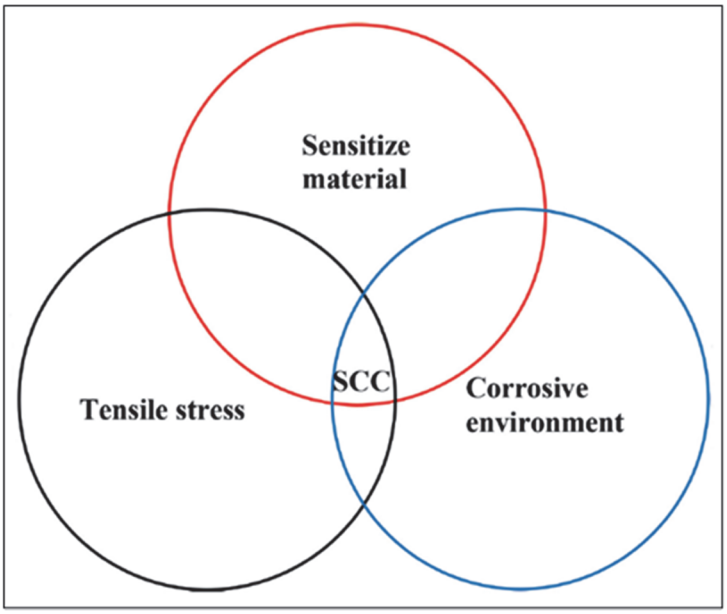

Figure 1.1 Relationship between SCC factors [4]

The SCC mechanisms are classified into anodic and cathodic. Anodic SCC is governed by anodic metal dissolution at the crack tip; on the other side, the cathodic SCC, mostly occurring in welded joints, is governed by hydrogen diffusion into the metal, thus provoking hydrogen embrittlement and HIC. But, during corrosion, both mechanisms occur simultaneously, and the governing mechanism is characterized by the rate of particular reaction [4].

During the SCC crack growth, three regions are typically observed above threshold stress-intensity level (K_{iscc}) - (i) low K values, when crack propagation rate increases rapidly, (ii) intermediate K values, when crack growth rate approaches almost constant plateau and, finally, (iii) when K values approaches K_{IC}, rapid crack growth and the onset of final failure [5].

Many review papers exist, concerning chemical, electrochemical and mechanical aspects at the crack tip. The most recent in-depth review was published by Bland et al. [6]. There are a large series of papers focused on mechanisms and modeling of SCC [6], [7-10]. Interested reader can find detailed modeling analysis in polemical papers between Shoji and Hall [7], [11-15]. A finite elements approach to SCC can be find in some recent papers [8], [9], [15-19].

Mild steel is used for external structures such as topside, jackets, legs and cranes [10]. Welded joints are basic structural components used for marine engineering. The steel used for these structures must meet requirements, specified in Eurocode 3. The normal mild steel referred to in these standards is usually a yield curve of 350 to 460 MPa, [11]. Steel with a capacity of more than 460 MPa is also currently available. The use of such a steel in for components in structures can reduce processing costs and materials due to their good weldability and high strength. In addition, not only mechanical properties, but also the corrosion resistance of a high-grade steel is of primary importance for applications for components in structures, since they are often exposed to highly corrosive environments with humid conditions, [12].

The last five decades have made significant progress in the development of mild steel for applications in pipelines, offshore constructions, ships and buildings. Such improvements were due to the need to achieved optimal combinations of

weldability, toughness and strength at reasonable prices. Focus in the improvements was on the zone of influence of the heat of the weld, its microstructure and properties, welding process and heat input, preheating and thermal treatment after welding. Although significant improvements in weldability through reduction of the carbon equivalent have been achieved over the years, the consequence is the increased dependence on thermomechanical processing and the transition to the mechanisms for strengthening with microwave insulation, far from the mechanisms dominated by carbon for which the original understanding is based [13].

Mild steels, or micro-alloyed steels, are not considered as alloyed steels because they are designed to satisfy specific mechanical properties (yield strength larger than 275 MPa). They have low carbon content (0.05 to 0.25% C) for better formability and weldability, while the content of manganese is up to 2.0%, with Mo, Cu, N, V, Nb, Ti and Zr are used in different contents, [14], [15]. Further reduction of detrimental effects of the Corrosive Environment (CE) was enabled by introduction of new production methods such as controlled rolling and hardening, [16].

Mild steel alloys are used in advanced marine objects such as ship and marine ships, due to their sufficient strength and excellent weldabilty, [17]. Recent studies behaviour showed the high sensitivity of SCC [18]. In addition, the use of these alloys requires welding and setting up connection procedures. The welding process induces structural changes which can influence local corrosive behaviour of the alloy. In addition, welded joints often have defects due to welding, as well as the remaining stresses, [14] , [19]. Thus, the risk of Stress Corrosion Cracking (SCC) is often present causing unexpected failures without noticable external indicators, which will greatly limit its application. The cathodic protection is used to prolong steel operating time, but this can cause much more serious SCC problems. Therefore, the investigation of SCC behaviour of welded steel under cathode potential is of great importance [20].

The stress corrosion cracking problem must, therefore, be considered in the context of other constraints on design and maintenance, including costs. SCC is generally defined as the initiation and/or propagation of SCC in the presence of both tensile stress and corrosive environment. The occurrence of SCC is commonly recognized by brittle cracking features in normally ductile metals, meaning that the

catastrophic capability of stress corrosion cracking is manifested through an effective reduction in fracture toughness. Consequently, stress corrosion cracking is a serious and growing concern in many industries, one of which is the shipbuilding industry [21] Figure 1.2 shows a sketch of pit corrosion and SCC initiation.

Figure 1.2 Sketch of pit corrosion and SCC initiation.

1.2 Defining the problem

Recognizing an increase in cracks that support the environment or a long-term burst of stress has been identified as the main threat to the material security of construction materials. Reducing the lifespan of equipment by cracking corrosion has serious implications for the technological applications of metal surfaces [22].

It is important to take into account the burst phenomena, which are considered to be voltage breaking (SCC), which this group of alloys can introduce in different degrees. In addition to SCC, mild steel is also sensitive to other types of brittle fractures, especially the cracking hydrogen (H), and too brittle fractures due to insufficient material. It is difficult in distinguishing SCC and H in operating conditions [23]. The overall appearance of stress corrosion cracks in mild steel is the same as hydrogen embrittlement cracks (except that SCC can leave corrosion products on the fracture surfaces). In many cases, the details of the SCC fractions and hydrogen fractions can not be distinguished. Many service defects involving mild steel in environments are likely to result from hydrogen. Cracking may occur in the HAZ or weld metal, and it may be longitudinal or branches see (Figure 1.3 and Figure 1.4).

SCC demands vary somewhat in HE, where the only requirement is to provide a hydrogen source, together with a hydrogen-capable substance. Other SCC mechanisms are more specific and usually occur when the metal is in general corrosion due to the protection of the surface of the film, although SCC may occur at

low temperatures in some positions. Cracks continue under low pressure and usually arise as a result of residual stresses of welding or making. The fracture is usually through the granules, although it can be converted into the path between the cells due to the sensitization of the steel [24].

Figure 1.3 SCC between BM and HAZ

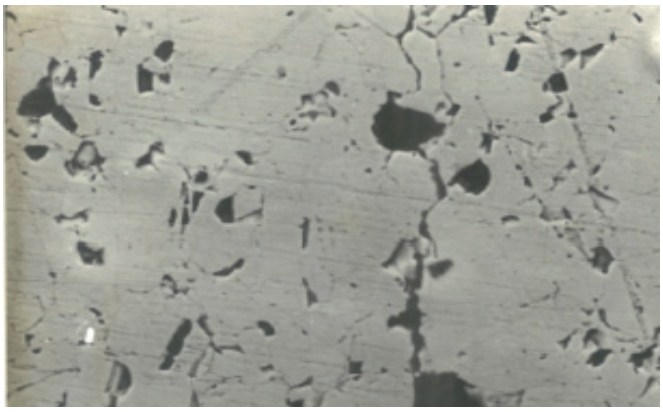

Figure 1.4 Surface SCC

There are two hypotheses for studying this phenomenon: First, failure is either due to an easily corrosive "path" within the material and another form of hydrogen embrittlement (HE), with the release of hydrogen through the cathodic reaction of corrosion. In some cases, research has shown that public failure occurs as a result of hydrogen embrittlement (HE). It can be expected that in the study of the problem of HE with steel, this phenomenon is especially important in the case of alloys of high alloys. The failure of stress corrosion in welded joints in high-strength steel may be particularly probable for several reasons. If, after welding, the voltage is not produced, the residual welding pressure remains. In the welding area, these pressures will be very narrow, and because they are usually of high stress, risk of

cracking is increased. Even with stress relief therapy, local pressure concentrations are usually left on the seams. Depending on the project, welded joints can be related with cracks where typically aggressive chemical species occur, which increases the likelihood of failure. Metal changes that occur during the thermal welding cycle can occur in local microstructures that are particularly sensitive to SCC. Thus, welded joints are often vulnerable to SCC attack, although the base metal is immune. One should notice that not enough information is available on SCC for welding high-strength steel. Many environments can cause stress corrosion [25].

SCC is one of the most damaging types of failures and its practical importance is affected under the combined influence of consistently applied pressures and an active environment, [26].

Although many research papers have been written over the past decades to explore the effect of different parameters on the stress fracture corrosion of mild steels in different environments, this phenomenon is still present for weld engineers especially for welded joints in actual steel structures. The importance of this study is observed according to researchers around the world:

- HSLA-65 (ASTM A945) represent new steel for shipbuilding industry.
- presently this phenomenon is not completely understood and hydrogen embrittlement detection, in particular, seems to be one of the most difficult aspects of the problem [21].
- laboratory tests have not always accurately modelled field-welding behaviour, particularly for modern HSLA steels, [12].

However, for earlier reasons and more topics about stress corrosion cracking for mild steel is presented in more detail in the fourth chapter of this thesis, in general.

1.3 Objective of the thesis

The overall objective of this work is to obtain a theoretical background and a more coherent understanding of the effects of stress corrosion cracking of mild steel. The scientific and main objective of the dissertation is to develop a numerical simulation using finite elements and experimental and determine the impact of SCC on mild steel welded joints.

1.4 Scope of the Work

In engineering problems, the problem often begins with the physical system, which is here the SCC phenomenon. To analyze many problems, a mathematical model is created. The solution of the mathematical model depends mainly on the form itself. In some simple cases, the exact (theoretical) solution can be created. On the other hand, the numerical solution is adopted as a perfect option in most practical situations. Accordingly, the method of elements selected for the current study will be applied to the approximate numerical solution. Therefore, numerical results are obtained from numerical simulations. To this end, the quality of the results will then be determined and determined by comparing the numerical and experimental results. In the end, redefining the relevant model at one or more stages depends on the degree of satisfaction of the analyst with the results achieved. Figure 1.5 illustrates the sequence of these phases.

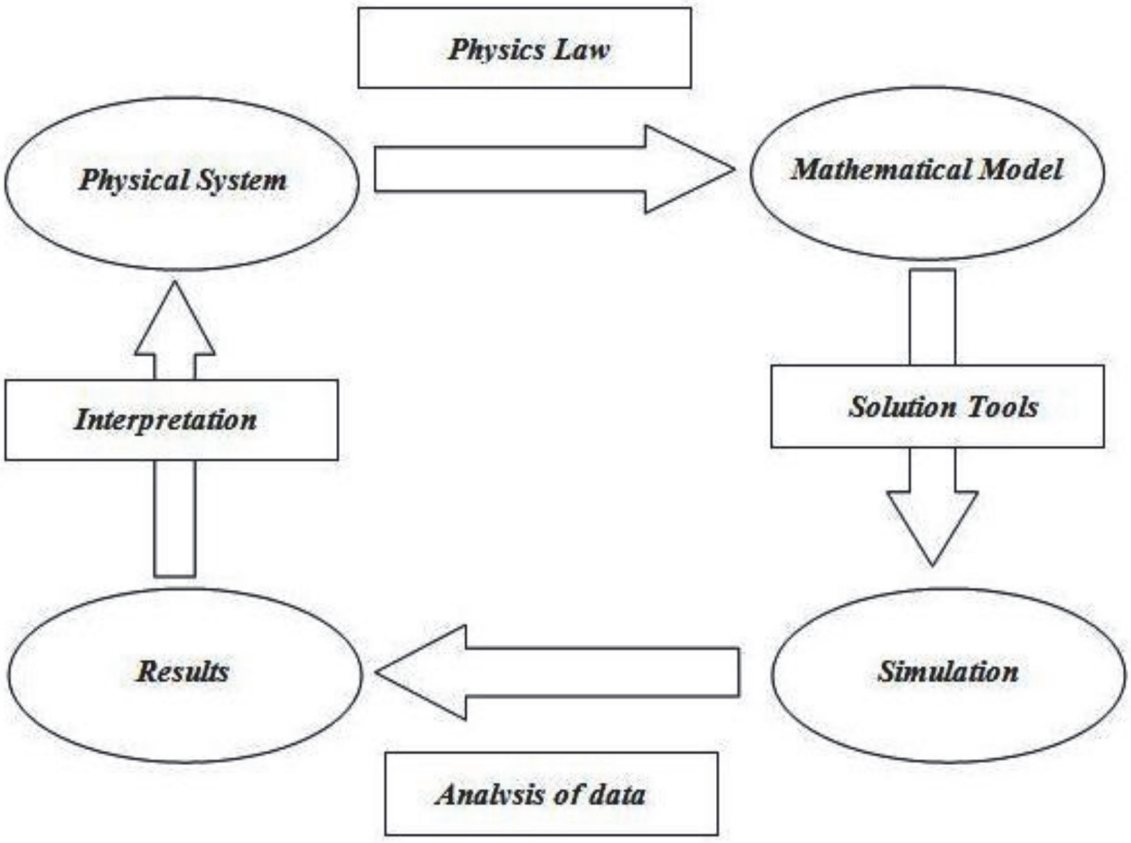

Figure 1.5 The sequence of the engineering problem analysis

1.5 Methodology used

The methodology of the applied research focuses on the following: First, the theoretical foundations of the thesis, which is the correct and deep understanding of the phenomenon of cracking stress corrosion, and the impact on the weld joints of steel construction, and the study literature dealing with research on this phenomenon. Second, the experiments will be carried out by the tests of the sensitivity of stress cracking corrosion and described by numerical simulation using the analysis of the limited elements in order to verify this phenomenon and its impact on the surfaces of the welded metal The present thesis is organized in six chapters, an introduction to the topic is included in chapter 1. Chapter 2 Literature review, this chapter provides a deep review of the phenomenon of stress cracking corrosion and its impact on mild steel over the past years. Chapter 3 deeply examines the fundamentals of mild steels. Chapter 4 examines the mechanics of stress cracking corrosion. Chapter 5 this chapter deals with numerical simulation, i.e. application of extended finite element method. Finally, the results and discussions and conclusions are presented in Chapter 6.

CHAPTER 2 Literature review

2.1 Introduction

As mentioned earlier in Chapter 1, controlling stress corrosion cracking is not an easy task to do without a strong background on the subject. Fortunately, this topic has attracted the attention of many researchers around the world in the past decades. This chapter summarizes the most important developments and findings found in the specialized research literature on avoiding stress corrosion cracking in recent years.

2.2 Basic aspects of SCC General

SCC is an old phenomenon known here as a kind of material failure that occurs when some materials are subjected to tensile stress in an erosive environment. Requires both tensile stress and the presence of a particular corrosion medium [21]. Removal either prevents cracking or stops cracking growth that has already spread.

2.3 Brief history

Stress Corrosion Cracking (SCC) is a progressive fracture mechanism that can occur in almost all metals. It was first identified by the British army in India at the end of the 19th century when cracks appeared in boxes of ammunition copper cartridges. The cartridge case developed high tensile stresses when the bullet was introduced, resulting in high temperatures, high humidity and traces of ammonia in the air, causing SCC [26], [27].

The actual beginning of the scientific interest of the environment-assisted cracking of metals (specifically SCC and HE) was in the late 19th century. Early evidence showed that the SCC study had a practical application by the British Army in India in the latter half of the 19th century for cracks in boxes of copper ammunition cartridges. The cartridge case developed tightened pressure when the bullet was introduced, resulting in high temperatures, high humidity and ammonia effects in the

air, causing SCC, [5]. Below is a sequence of events on the developments that have occurred for this phenomenon from the beginning of the twentieth century until recent times.

- Early in the 20th century, SCC was observed in martensitic steel, but the problem didn't become widely recognized for SCC until the era of the aerospace programs. Also during this period, the cracking of mild steel due to nitrates became of practical importance in the chemical industry. SCC occurs when the alloy is almost inert to the environment which does the cracking. During the 1930s when stainless steel came to be used, SCC was observed in this class of allays especially in chloride at elevated temperature. Also during this time, magnesium alloys for military aircraft were found to be susceptible to SCC in moist atmospheres [21].

- The 1940s and 1950s were a time when the seriousness of the SCC problem, the need to identify SCC sensitive materials and environments that facilitated physical failure, and the urgency of defining the research agenda were clear. In 1944, the first major seminar - a seminar on metal cracking caused by stress and corrosion - was organized by ASTM and AIME in Philadelphia, USA [29]. A similar seminar was also held in Boston, USA, in 1954 on stress corrosion cracking.

- In the 1960s, fracture mechanics became a serious consideration for studying environmental effects on the mechanical properties of materials. In early 1966, the Advanced Research Projects Agency (ARPA) of the US Department of Defense asked the Marine Research Laboratory to conduct an intensive research into the problem of stress corrosion caused by high-strength alloys after realizing the importance of the technical complexity of the gravity of this phenomenon to designers of the aerospace and marine industries, From the difficulty of fragile fracture with the chemical reactions that occur within the cracks and cannot be accessed as shown in Figure (2.1). The agency also recognized new developments in surface physics and surface chemistry that could eventually lead to advances in metal fatigue corrosion. In 1967, the International Conference at the University of Ohio, USA, was the first

conference to address the key aspects of stress corrosion cracking discussed in the SCC phenomenon of all major alloy systems [30].

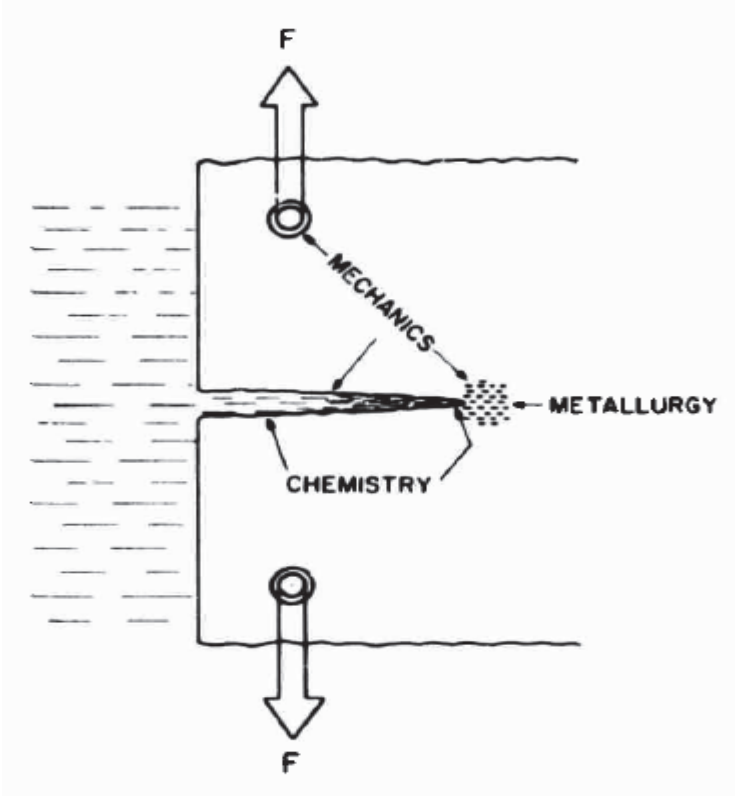

Figure 2.1 The three scientific elements of stress-corrosion cracking.

- During the seventh decade of the last century, there was a great interest in (SCC), which focused on identifying the mechanisms of stress corrosion cracking and the growth of cracks. Held at, University of Surrey, United Kingdom 1977 International Conference on Mechanisms for Cracking of Sensitive Materials.

- In the eighties of the last century, the most important achievement during this period was the "modelling and measurement of cracks and their bad effects on the spread of cracks at the loading of static and dynamic," held this conference at the National Physical Laboratory, the United Kingdom in 1984. The conference was one of the most important conferences that had a great impact on this phenomenon [27].

- In the 1990s, many types of research were interested in the topic, in particular, many conferences were held. One of the major differences in

research was the widespread and positive use of new techniques, including high-resolution analytical methods, and computational methods for study SCC in different environments [5].

- In the recent years, there is growing concern about SCC phenomenon on wide ranges in the welding technology in the deference metals and environments around the world, there are many kinds of researches and studies have been exposed to this phenomenon, such as:

- The effect of SCC for steel 44340 and 3.5 NiCrMoV under the hydrogen charge with a different application of stress was studied [28]. Results show that the speed of SCC is lower in samples exposed to distilled water, but there is a significant similarity between the speed of the incision with the stress rate applied in both cases. The surface morphology of the samples was mostly between granular cells and was apparent at the highest applied stress gradients [28].

- The installation for newly formed surface creation of the metal has been developed, [26]. Experiments were carried out in model solutions of NaCl on samples of various shipbuilding metals. Shipbuilding metal potentials without oxide film in the marine and ocean water have been obtained. The results show how much the steel potential value was critical "inside" the crack under corrosion-mechanical and fatigue destruction. The obtained results show that the electrochemical corrosion account is possible at the application of high-tensile steels, which used in dynamically loaded constructions in corrosion environments. Hereof also follows that steel polarization potential for cathodic protection from local fractures is necessary to define on the new-formed surface. The observed phenomenon immutability potential of the metal with a minimum of surface charge on the new formed surface has important theoretical and practical significance for electrochemical protection from corrosion and mechanical fracture of vessels and ocean structures [26].

- Stress corrosion cracking (SCC) behavior and mechanism of E690 welded joint in a simulated marine atmosphere containing SO2 were investigated using slow strain rate tests (SSRT) method and electrochemical measurements. Results showed that it had very high SCC susceptibility in this

environment with a combined mechanism of anodic dissolution and hydrogen embrittlement (HE). The intern critical heat-affected zone in the welded joint was the most vulnerable location to SCC because this zone has less strength, more negative potential, and higher corrosion current density [30].

- Using the finite element method, the mechanical effect of nonlinear stress corrosion cracking on the stress rate at the tip of the crack, for (316L) in a model chloride medium was studied in [31]. Slow stein rate test was applied (SSRT). The results and investigations revealed the spread of cracks in the surface of the metal and its ramifications to multiple branches, and also some important information on the impact of the microscopic structure of metal erosion [31].
- Two options of finite element (FEM), impact function (IFM) were used to evaluate the impact of SCC on weld metal and heat-affected zone and their impact on the growth of cracks due to the residual stresses, [32]. The growth of cracks has been shown to be largely influenced by the initial location and the remaining stress distributions. The highest growth rate of cracking is obtained when the SCC crack grows along the z-axis, where ring tension is greatest in the focal welding area. The IFM evaluation also showed conservative results. In the asymmetric welding area, the effect of cracking is shown differently depending on the initial arrangement of the cracks [32].
- In 2015 using the finite element method, Wang and others proved that corrosion product films on the surface of the metal had a significant role in the growth of the SCC. The flat specimens and the U-shaped edge were examined in terms of the stress caused by the of the corrosion product films. The study showed the effect of the area of stress in front of the tip of the incision in the samples by Young's modulus of the corrosion product films and the thickness of the layer and the geometric shape of the crack, [10].

2.4 Characteristics of SCC

The following points summarize most of the characteristics of SCC:

1. Tensile stress is required. This stress may be supplied by service loads, cold work, mismatch in fit-up, heat treatment, and by the wedging action of corrosion

products.

2. Just alloys and not pure metals are affected, though there may be exceptions to this rule.

3. In general, only a few chemical species present in the environment are effective in causing SCC of certain alloys.

4. The species responsible for SCC, in general, need not be present either in large quantities or in high concentrations.

5. With some alloy/corrode combination, such as titanium alloys and crystalline sodium chloride, or austenitic stainless steel and chloride solutions, temperatures substantially above room temperature may be required to activate some process essential to SCC.

6. An alloy is usually almost inert to the environment which causes SCC.

7. Stress corrosion cracking is always fragile under the microscope, even in very heavy alloys in tests of purely mechanical failures.

8. There seems to be at least some tension in some systems where CSC does not occur.

2.5 Sequence of Events in SCC

In the most general case, if a smooth specimen is placed in a corrosive environment in which it will eventually undergo SCC, the sequence of events is as shown in figure 2.2. First a corrosion pit forms. There is an important feature of most corrosion pits, the significance of which is not always appreciated, a porous cap of corrosion products which must be removed in order to see the pit itself. This cap impedes exchange between the corroding within the pit and the bulk corroding outside the pit, but it permits inward migration of anions such as chloride[30].

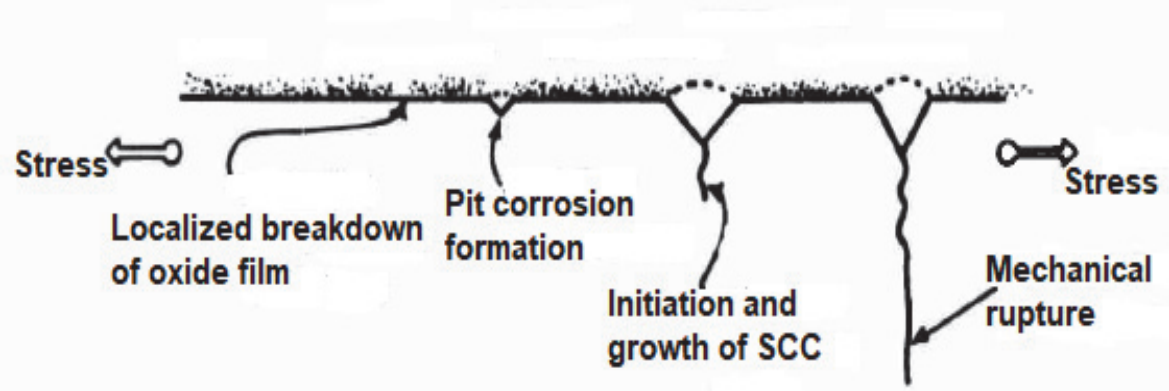

Figure 2.2 Sequence of Events in SCC

Generally, the pH within corrosion pits also differs from that outside the pit. The function of a corrosion pit in initiating SCC was once widely thought to be purely mechanical, to concentrate stresses. It now appears that the essential function of the pit when it initiates SCC is not primarily mechanical, but rather it is to provide a mechanism for altering the solution chemistry locally to one favorable for SCC.

2.6 Stress Corrosion Cracking Growth Models

Cracking stress has a variety of mechanisms that can be chemical or mechanical. Many factors influence these mechanisms, which can be mechanical, heat, chemical, or environmental. Some of the models used to assess this phenomenon (SCC) include a crack in the film that subsequently degrades as a result of crack branching. The diffusion of hydrogen and oxygen between the grains through the spaces between them, which causes internal stresses [40]. It is difficult to fully explain and clarify the mechanism of (SCC) at the same time. The mechanisms affecting (SCC) cannot be predicted at all, but depend on the surrounding conditions of the causative environment, the manufacturing process, and the stresses according to the place at the time of this phenomenon [41].

2.6.1 Rios et al., Model

This model attempted to agree between mechanisms. It emphasized that there are several factors that cause a defect in the grain boundaries, which leads to the failure of the plastic area at the tip of the crack, which leads to the rapid growth of the crack. Some factors causing (SCC) such as residual stress, intergranular carbides, and different temperatures. The crack does not spread unevenly but rather

concentrates on sinuous areas forming a squeeze, such as (u-bend) [42]. Crack growth rate (CGR) is proportional to the subtle degree of residual stress within the alloy (SCC). The stress is slow at the end of the crack that is part of this process [43].

2.6.2 Jivkov et al., Model

It was found in 2008 that the development of cracks and growth begins at the side of the crack, as a result of several variables and factors dependent on the geometry and the stress intensity factor (K). This model connects, between stress intensity factor (K) to the failure-prone portion, depending on the length and location of the crack in the sample. The crack tip is calculated using a special model specifically across granules.

2.6.3 Hall Model

In this model SCC occurs due to plastic failure during creep at the crack tip, enabling correlation of stress with stress intensity factor K [41].

2.6.4 Scott Model

This model is used only for steam generator tubes, [44]. It is a simple model involving the stress intensity factor, as shown in Figure 2.5, where the comparison with experimental data is given, [41].

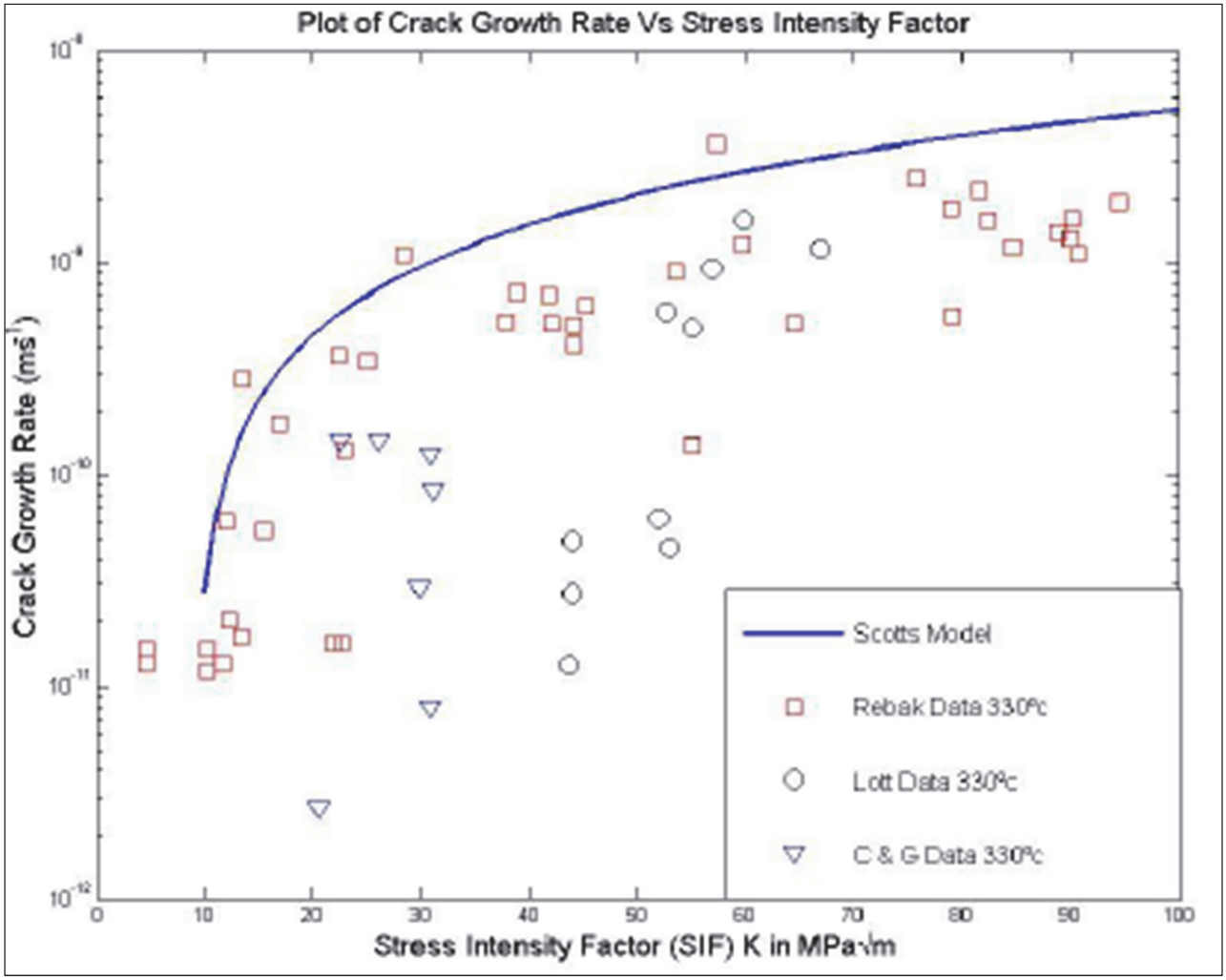

Figure 2.3 Stress intensity factor vs crack growth rate [41].

2.6.5 The Slip Dissolution -Film Rupture Model

This model introduces film formation and rupture, as well as its reactivation, depending on the crack tip state [40], [41]. It correlates Stress Intensity Factor (SIF) with crack growth rate, Fig. 2.5.

3. CHAPTER - High Strength Steel

3.1 Introduction

This chapter covers an aspect of mild steel that is classified as one of the steels widely used in the industry. High-strength steel is one of the types of this grade whose yield strength is not less than 450 MPa, which often contains 0.15 wt% C, 1.65 wt% Mn, and also has low levels (less than 0.035%) of P, S, and others, [45]. This type of steel has many uses, as we find it used in structures, construction, pipelines, shipbuilding and many other marine applications [46]. It is used to develop applications that require the design to withstand particularly high stresses, and which are often very close to the yield stress [47].

3.2 Definition of High Strength Steels

The conventional method [48, 49] to obtain this type of steel, when producing various types of steel, to develop optimum strength, the steel must first be completely transformed into martensite, and for this to be achieved the steel must be quenched at a rate fast enough to ensure that the decomposition of the austenite formed during the cooling of products such as pearlite and ferrite must be avoided. And by cooling to a martensite form which is subsequently heated or tempered, at medium temperature, by increasing the hardness of the formed steel without very large losses in strength. This is what is known as high-strength steel [48].

Different sectors in industry, have always demanded minimum construction mass to improve performance and production. To achieve this goal, good formability and weldability of high-strength steels is one such important method. Cold rolled steel and quenched steel with medium and high yield strength levels of 740 MPa and 1100 MPa respectively are used with success in trucks, dumpers, cranes and similar products. For new types of high-strength steels, the production cost can be reduced by reducing the weight by relying on efficient designs due to its yield strength. The design procedures and production techniques used must take into account formability, weldability, hardness, torsion, crush resistance and fatigue, take advantage of the full potential of this type of steel [49].

3.3 Classification

Depending on the manufacturing and finishing method, product shape, microstructure, heat treatment, and given the level of strength required as specified, the steels are classified into different systems in the EN 10113-7 standard [50]. Steel grades are classified into three groups, according to EN, respecting the production process.

3.3.1 **Normalized steel grades (EN 10113 part 2)**

Normalization process, during which metal is heated to a certain temperature that enables the movement of grains, followed by cooling to the ambient temperature in the atmosphere. Hence, a microscopic composition of perlite granules with some ferrite is obtained. Better fabrication property and higher hardness ability are obtained in natural steel as compared to annealed (oven-cooled) steel [51].

3.3.2 **Thermo-Mechanical controlled Processing steel grades (EN 10113 part 3)**

This is the most efficient process for minimizing the size grains. Thermo-Mechanical Control Process (TMCP) involves control of both thermomechanical stability and rapid cooling. Thereby, reduction of thickness by rolling is largely controlled near the temperature A_{r3}. For this, the use of TMCP changes microstructure as well, [21] [51].

3.3.3 **Quenched and Tempered (Q&T) high strength steel grade (EN 10137 part 2)**

In this type of steel should be combined, fast cooling and controlled stability between grains, to obtain steel with advanced mechanical properties more than ordinary steel so that this steel has high ability to form and welding. Many steel grades were produced with a yield strength of 450 MPa, using the TMCP method. Recently, to overcome this shortcoming in the production of high strength structural steel, the Q&T method has been used concerning normal products, strength limits and section thicknesses [51], [52].

By cooling the steel from the pure austenitic stage whose temperature ranges between (850-950 °C) until it reaches the martensite stage at room temperature or

less, and this is done by applying rapid cooling in certain cooling media such as (water, brine, oil, etc.), For the purpose of obtaining low alloy steels. The martensite phase is a brittle phase due to the increased carbon content, which in turn increases its hardness.

Tempering is one of the main steps that are taken in steel production. To increase the strength of the metal and reduce its brittleness, residual stresses are eliminated by heating the hardened steel to a medium temperature. An increase in temperature is accompanied by a decrease in the region's properties, and this leads to an increase in tensile strength, elongation and stiffness [30]. The level of yield strength of high-strength steels varies with different production methods. Table 3.1 shows a group of types of high-strength steels for marine structures.

Table 3.1. High strength steels used in offshore [53]

Yield Strength (MPa)	Process route	Application
350	Normalized TMCP	Structures Structures & Pipelines
450	Q & T TMCP	Structures & Pipelines
550	Q & T TMCP	Structures & Moorings Pipelines
650	Q & T	Jack-ups & Moorings
750	Q & T	Jack-ups & Moorings
850	Q & T	Jack-ups & Moorings

3.4 Hardenability

There are variation [54] about the meaning of hardness and hardenability. During cooling the steel can harden to a certain depth, this is known as the hardness property of steel. Hence, hardness is a physical property, independent of cooling rate, what mainly depends on chemical composition and grain size. Damping intensity is the structures obtained by the damping section and is a function of both the stiffness and the quenching process. Thus the quenching of the sample depends to a large extent on its microstructure, causing it to appear with different hardness values. Depending on carbon content and the steel structure. This defines hardness as a measure of a material's resistance to plastic deformation.

Several researchers explained that, in the early 1930s, the concept of hardness developed, the tempered martensite hardness increased more or less linear from cca 0.05 to 0.5% of C. From Figure 3.1 one can see that the quenched stiffness decreases when the carbon content in austenite is more than 0.8%, which is much softer than martensite due to the presence of retained austenite [54].

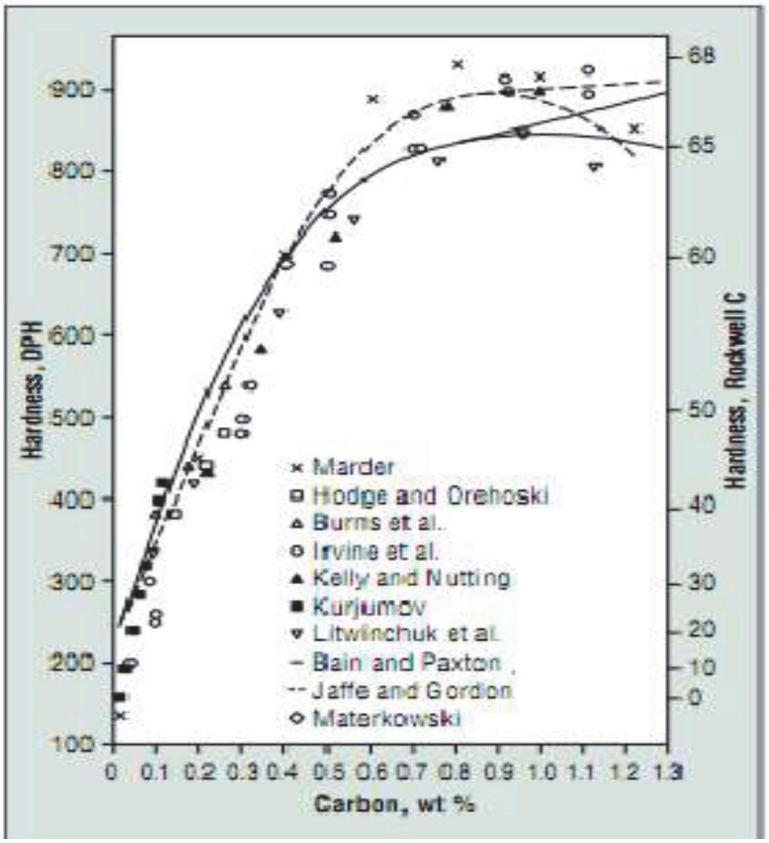

Figure 3.1 Summary of extensive as-quenched hardness data from the literature for Fe-C alloys and steels by Krauss, [54]

3.5 Hardening Mechanisms [55]

Solid solution hardening, grain refinement, as well as precipitation hardening are the different mechanisms that can affect the strength. Refining grain size is the only reinforcement mechanism that increases durability at the same time, so it is considered the most unique mechanism. The relationship between grain size and yield strength of C-Mn steel is shown in Figure 3.2.

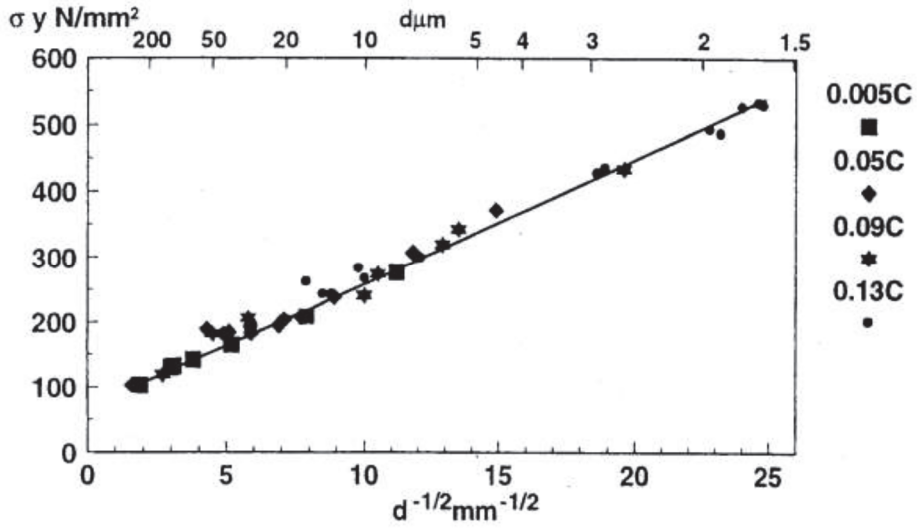

Figure 3.2 Relation between lower yield strength and the grain diameter.[40]

3.5.1 Microalloyed steels [55]

Microalloyed steels are alloys that can be obtained by adding a few elements in small quantities, such as V and Nb. Since grain refining is limited, alternative strengthening mechanisms must be employed to further increase yield strength. When designing fine grain steels, the deposition and hardening of pearlite should be used to a greater extent than is expected. Vanadium is often used to obtain the required level of solidification and precipitation at the reheating temperatures used in the rods heat treatment of high strength alloys, due to the limited solubility of some elements at these temperatures.

Microelement compounds - V(C or N) precipitation during transformation or even afterwards, strengthen the microstructure. Proper quantity of V and N is needed to produce required level of strengthening.

3.5.2 Thermomechanical Treatment (Rolling)

Usually at temperatures just below the plate reheating temperature, initial rolling passes of the steel are performed, so that the deformation steps follow the rapid recrystallization and grain growth, [54] [55]. The addition of austenite grain growth inhibitors, when performing a heat treatment, repeated deformation and recrystallization steps are combined to initially improve the austenitic grain size and reduce its growth after recrystallization. By frequent recrystallization, due to optimal formations and the adoption of rather difficult reduction schedules, the best sizes of

recrystallized austenite grains resulting from this process are around 15 μm. Depending on the cooling rate, the transformation can produce iron pellets 6-8 microns in size. It is at this point that controlled rolling is not only possible but is also beneficial for structural homogeneity [55].

By using additional micro-dye elements suitable particle sizes of austenite can be obtained, and in conjunction with a controlled rolling sequence, the recrystallization of austenite is greatly impeded. The shape of the grains and the surface area are affected by the evolution of this process much greater than that occurring in recrystallized austenite. During the process, both austenite recrystallization and CN precipitation reactions are affected. However, as shown in Figure.3.3, since about the middle of the last century, instead of hot and calibrated rolling, thermomechanical rolling has been used. When adding materials up to X70 niobium and vanadium mixed with steel, low carbon steels can be produced. By using this method, it becomes possible to produce high-strength steels like X80, which have low carbon content and high weldability. The strength is greatly increased by adding molybdenum, copper and nickel, to a level of up to X100 when the steel on the plate is processed by mechanical thermal rolling in addition to modified accelerated cooling[52].

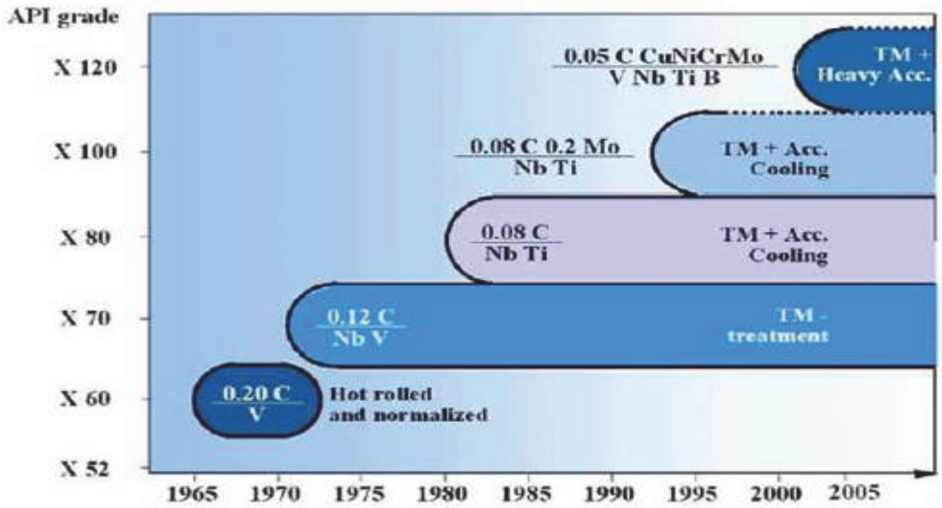

Figure 3.3 History in Line Pipe Steels (Large Diameter Pipe) [52]

Great importance is given to the effect of austenite formation, and the transition temperature range (according to the alloy content, deformation and cooling rate). The mechanical properties of the carefully cast plate and the final grain size are factors

determining the conversion of the microstructure from austenite to ferrite. Also, the temperature range for the conversion of austenite to ferrite continues to be controlled beyond the production of a minimum level of austenite grains to determine its interaction motion. With controlled cooling, an increased growth rate can produce an accurate size of ferrite grains [55]. Hence, it is possible to design a rolling strategy, to produce the best possible size for recrystallized austenite grains. It is of utmost importance that the rolling process is controlled by recrystallization. During the controlled rolling, the cooling acceleration of low-carbon fine alloy steel products and its effect on the microstructure are shown in Fig. 3.4. The range of conversion of austenite to ferrite must be controlled so that the maximum purification of the ferrite grain is achieved. However, compared to the two, the grain size that can be produced from ferrite when converting from the austenitic grains flattened by rolling under the temperature of recrystallization is better than the size of the ferrite grains that can be produced when converting from recrystallized austenite. A moderate grain size which is coarser than the grain size can be achieved in sheets rolled in high strength steel.

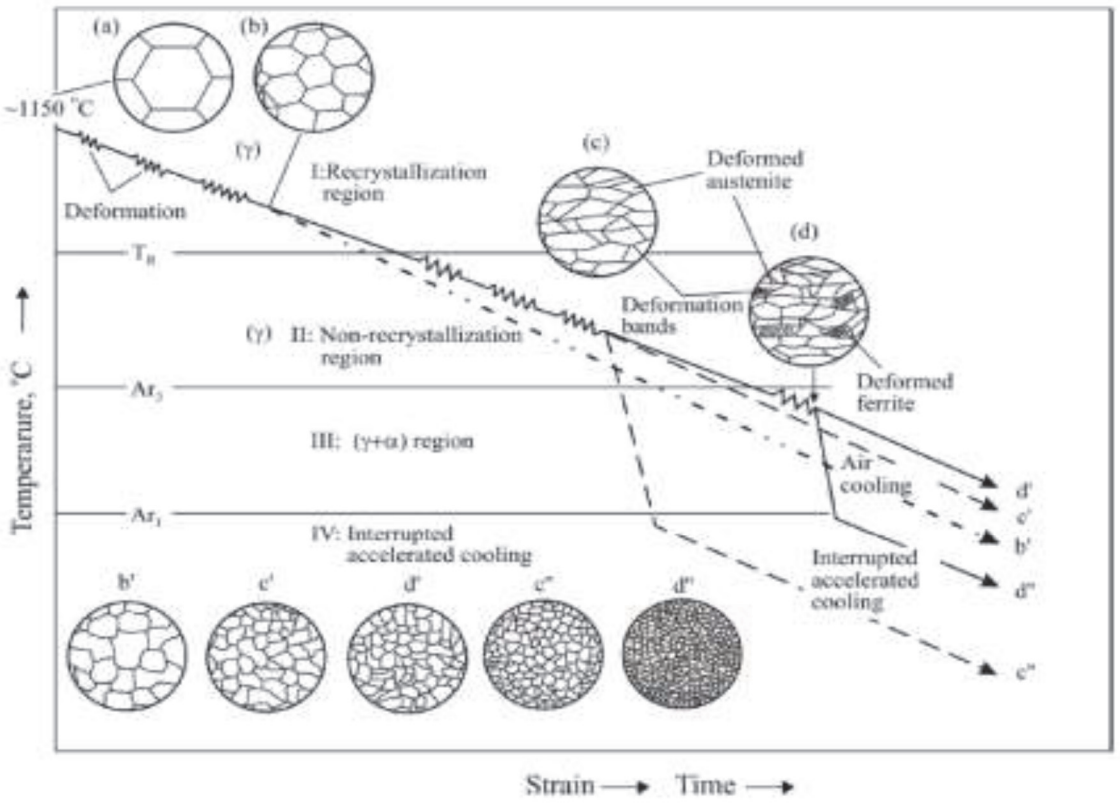

Figure 3.4 Schematic diagram of the influence of accelerated cooling on the microstructure of low-carbon micro alloyed steel products during controlled rolling [54]

However, about twenty years ago, the ISP (Inline Strip Production) line was developed in ATA Averdi steel plant in Italy with a production capacity of 5.105 tons/year. This line (Figure 3.5) consists of the continuous casting machine for concast slabs 60 mm thick with the burnishing mill stand for squashing the slab with the liquid core to 43 mm, roughing train, a furnace for inductive heating of the strand, Ceremony-type furnace with the strand coiler and decoiler, ensuring maintaining the correct feedstock temperature, mill scale breaker, finishing train, laminar flow cooling, and a coiler for the finished product [54].

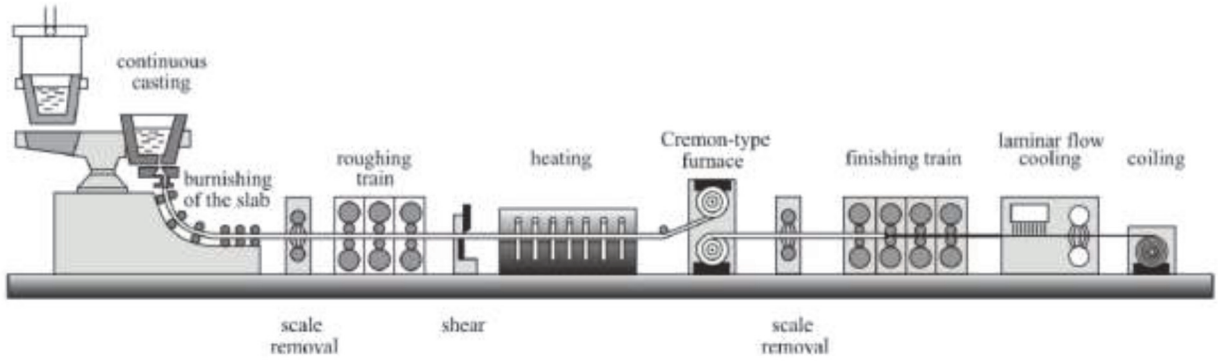

Figure 3. 5 Schematic diagram of an integrated production line of rolled plates in ISP (In-line Strip Production) process. The steel may be up to 1 mm thick [54]

3.5.3 Processing methods of HSLA Steels [14]

Given this, and to improve the mechanical properties of some Special Steel (HSLA) and its various forms, hot-rolled HSS products may include special treatment. These processing methods include:

- To obtain fine austenite grains the rolling must be controlled to precipitate HSLA steels and/or highly deformed austenite grains. The austenite granules are converted into fine ferrite grains, during the cooling process, meanwhile, while the yield strength is improved the durability is greatly enhanced. Figure 3.6 illustrates the balance of strength and durability of integrated steel tubes, as well as demonstrates mechanical heat treatment concerning mechanical properties.
- To produce fine ferrite grains during austenite conversion the rolled HSS steels are controlled, this is done during rapid cooling. The cooling temperature increases precipitation so that it cannot be fast, nor can it be slow enough to form ferrite. The effect of accelerated cooling on grain size is shown in Fig. 3.7, and it is noted that faster cooling gives finer grain size.

- To obtain HSS annealed steels for improved formability, the two-phase microstructure also shows lower yield strength and provides a better combination of ductility and tensile strength compared to normal HSS steels. High strength steel is also formed into cold-rolled sheets.

The main advantage of HSS forgings (HSLA hot rolled products) is that it has a yield strength ranging from 275 to 485 MPa and can be higher, which can be achieved without heat treatment. Typically, the basic configurations of ferrite - pearlite forgings with fine alloys are from 0.3 to 0.5% C and 1.4 to 1.6% Mn. Also, low carbon steel forgings of this type are improved under the same conditions.

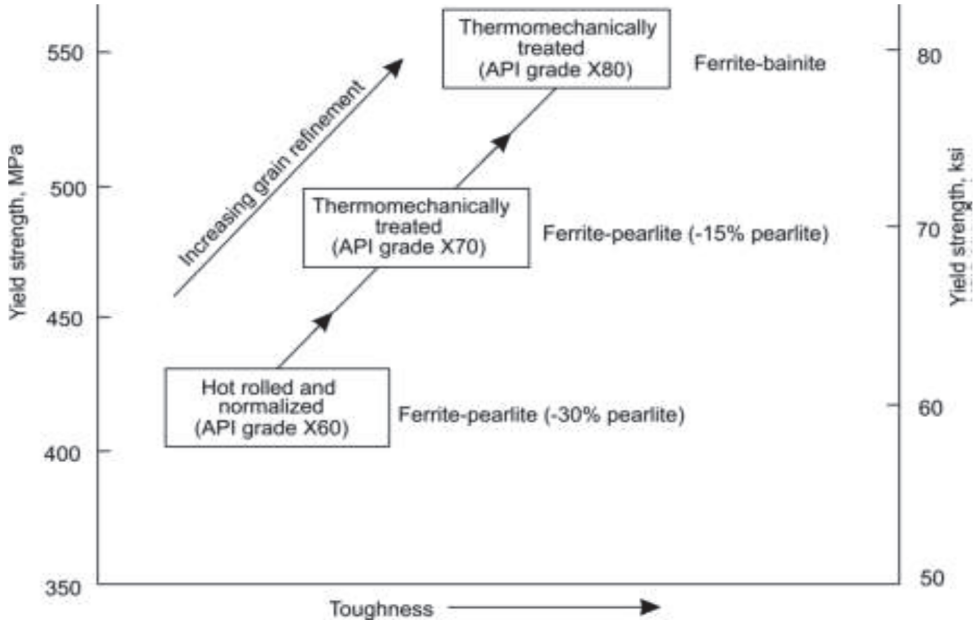

Figure 3.6 Effect of microstructure and production process on the mechanical properties of line pipe steels [14]

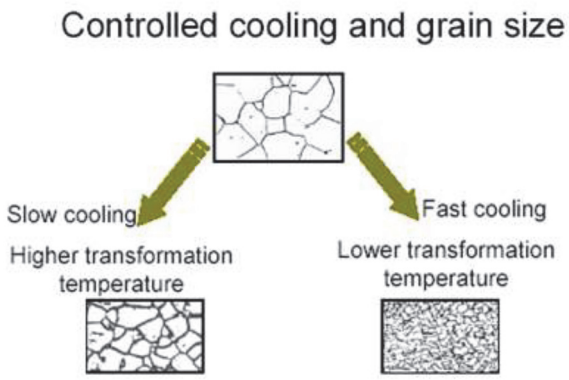

Figure 3.7 Controlled cooling and grain size. [56]

3.6. Chemical Composition and Properties of HSLA Steels [56]

High-strength and low-alloy steel (HSLA) identifies steels that have several benefits and advantage over regular carbon steel, which has a low carbon presence. In general, it must have a set of high mechanical properties, such as high strength, along with improved toughness, ductility, excellent formability and weldability, and additional resistance to atmospheric corrosion. Due to its excellent properties, HSLA steel is widely used in the industry, as we find it used in automobile chassis, oil storage tanks, bridges, and tanks designed to withstand high pressure. Usually, the percentage of carbon in HSLA steels is low, which is mostly less than 0.15%, compared to ordinary carbon steels. These excellent properties are obtained by adding different alloy elements in very small quantities if compared to conventional steels, and this type of steel is known as fine alloy steels. There is a very great possibility to add a lot of elements, including carbon, manganese and silicon, to steel to achieve additional strength and improve its properties. Also, to ensure that these features are achieved, among the elements that can be added are chromium, nickel, niobium, boron, molybdenum, titanium and copper.

3.6.1 Multivariate Interaction in HSLA Steel [56]

The alloying elements added to the steel interact with the proportion of iron and carbon contained in the steel, resulting in different hardening effects. And by strengthening the solid solution, these added elements work to harden the steel. When combined with carbon in various fine and random carbide deposits, the elements of the steel alloys are solid when the precipitation hardens. The diffusion of these elements is affected, which results in many complex interactions between industry elements. Alloys. The precipitation is improved when several elements combine to form a carbide compound. Due to small quantities of alloying elements, the solid solution is strengthened, and to a lesser extent, the grain is refined. By adding alloying elements, the steel is strengthened. The cooling rate, deformation range, time and temperature are sensitive enhancers to the curing environment. For example, sediment formation is greatly influenced by the solubility and diffusion of fine alloy elements, as a result of temperature control. Grain growth is a thermally activated process, during steel processing, the temperature and time have a great influence on the grain size.

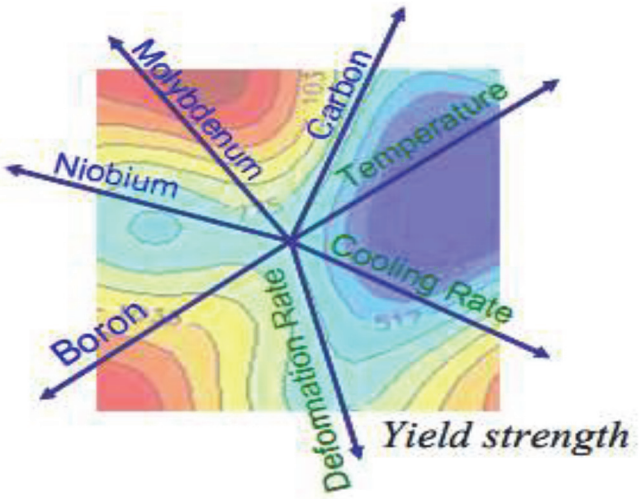

Figure 3.8 Multidimensional nature of micro alloyed steel with complex interactions and different contributions to the final mechanical property [56]

3.6.2 Material specifications for HSLA steel

Much of the steel used in rolling or normalizing, is documented by the American Society for Testing and Materials (ASTM). Table 3.2 documents many ASTM specifications covering high quality HSLA steels in the presence of special elements. Certain ASTM, ASI, API and MIL specifications outline the chemical formulations, tests and additional procedures relevant to each application. The user may request special applications or supplementary tests for the task [5]. However, high-strength alloy steels will be tested in this work and its specifications will be described later.

Table 3.2 Compositional limits for HSLA steel in ASTM specifications properties [53]

ASTM specification(a)	Type or grade	UNS designation	Heat computational limits, % (b)									
			C	Mn	P	S	Si	Cr	Ni	Cu	V	Other
A 242	Type 1	K11510	0.15	1.00	0.45	0.05	...	...	...	0.20 min	...	...
A 572	Grade 42	...	0.21	1.35(c)	0.04	0.05	0.30(c)	...	...	0.20 min(d)	...	(e)
	Grade 50	...	0.23	1.35(c)	0.04	0.05	0.30(c)	...	...	0.20 min(d)	...	(e)
	Grade 60	...	0.26	1.35(c)	0.04	0.05	0.30	...	...	0.20 min(d)	...	(e)
	Grade 65	...	0.23(c)	1.65(c)	0.04	0.05	0.30	...	...	0.20 min(d)	...	(e)
A 588	Grade A	K11430	0.10–0.19	0.90–1.25	0.04	0.05	0.15–0.30	0.40–0.65	...	0.25–0.40	0.02–0.10	...
	Grade B	K12043	0.20	0.75–1.25	0.04	0.05	0.15–0.30	0.40–0.70	0.25–0.50	0.20–0.40	0.01–0.10	...
	Grade C	K11538	0.15	0.80–1.35	0.04	0.05	0.15–0.30	0.30–0.50	0.25–0.50	0.20–0.50	0.01–0.10	...
	Grade D	K11552	0.10–0.20	0.75–1.25	0.04	0.05	0.50–0.90	0.50–0.90	...	0.30	...	0.04 Nb, 0.05–0.15 Zr
	Grade K	...	0.17	0.5–1.20	0.04	0.05	0.25–0.50	0.40–0.70	0.40	0.30–0.50	...	0.10 Mo, 0.005–0.05 Nb
A 606	...	...	0.22	1.25	...	0.05	...	...	...	...	...	...
A 607	Grade 45	...	0.22	1.35	0.04	0.05	...	...	...	0.20 min(d)	...	(e)
	Grade 50	...	0.23	1.35	0.04	0.05	...	...	...	0.20 min(d)	...	(e)
	Grade 55	...	0.25	1.35	0.04	0.05	...	...	...	0.20 min(d)	...	(e)
	Grade 60	...	0.26	1.50	0.04	0.05	...	...	...	0.20 min(d)	...	(e)
	Grade 65	...	0.26	1.50	0.04	0.05	...	...	...	0.20 min(d)	...	(e)
	Grade 70	...	0.26	1.65	0.04	0.05	...	...	...	0.20 min(d)	...	(e)
A 618	Grade Ia	...	0.15	1.00	0.15	0.05	...	...	...	0.20 min	...	...
	Grade Ib	...	0.20	1.35	0.04	0.05	...	...	...	0.20 min(f)	...	...
	Grade II	K12609	0.22	0.85–1.25	0.04	0.05	0.30	...	...	...	0.02 min	...
	Grade III	K12700	0.23	1.35	0.04	0.05	0.30	...	...	...	0.02 min	0.005 Nb min(g)
A 633	Grade A	K01802	0.18	1.00–1.35	0.04	0.05	0.15–0.30	...	...	...	...	0.05 Nb
	Grade C	K12000	0.20	1.15–1.50	0.04	0.05	0.15–0.50	...	...	...	...	0.01–0.05 Nb
	Grade D	K02003	0.20	0.70–1.60(c)	0.04	0.05	0.15–0.50	0.25	0.25	0.35	...	0.08 Mo
	Grade E	K12202	0.22	1.15–1.50	0.04	0.05	0.15–0.50	...	...	...	0.04–0.11	0.01–0.05 Nb(d), 0.01–0.03 N

3.7 Advanced High Strength Steels

In this Chapter different Advanced HSS are presented, classified according to their microstructure and production process.

3.7.1 Dual-phase steel (DP)

The dual-phase steel microstructure, Figure.3.9, shows matrix of fine ferrite and hard martensitic islands. The cooling is carefully controlled to produce a ferrite martensite structure from austenite if it is hot rolled. Upon rapid cooling, the final structure is produced from a double-phase structure of ferritic austenite, resulting in some of the austenite being converted into martensite, during continuous hardening [57].

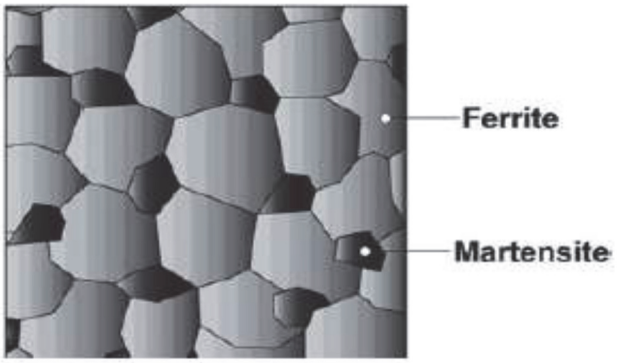

Figure 3.9 DP microstructure schematic [45]

The soft, elastic ferrite in the finished double-phase material, exceptionally, absorbs the pressure around the martensite islands, resulting in high stiffness and

fatigue strength, resulting in uniform elongation. Double-phase steels can be developed with additional production strength ranging from low to high Yield strength to UTS ratios, which allows a fair number of applications in different places.

3.7.2 TRIP steel

This type of high strength steel is widely used in marine applications as well as in the automotive industry. TRIP takes advantage of a multi-stage microstructure with fine ferrite content in difficult stages. The schematic diagram shown in Figure.3.10 shows the microstructure of this species. The matrix contains a large amount of retained austenite (up to 5%), along with the martensite content. TRIP shall contain an acceptable proportion of bantite, to stabilize the austenite diffuse below carbon at ambient temperatures. To accelerate the formation of ferrite/bainite, Aland/or Si must be added, and the formation of carbide in the designated area is reduced [58].

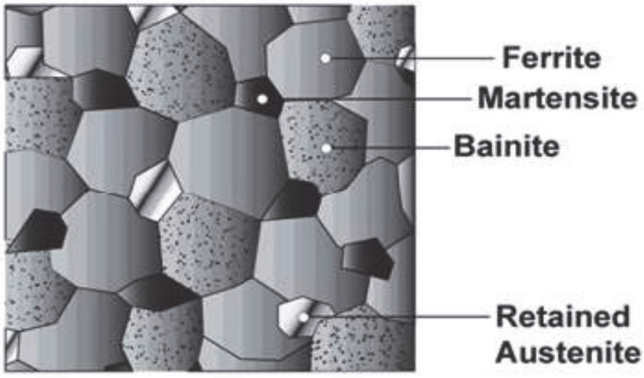

Figure 3.10 Schematic of a typical TRIP microstructure [59]

3.7.3 MnB steel

The die-cooled hot-stamped steel contains Mn B, which makes it have high strength, a hot stamping process is formed for the steel, then pressure is formed when the blanks are heated to austenite, and this process takes place when the blanks are still red and smooth. Consequently, the absorption properties deteriorate which increases the environmental problem due to the addition of alloying elements, [60]. The synergetic effect of alloying elements on the phase transformation occurrence is shown in Figure 3.11, [60].

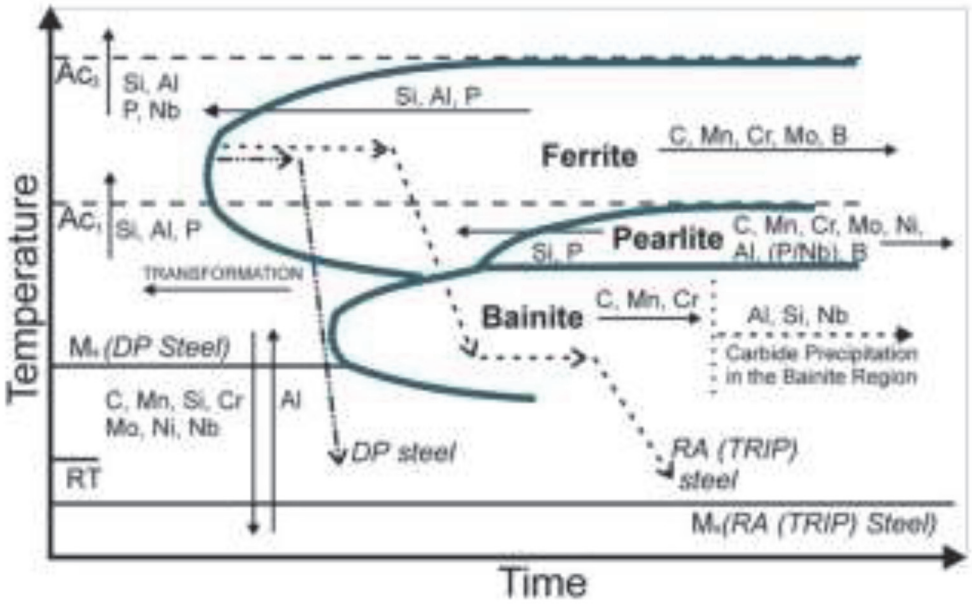

Figure 3.11 Influence of alloying elements on TTT behaviour. [46]

The stress and strain behavior of different steels (HSLA, DP, and TRIP) which have the same yield strength is illustrated in Figure 3.12.

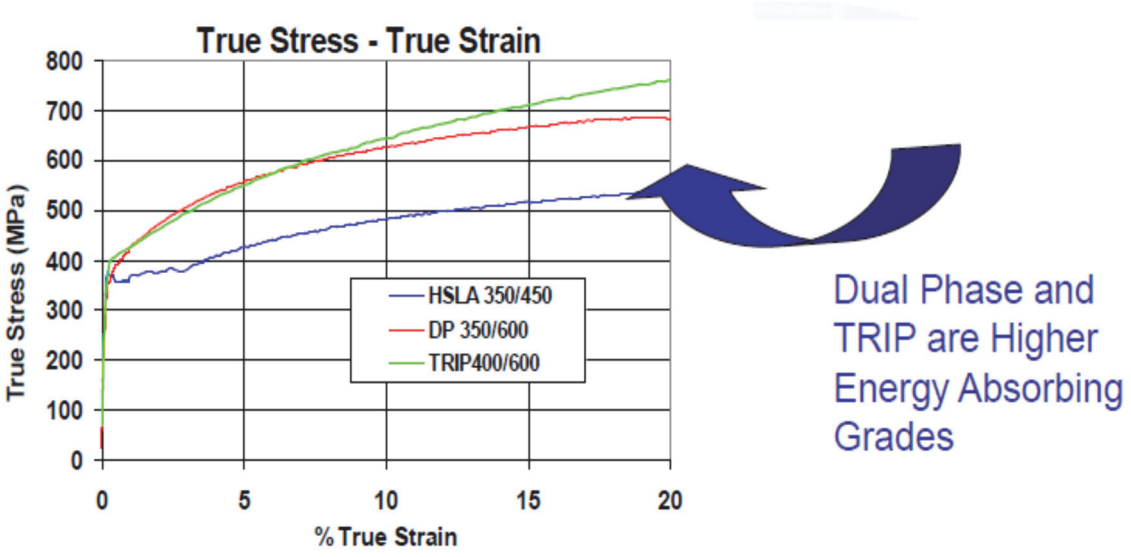

Figure 3.12 Advanced High Strength Steel Processing

Figure 3.13 shows the different types of steels including conventional high-strength steels, low-alloy steels (HSLA), light and steels, isotropies, newer grades of high-advanced steels, durable steels such as double-phase, and martensitic steels such as "AHSS".. The mixture stems mainly from its high capacity for stress

hardening, as a result of the low yield strength to the ratio of maximum tensile strength. Figure 3.14 shows the third generation of AHSS steel [62].

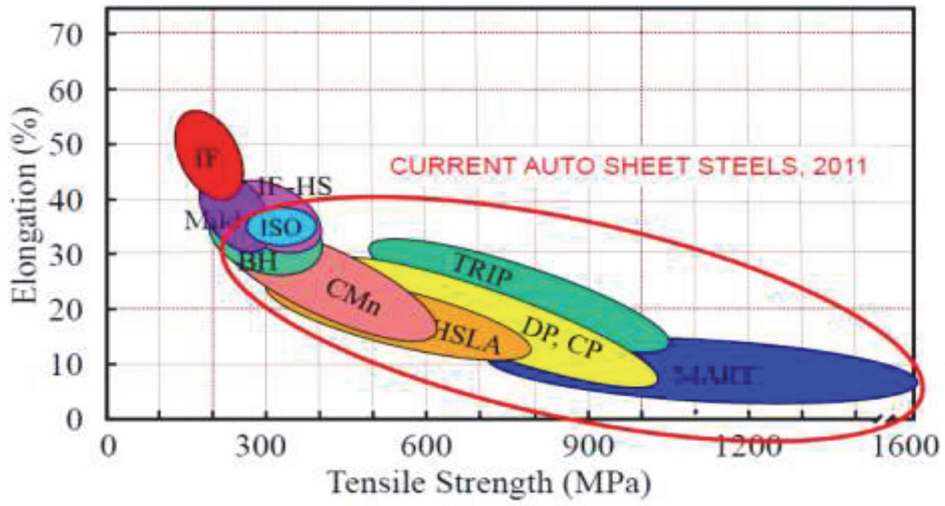

Figure 3.13. Tensile strength and elongation relationship of different HSS, [61]

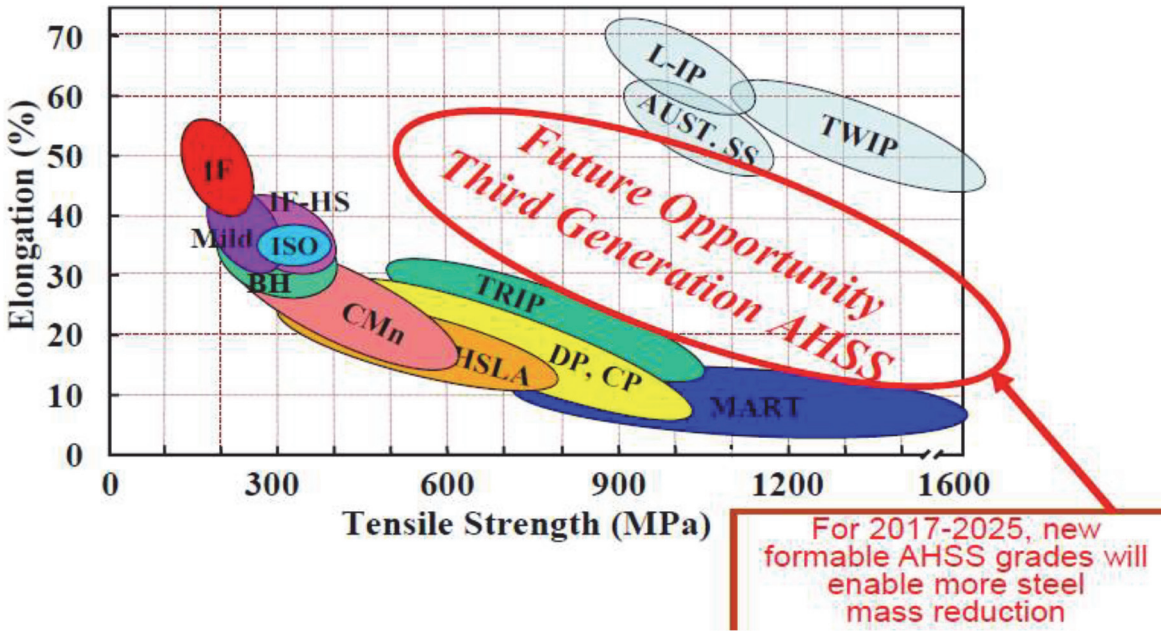

Figure 3.14 Third Generation of AHSS, [61]

Chapter 4 Mechanisms of Stress Corrosion Cracking (SCC)

4.1 Definition of Stress Corrosion Cracking

SCC is a weakening of engineering materials and their disruption and appears on the material after a while due to its slow diffusion as a result of the surrounding environment. As a result of the stress applied to the material in the medium with the synergistic reaction during the corrosion that reaches the material this phenomenon occurs [49].

SCC is defined as a type of subcritical cracking of materials, and as a result of the joint and synergistic interaction between the stress applied to the material, the environment that causes corrosion, and the presence of sensitive materials, the phenomenon of stress corrosion cracking occurs [64]. When a stress is applied that is well below the permissible service fatigue and without apparent general wear behaviour, SCC causes a material failure, with severe consequences within a certain period [65]. Several research has been done over the past years to study the phenomenon of SCC, which has established the general behaviour of SCC for different materials. Despite this, there is no reliable theory that can fully explain all of the behaviour to the SCC observed under clear circumstances, so the general concept of SCC remains widely hypothesized and is under investigation. Since there are no satisfactory automated models that impede efforts to predict SCC failure, to obtain accurate results for SCC, the automated investigation is one of the most important methods used to study this phenomenon [66]. The difficulty in understanding the basic mechanisms of SCC has major aspects, which are represented in the following three aspects: the inconsistency of experimental data for some researchers, the difficulty of accurately characterizing the materials inside the cracks, the complexity of the interactions between the different corrosion reactions and the mechanical stress. If all three basic requirements are fulfilled simultaneously, then only SCC can occur, namely, sensitive materials, tensile stress, and corrosive environment, but if any or one of them changes it will have the largest impact on SCC behaviour. These include, but are not limited to: alloy composition, metallic condition, stress intensity factor or size and method of applied stress, temperature, stress, pH, composition and concentration of the corrosion solution, electrochemical

potential, with stirring or mixing [67]. A certain corrosive environment can cause SCC in one substance; it does not necessarily affect another substance.

Cracks from SCC are not visually distinguishable, but can only be observed microscopically. The shape resulting from crushing through this phenomenon can be along the boundaries of the grains (intergranular) or across the granules (transgranular), depending on its properties according to the system followed for this phenomenon. Figure 4.1 shows the types of SCC.

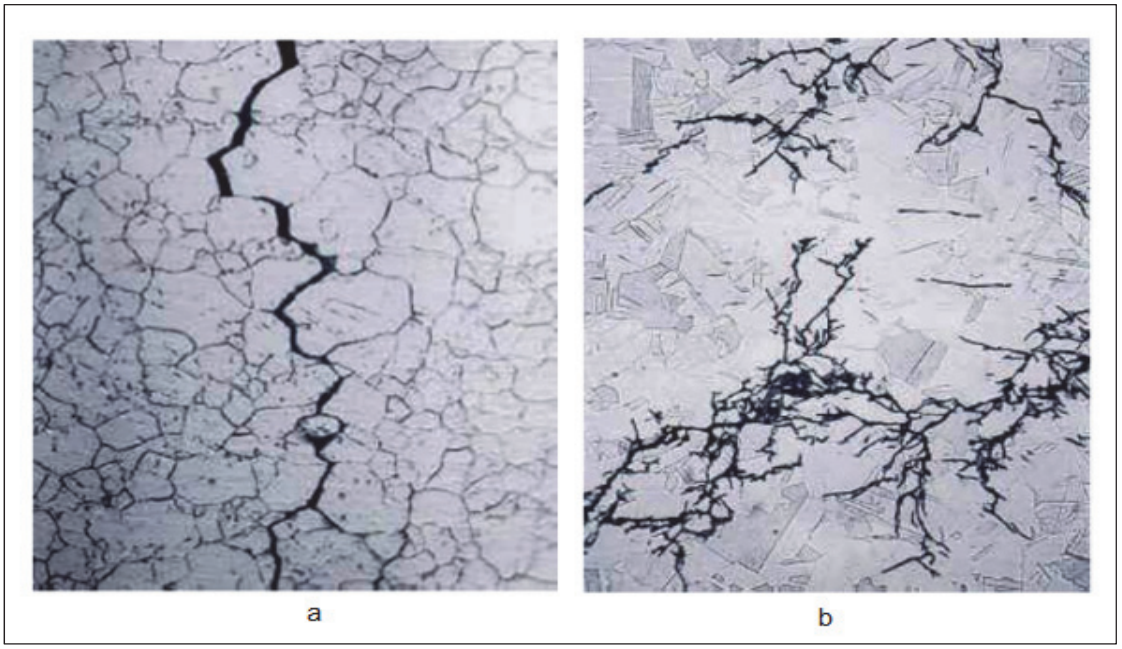

Figure 4.1. Types of SCC a) intergranular, b) transgranular.

4.2. Stress Corrosion Cracking models

There is still a severe shortage of SCC models that includes an integrated mechanism, through which it is possible to develop an explanation that includes all aspects of the SCC phenomenon, both laboratory and field. Several mechanisms have been presented, each of which has the potential to elucidate a specific aspect of SCC behaviour. These mechanisms include, for example, anodic degradation, hydrogen fractionation, and surface absorption [35].

The specific interpretation of the anode degradation mechanism can vary for researchers in this field, but the original concept of the mechanism remains unchanging. The generalized anodic degradation mechanism for cracking caused by stress corrosion in metals and their alloys, as it has been described as follows:

Localized corrosion occurs along the anodic path of sediments or regions, due to heterogeneity in sediment distribution with different electrochemical anodes in relation to the alloy matrix, often occurring at grain boundaries. Cracks occur between the granular cells, due to the rapid dissolution of the anode deposits, which leads to re-decomposition.

Tensile stress concentrates at a defect tip. The protective membranes are torn at the end of the incision, due to the enhancement of the local stress field that causes the slip strips to move. The crack growth process is then repeated by sliding off the anodic deposits as a result of rupture of their protective membranes. The stretching of the crack becomes continuous if the rate of crack tip stress is greater than the rate of recharging. The fissure may grow slowly and intermittently, if these slips do not occur, and remain thus awaiting the activity of these slips, and the chemical reaction begins again, and rupture of these membranes occurs. Figure 4.2 shows schematically of the SCC mechanism.

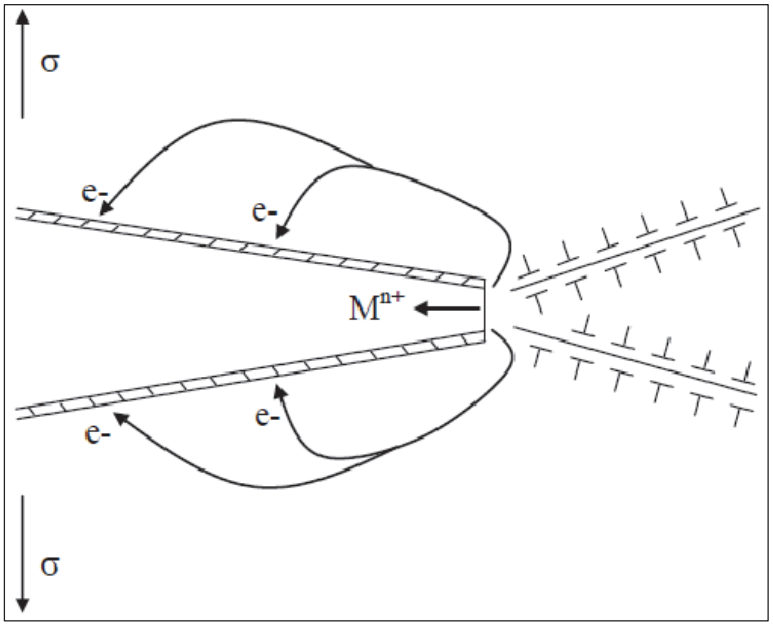

Figure 4.2: Schematic of anodic dissolution mechanism.

Depending on observations that were recorded through the relationship between SCC and hydrogen, several researchers proposed a new mechanism for SCC, and hydrogen embrittlement, [68-73]. This mechanism carefully studied the role of hydrogen in SCCs in many metals and their alloys, as it was agreed with

overwhelming evidence that the SCC mechanism involved hydrogen embrittlement. During hydrogen erosion, the cathodic reactions are generated by:

$$H_2O + e^- \rightarrow H + OH^- \quad (1)$$

and

$$H^+ + e^- \rightarrow H \quad (2)$$

In neutral as well as acidic solutions, a portion of atomic hydrogen binds together on the surface of the metal, forming molecular hydrogen. Atomic hydrogen can enter the material network, resulting in embrittlement effects through a variety of mechanisms such as hydrogen pressure, [74], surface adsorption, [75], cohesion, [76], flow of reinforced plastic, hydride, [77], Hydrogen trapping, [78]. Hydrogen can play a role in weakening the protective membranes and stimulating the chemical activity of the anode, which leads to reciprocal plastic slip. When tensile stress is effective in the process, there is a possibility that the cracked material will fail at a stress level below the yield strength level. The role that hydrogen plays in enhancing stress at the fissure tip leads to a distinction between the anode dissolution mechanism and the hydrogen fractionation mechanism. The following figure 4.3 illustrates this mechanism.

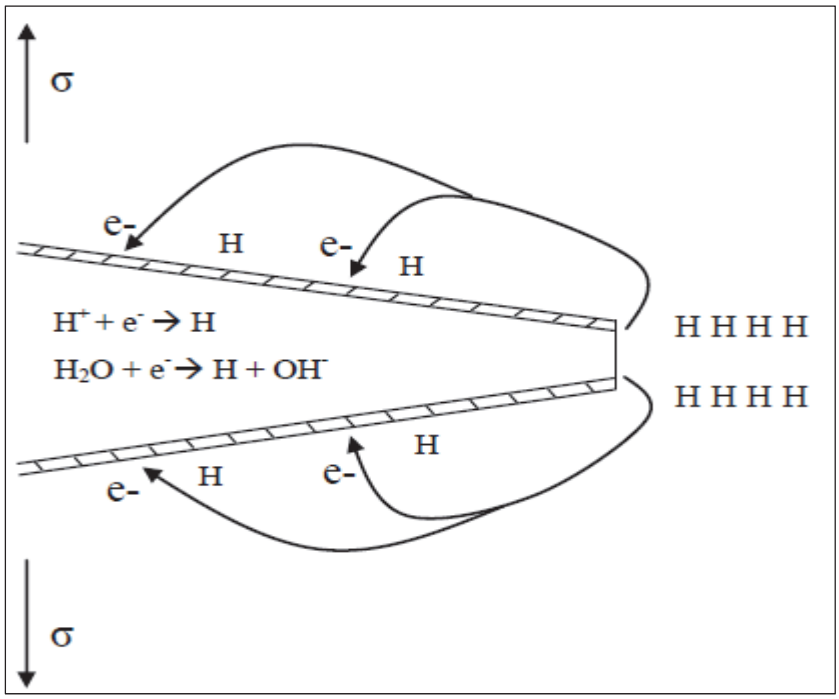

Figure 4.3: Schematic of hydrogen embrittlement mechanism.

The absorption of the surface active ingredients of the medium onto the metal surface can reduce the resistance and deformation of the solid materials. The emission of dislocation of the granules on the reinforced surface of the fissures ends promotes the fusion of the fissure-end with voids formed before the incisions. Brittle cracks or fractures are produced between the granular cells. This process, similar to hydrogen embrittlement, except that it is confined to the surface, also some other elements can produce this effect instead of hydrogen. Figure 4.4 illustrates the hydrogen embrittlement mechanism.

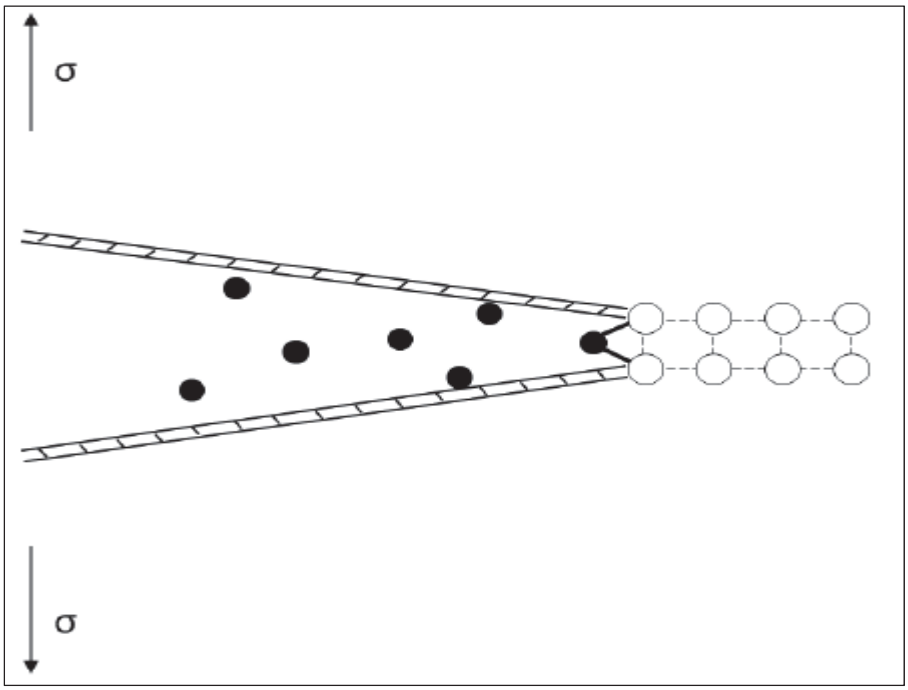

Figure 4.4: Schematic of surface adsorption mechanism.

Given the degeneration/rupture of the membrane model, the crack is unstable, but it repeatedly follows the sequences as shown in Figure.4.5: (1) the stress is mainly concentrated at the tip of the crack, (2) the exposures of the causative surface of the local rupture to the fracture of the protective film, (3) The slit growth, due to the consumption of electrons on the rest of the metal surface (cathode), as the anode decays the bare metal, (4) the presence of the oxide on the bare surface of the metal causes the slit growth at the same time, and (5) When the oxide film reaches the critical thickness, the crack stops growing (this process is known as re-passivation). The previous points represent the scope of work of the Ford-Anderson model [79].

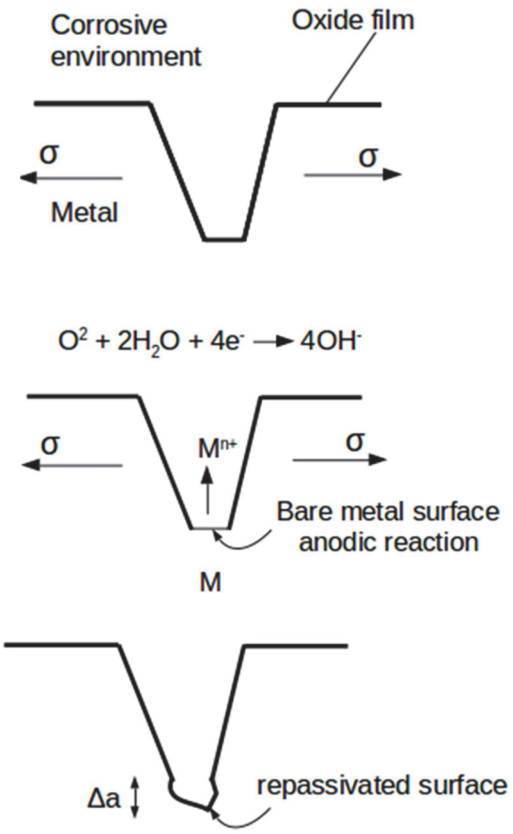

Figure 4.5. Schematic sequences of the film rupture model.

The crack ends mainly undergoes anodic dissolution of the metal, while the cathodic reaction is supported by the crack mouth. There is a possibility of corrosion at the end of the slit due to separation of the anode and cathode, this corrosion is more negative than that at the mouth opening. As an outcome, the crevice end is polarized under free corrosion conditions with aluminum oxide causing anodic dissolution of the bare metal:

$$M \rightarrow M^{+n} + ne^- \tag{3}$$

while two possible cathodic reactions may be occurring at the crack mouth:

$$O_2 + 2H_2O + 4e^- \rightarrow 4OH^- \tag{4}$$

$$2H^+ + 2e^- \rightarrow H_2 \tag{5}$$

Which one cathodic reaction occurs at the crack mouth, may be critical in determining which kind of SCC is operable. It depends on pH value, oxygen supply,

chemical conditions on the metal surface, etc. In particular, anodic reaction of the ferrous alloys can be described by:

$$3Fe + 4H_2O \rightarrow Fe_3O_4 + 8H^+ + 8e^- \quad (6)$$

Additionally, in stainless steels with nickel and chromium as a main alloying elements:

$$N_i + H_2O \rightarrow N_iO + 2H^+ + 2e^- \quad (7)$$

$$2Cr + 3H_2O \rightarrow Cr_2O_3 + 6H^+ + 6e^- \quad (8)$$

On the other side, in diluted aluminum alloys, anodic dissolution reaction is:

$$2Al + 6H_2O \rightarrow 2Al(OH)_3 + 3H_2 \quad (9)$$

Ford and Andersen proposed a theoretical model for SCC crack growth rates considering electrochemical and mechanical aspects at the crack tip which is simultaneously subjected to corrosive environment and tensile loading. The fundamental mathematical equation for active path corrosion model is Faraday's law [79].

$$\dot{a} = \frac{da}{dt} = \frac{M}{z\rho F} Q_f \frac{\dot{\varepsilon_c}}{\varepsilon_f} = \frac{M}{z\rho F} \frac{i}{1-m} \left(\frac{t_o}{\varepsilon_f}\right)^m \dot{\varepsilon_c}^m \quad (10)$$

where M is molar mass and z number of valence electrons, F is Faraday's constant, Q_f is the electric charge between two successive film rupture events, dotted ε_c is the strain rate at the crack tip and ε_f is the rupture ductility of the passive film, i is anodic current density immediately after the passive film rupture and m is re-passivation exponent. Equation's variable was grouped into materials constants (M, z, ρ, F), electrochemical (i and m) and mechanical (dotted ε_c) variables. This is the mathematical framework of the model.

4.3 Electrochemical Aspects of Stress Corrosion Cracking

Although SCC occurs without apparent general corrosion, the corrosion reactions within the initiated crack tip area, between the local solution and oxide films or bare metal, still plays an important role in crack initiation and propagation.

Corrosion, by definition, is the consequence of the chemical reaction between a metal or metal alloy and its environment [34]. During a corrosion reaction, metal or

metal alloy is being oxidized to metal ions and dissolved into solution, a process called the anodic reaction. Meanwhile, other species, such as H+, receive the extra electrons generated by the anodic reaction and are being reduced to hydrogen gas, through a process known as a cathodic reaction. The pioneering work on electrolysis by Michael Faraday established the relationship between the current exchanged and mass of materials involved in chemical reaction during the corrosion process. Starting with his work and electrochemical principles he established, Butler and Volmer added concepts from thermodynamics to derive one of the most fundamental relationships in electrochemistry [37].

The process that alters the corrosion current by changing the applied over-potential is call polarization and the plot of potential *vs.* current is called the polarization curve. Some types of metals and alloys, when exposed to a certain corrosive environment

While maintained at a specific range of potential, a layer of the oxide film will be formed, which blocks the corrosion reaction and thus decreases the corrosion current. This phenomenon is called passivation [36]. Figure 4.6 illustrates a typical polarization curve for material with passivation behaviors. The two grey areas indicate zones of susceptibility to stress corrosion cracking. As a result, the electrochemical potential strongly affects general corrosion, as well as SCC [37].

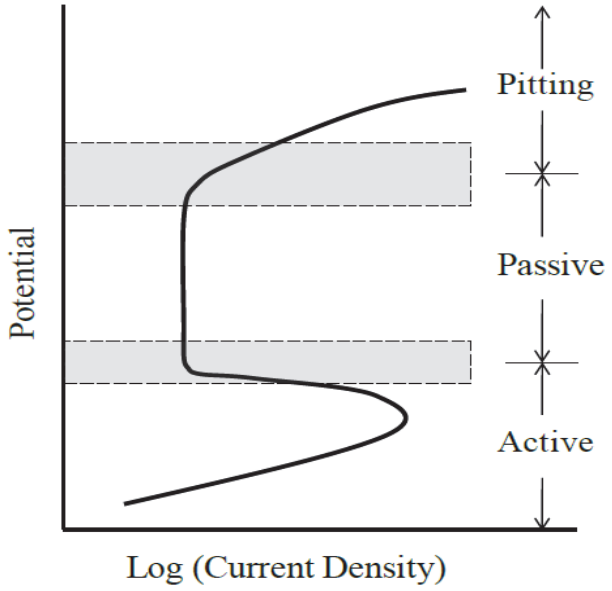

Figure 4.6. Typical polarization curve of metal with passivation behavior

The experimental data of anodic current can be represented by [81]

$$i_a = \frac{i_{corr}\exp[\frac{2.3}{\beta_a}(E-E_{corr})]}{1+\frac{i_{corr}\exp[\frac{2.3}{\beta_a}(E-E_{corr})]}{i_{rp}\exp[\frac{2.3}{\beta_{rp}}(E-E_{rp})]}} \quad (11)$$

where E_{corr} is corrosion potential, i_{corr} corrosion current density on bare surface, E_{rp} and i_{rp} are their equivalents on re-passivating surface, β_a is Tafel slopes for anodic reactions on bare surface, β_{rp} its equivalent on re-passivating surface. Ccorrosion current density. i_{rp} is the function of pH as defined by Freundlich adsorption equation [82]:

$$\log i_{rp} = logk - npH \quad (12)$$

where k is a constant, and n is related to the valency of the cations: n = 0.5, 0.33, and 0.25 for monovalent, divalent and trivalent ions. The cathodic current density is

$$i_c = \frac{i_{corr}[\frac{2.3}{\beta_c}(E-E_{corr})]}{1+\frac{i_{corr}[\frac{2.3}{\beta_c}(E-E_{corr})]}{\frac{nFD_Hc_H}{\delta}}} \quad (13)$$

where n is charge number of cell reaction and δ is diffusion layer thickness, D_H and c_H are diffusion coefficient and concentration of hydrogen, respectively. Parameters to construct polarization curve are shown in Table 4.1, and calculated curves are shown in Figure 4.7.

Table 4.1. Parameters for polarization curves [21].

E_{corr} (V)	i_{corr} (Am^{-2})	i_{rp}(Am^{-2})	β_a(V dec^{-1})	β_c(V dec^{-1})	β_{rp}(V dec^{-1})
-0.86	1 x 10^{-2}	1 x $10^{-3-\ n\ x\ pH}$	0.12	0.72	-0.28

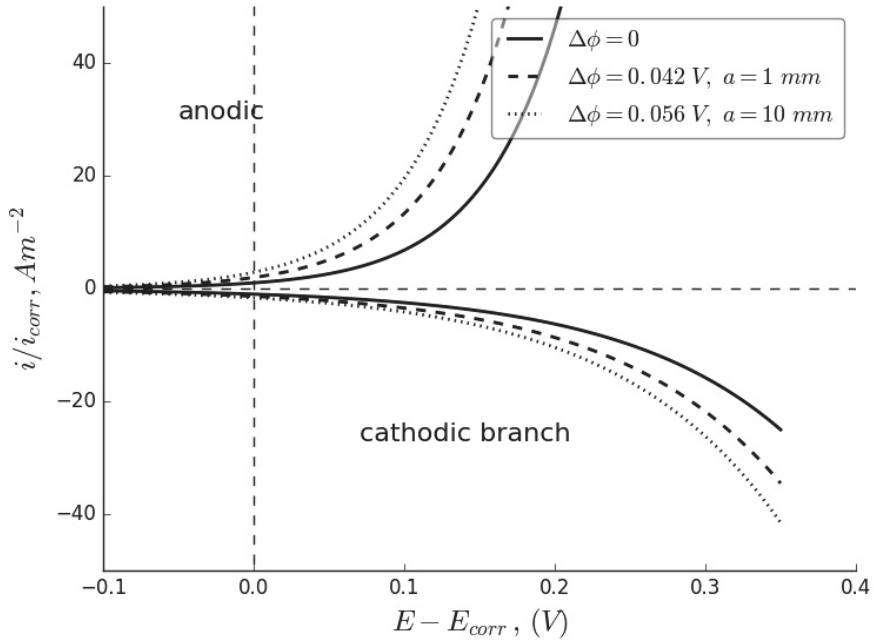

Figure 4.7. Polarization curves obtained from Equations (11) and (13).

4.4 Mechanical Aspect of Stress Corrosion Cracking

There are four necessary factors for SCC:

(i) A material is subordinated to SCC.

(ii) Corrosive environment.

(iii) Mechanical load.

(iv) Time.

For SCC to occur, mechanical loading is an important aspect, it is considered one of the basic requirements for this phenomenon. SCC is a concern of many engineering constructions, including pipelines, pressure vessels and turbines. The SCC is a brittle, or quasi-brittle failure, with virtually no loss of material and visible corrosion. It is generally described as a "branched river" with a main crack and a secondary or tertiary crack with multiple branches. Cracks occur below the yield strength of the material and may be inter-granulated or trans-granulated. The initiation and propagation of SCC is a complex process of degradation, depending on the microstructural, mechanical and environmental parameters [83].

SCC mechanisms can be divided into anodic and cathodic. The first one is the controlled anodic dissolution of metal and the second one is the hydrogen uptake that causes the hydrogen embryo and is called "hydrogen-induced cracking". A

representative example of the mechanism of anodic stainless steel, while cathodic reactions are high- strength steels[1]. Anodizing mechanism, both models are widely accepted "sliding model" and "tear film model". In the film rupture model, a passive surface film, usually of oxide, protects the base metal from a corrosive environment. The applied loading causes the film to break the exposure of the base metal to corrosion. The rupture film will occur preferentially in the strain concentration regions, such as small cracks or defects. The growth rate of the crack depends on the competitive cracking and re-passivation sequences in the oxide film. Three basic loading modes are illustrated in Figure 4.8. As a result, when conducting SCC tests, both the loading mode and stress intensity must be prescribed in order to ensure accurate and reliable experimentation.

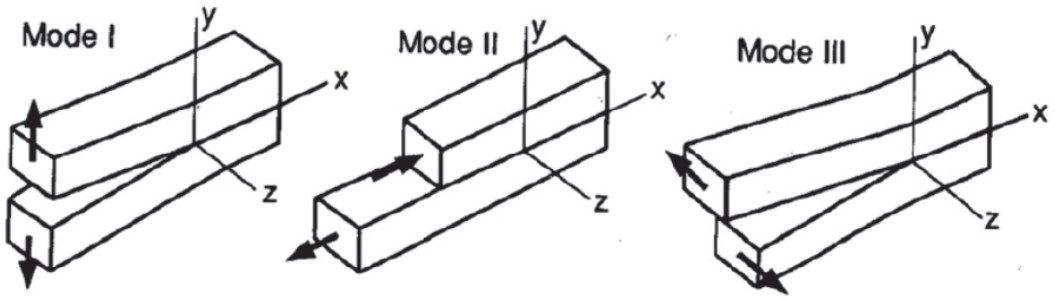

Figure 4.8.: Schematic of three different loading modes.

The crack tip strain rate (CTSR) can't be experimentally measured, but has to be derived from theoretically proposed strain field ahead the crack. Total CTSR can be separated into the two components - stationary (or, perhaps, quasi-stationary) and advancing crack, i.e.:

$$\frac{d\varepsilon(r,t)}{dt} = \left(\frac{d\varepsilon}{dt}\right)_K - \dot{a}\left(\frac{d\varepsilon}{dr}\right)_r \tag{14}$$

The physical meaning of the above equation is as follows: the first term is the strain rate at distance, (r), from the crack tip, and the second term is the strain rate generated due to crack advances with the velocity da/dt trough the strain field. Hutchinson, Rice and Rosenberg developed a strain field distribution (HRR-field) for a stationary crack tip [84, 85]:

$$\varepsilon = \frac{\sigma_y}{E}\left(\frac{\alpha}{r}\frac{K^2}{{\sigma_y}^2}\right)^{\frac{n}{n+1}} \tag{15}$$

where K denotes the Stress Intensity Factor (SIF), r is characteristic distance in front of stationary crack, and n is strain hardening exponent from the Ramberg-Osgood strain-stress equation:

$$\varepsilon = \frac{\sigma}{E} + \alpha \frac{\sigma}{E} \left(\frac{\sigma}{\sigma_o}\right)^n \tag{16}$$

Graphical interpretation of the two equations are shown in Figures 4.9 and 4.10.

Applying partial derivation to Eq. 15 yields the strain rate:

$$\left(\frac{d\varepsilon}{dt}\right)_K = \frac{2n}{n+1} \frac{\sigma_y}{E} \left(\frac{\alpha}{r} \frac{K^2}{\sigma_y^2}\right)^{\frac{n}{n+1}} \frac{\dot{K}}{K} \tag{17}$$

where K-dot denotes time derivative dK/dt.

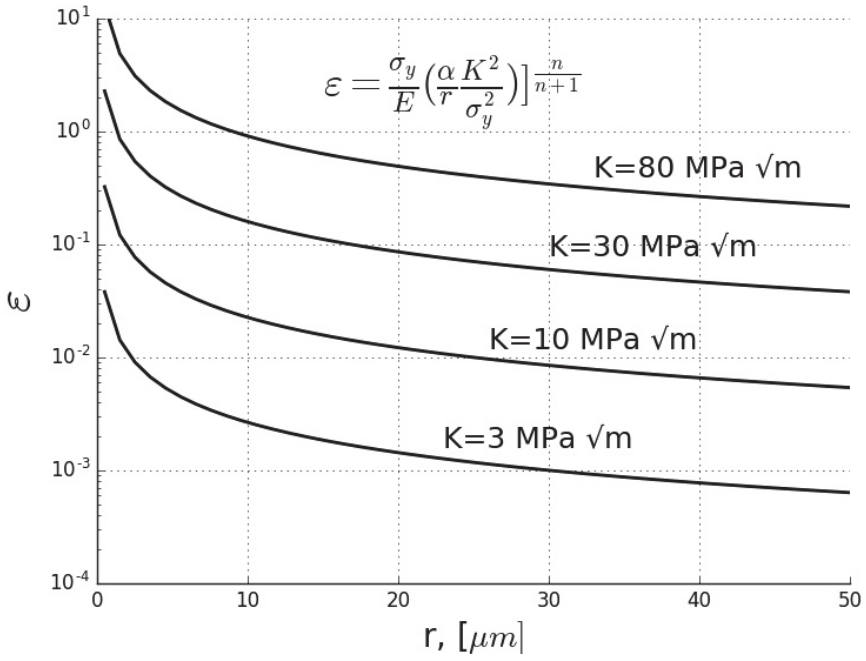

Fig. 4.9. HRR strain field in front of the crack tip distance r.

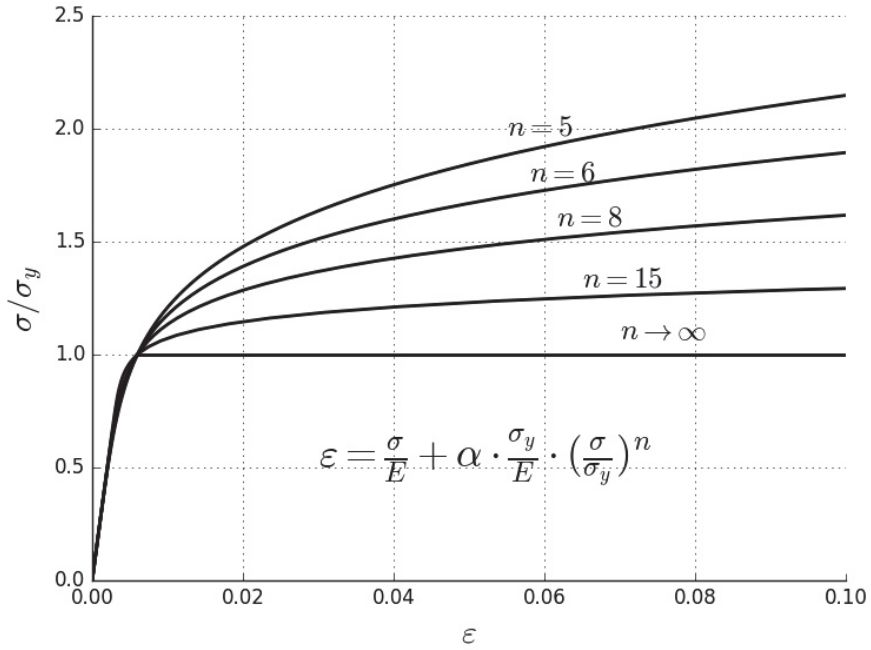

Fig. 4.10. Ramberg-Osgood equation.

Similar to the HRR-field, for the 'crack advance' strain field was proposed, [86]:

$$\varepsilon = \beta \frac{\sigma_y}{E} [\ln(\frac{1}{3\pi r} \frac{K^2}{\sigma_y^2})]^{\frac{2n}{n-1}} \tag{18}$$

as shown in Figure 4.11, while the strain rate component for a moving crack is time derivative of the above equation

$$-\dot{a}(\frac{d\varepsilon}{dt})_r = \frac{n}{n-1} \beta \frac{\sigma_y}{E} \frac{\dot{a}}{r} [\ln(\frac{1}{3\pi r} \frac{K^2}{\sigma_y^2})]^{\frac{n+1}{n-1}} \tag{19}$$

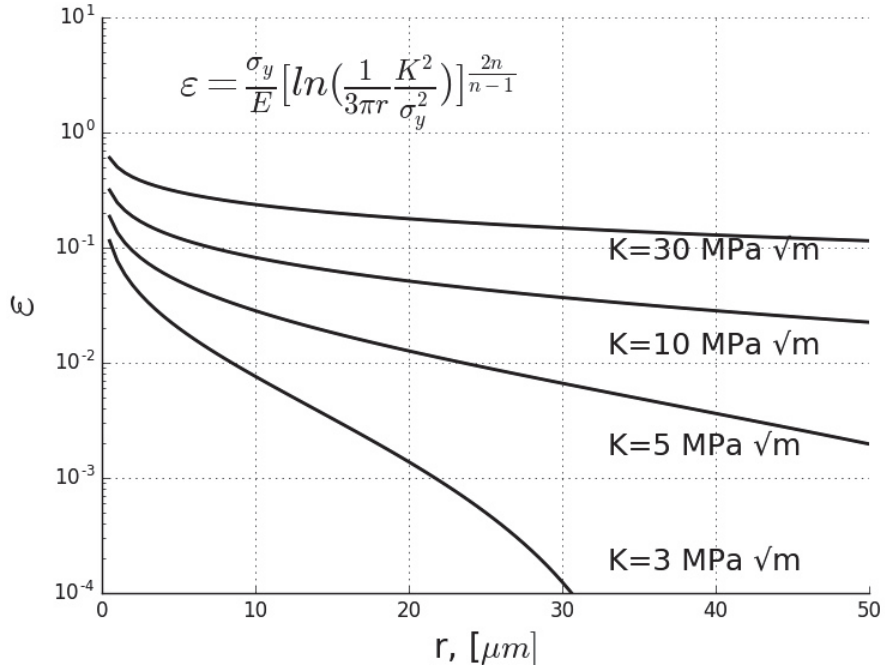

Fig. 4.11. Strain field ahead the moving crack tip.

Total strain rate (stationary plus moving crack) is sum of Eq.15 and 17.

$$\dot{\varepsilon}_c = \frac{2n}{n+1}\frac{\sigma_y}{E}\left(\frac{\alpha}{r}\frac{K^2}{\sigma_y^2}\right)^{\frac{n}{n+1}}\frac{\dot{K}}{K} + \frac{n}{n-1}\beta\frac{\sigma_y}{E}\frac{\dot{a}}{r}\left[\ln\left(\frac{1}{3\pi r}\frac{K^2}{\sigma_y^2}\right)\right]^{\frac{n+1}{n-1}} \tag{20}$$

where $\dot{K} = dK/dt$ is time derivative of SIF. While some fracture mechanics experiments can be conducted to establish time-dependence of K-factor, it is supposed to be more convenient to apply 'chain rule':

$$\frac{dK}{dt} = \frac{dK}{da}\frac{da}{dt} = \frac{dK}{da}\dot{a} \tag{21}$$

and, getting back, the final equation for crack growth rate is formulated:

$$\dot{a} = \frac{M}{z\rho F}\frac{i}{1-m}\left(\frac{t_o}{\varepsilon_f}\right)^m\left[\frac{2n}{n+1}\frac{\sigma_y}{E}\left(\frac{\alpha}{r}\frac{K^2}{\sigma_y^2}\right)^{\frac{n}{n+1}}\frac{dK}{da}\frac{\dot{a}}{K} + \frac{n}{n-1}\beta\frac{\sigma_y}{E}\frac{\dot{a}}{r}\left[\ln\left(\frac{1}{3\pi r}\frac{K^2}{\sigma_y^2}\right)\right]^{\frac{n+1}{n-1}}\right]^m \tag{22}$$

Both sides of above equation include $\dot{a}$, but it can be easily solved either in analytical or in finite elements formulation. Parameters used in this work are shown in Table 4.2.

Table 4.2. Parameters used in calculation.

M_{Fe} (kg/mol)	atomic mass of iron	55.8 x 10^{-3}
M_{Al} (kg/mol)	atomic mass of aluminium	26.9 x 10^{-3}
F (C/mol)	Faraday's constant	96485
z	number of exchanged electrons	2
ρ (kg/m^3)	density	7.8 x 10^6
t_o (sec.)	incubation period of repassivation	1 x 10^{-2}
ε_f	fracture ductility of passive film	1 x 10^{-3}
m	exponent of repassivation kinetics	2/3
σ_y (MPa)	yield strength	450
E (GPa)	Young modulus	200
ββ	Ryce parameter	5.08
n	Ramberg-Osgood exponent	6 -10
α	material constant in HRR-field	0.2 x 10^{-2}

Characteristic distance *r* was calculated from the plastic zone size ahead the crack [26]

$$r = \frac{0.305\lambda\frac{K^2}{\sigma_y{}^2}}{\lambda\frac{K^2}{\sigma_y{}^2}+1.16} \tag{21}$$

However, K and dK/dt are not independent variables, they are the function of applied stress σ, crack size *a* and geometry-dependent factor. Figure 4.12(a,b) shows two crack opening modes, simple tension (a) and pure opening mode (b). Analytical solution for both modes are almost the same, with only difference in geometry dependent correction, f(a/b),

$$K_I = \sigma\sqrt{\pi a}\sqrt{\frac{2b}{\pi a}\tan\frac{\pi a}{2b}}f(\frac{a}{b}) \tag{22}$$

details of which can be find elsewhere [27, 28]. Before we proceed to finite elements formulation, it might be of some interest to explain mutual relation between K and dK/da, which is shown in Figure 4.13.

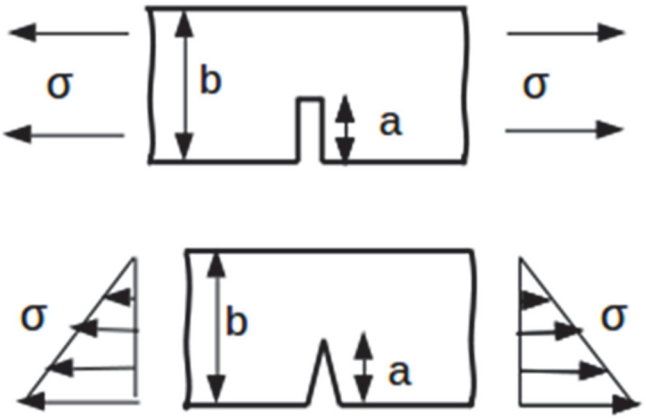

Fig. 4.12. Two different types of loading - a) tensile, b) compact tension (CT).

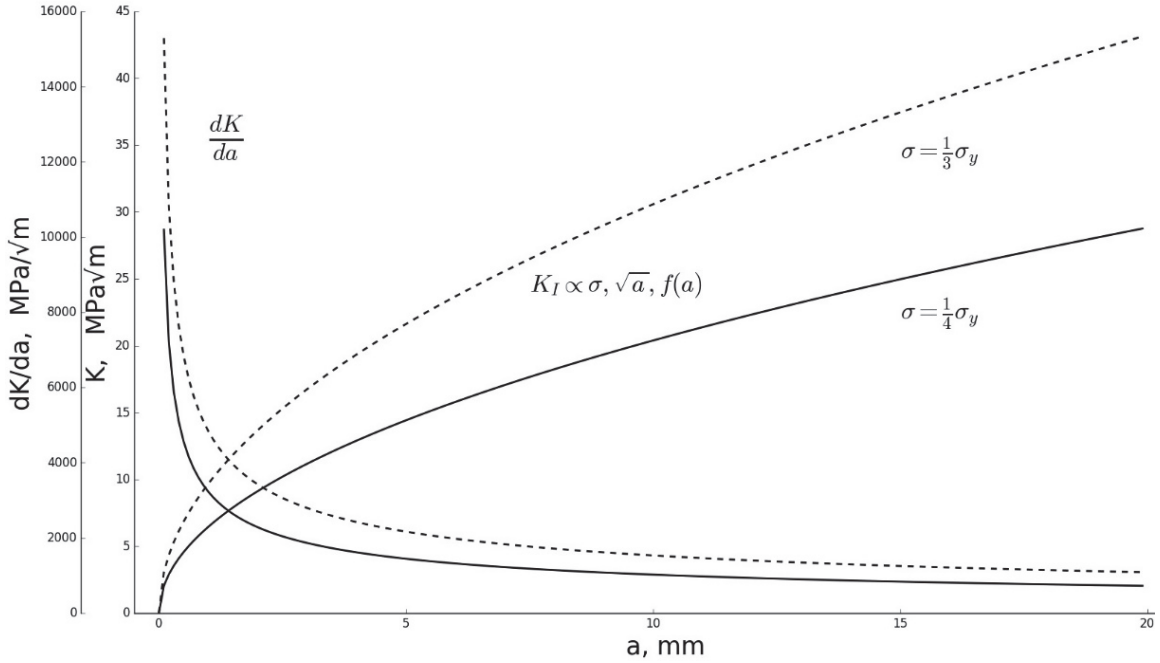

Fig. 4.13. K-function and dK/dt vs. crack size.

Assuming monotonously growing crack, with constant applied stress, K is increasing power law function (left y-axis) while, on the other side, dK/da behaves in quite opposite manner (right y-axis). Physical meaning of such behaviour is as follows: small stationary cracks (or small K-values) are dominated by rather larger values of $\frac{dK}{da}\frac{1}{K}$. On the other side, large moving cracks are dominated in a K^2 manner. However, in most general way, dK/da can be zero (when K=const. tests) or even negative (for decreasing K values).

CHAPTER 5 - Extended Finite Element Method (XFEM)

5.1 Introduction

Finite Element Method (FEM) has an important position in engineering since it can deal efficiently with challenging geometric forms. It is one of very few method to tackle non-smooth fracture tip stress and strain fields through a locally developed mesh, enabling compatibility with fracture mechanics singularities.

Nevertheless, if applied to crack propagation, FEM has to overcome problem of re-meshing at each propagation step. Numerous methods have been suggested without real success before the extended finite element method (XFEM) has been developed, [91, 92], after 1991, as shown in Figure 5.1.

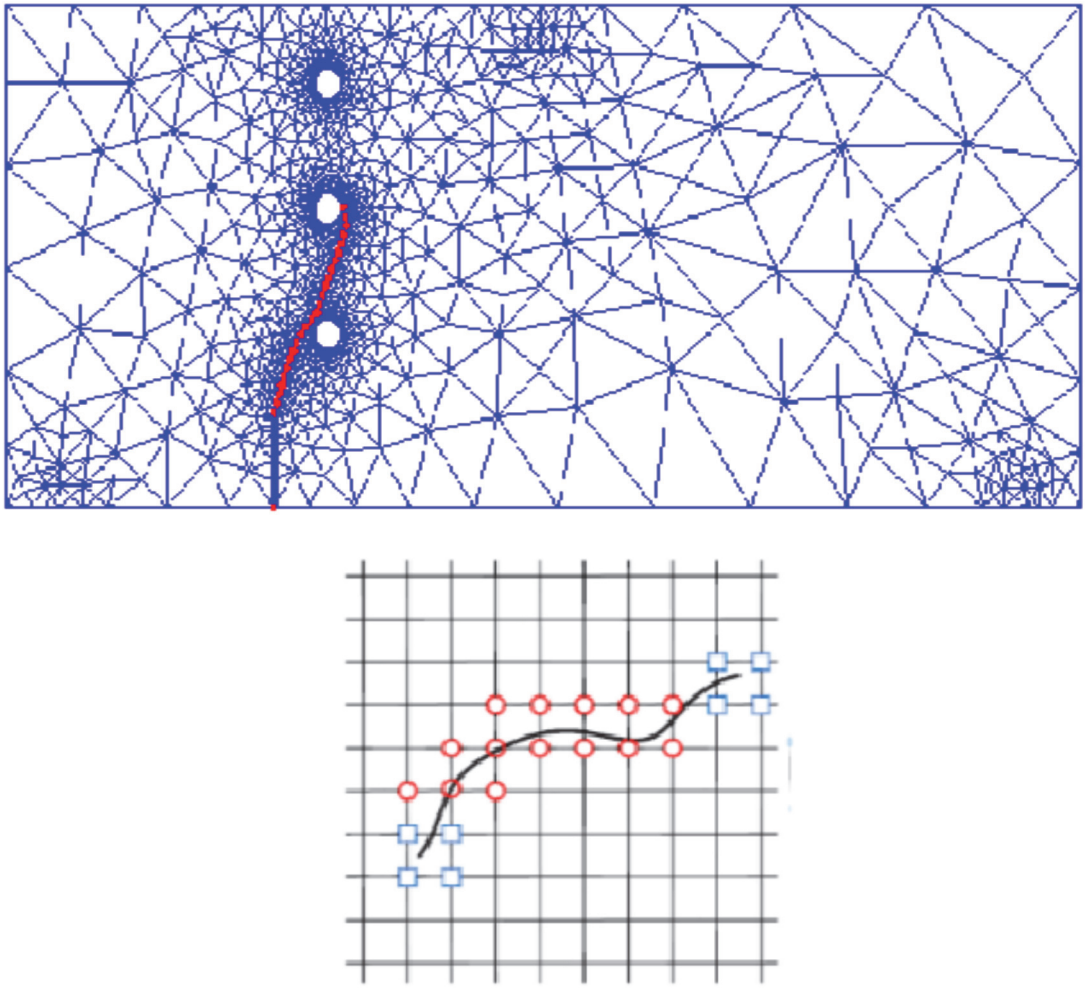

Figure 5.1 Comparison of 2D solid fracture analysis model using enriched x-FEM (upper) and extended x-FEM (lower)

The essence of xFEM are additional degrees of freedom in the nodes of elements where crack cuts through. The mesh is independent of crack propagation, so there is no need for re-meshing. This provides correctness in the calculation of stress and strain concentration.

5.2 Basics of extended finite element method

Modelling of crack propagation by classical FEM is practically impossible because it requires countless re-meshing steps. The xFEM provides possibility to model arbitrary shaped cracks, [93], because it uses additional functions to model singularity, thus avoiding re-meshing.

There are two types of these, so-called enhancement functions:

• Heaviside's function, which is discontinuous and introduces the special field, moving to the sides of the crack,

• Near Tip (NT) functions, representing the set of linear elastic asymptotic scroll function, defining displacements at the crack tip.

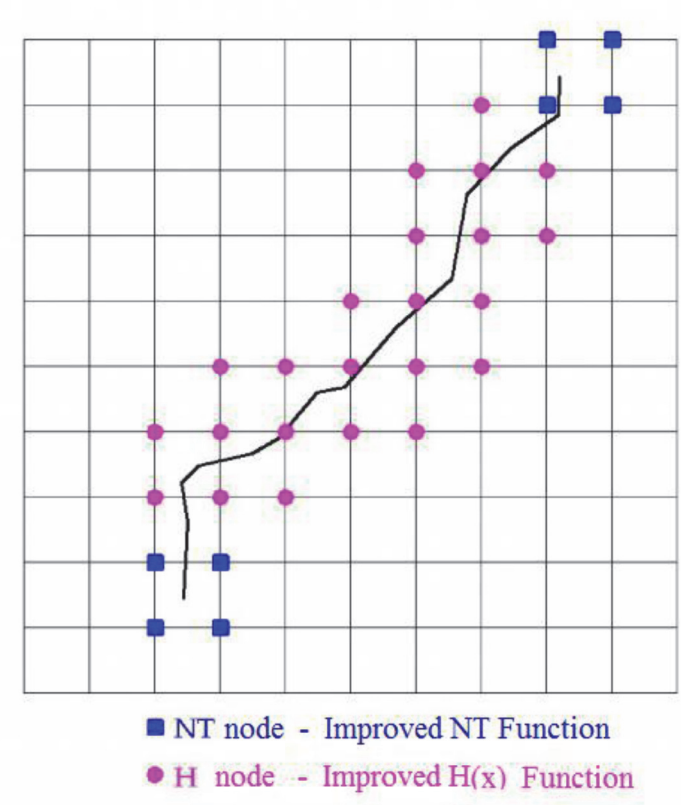

Figure 5.2 Nodes NT and H(x) improved function

Thereby two node types are involved, H node with 4 degrees of freedom (DoF), and NT with 10 DoF, Figure 5.2.

5.2.1 Defining of the displacement field XFEM

Nodes enriched in the two directions with 4 crack tip functions F_α(x) are defined as follows, [92]:

$$[F_\alpha(r,\theta), \alpha = 1-4\,] = \left[\sqrt{r}\,\sin\frac{\theta}{2}, \sqrt{r}\,\cos\frac{\theta}{2}, \sqrt{r}\,\sin\frac{\theta}{2}\sin\theta, \sqrt{r}\,\cos\frac{\theta}{2}\,\sin\theta\right] \quad .... \quad 5\text{-}1$$

The displacements now take the following form [1]:

$$u_{x\,FEM}(x) = \sum_{i\epsilon I} N_i(x)u_i + \sum_{i\epsilon J} N_i(x)H(x)a_j + \sum_{i\epsilon K}\left[N_i(x)\sum_{\alpha=1}^{4} F_\alpha(x)b_k^\alpha\right] \quad .... \quad 5\text{-}2$$

where N_i(x) is shape function and U_i is displacement vector. Hence, the additional DOFsa_{j}, $\mathfrak{b}_{\mathrm{K}}^{a}$ in 5-2 are only added to the enriched nodes.

5.2.2 The general form of the extended finite element method

Genaral equation can be now set for global stiffness matrix, displament and force vectors:

$$K.q = f \quad \ldots\ldots\ldots\ldots\ldots\ldots\ldots\ldots \quad 5\text{-}3$$

Global stiffness matrix is now:

$$K = \begin{bmatrix} K_{uu} & K_{ua} \\ K_{ua}^T & K_{aa} \end{bmatrix} \quad \ldots\ldots\ldots\ldots \quad 5\text{-}4$$

where:

K_{uu} - Classical FE stiffness matrix

K_{aa} - "improved" FE stiffness matrix

K_{ua} - coupling between classical and "improved" FE stiffness matrix.

Stiffness matrix in general can be calculated as follows:

$$K_s = \int_{\Omega^h} B_\alpha^T\, C\, B_\beta\, d\Omega \qquad \alpha,\beta = u,a \qquad \ldots\ldots\ldots\ldots \qquad 5\text{-}5$$

where C is constitutive matrix, B_u classical and B_a improved shape functions matrix, respectively:

$$B_u = \begin{bmatrix} N_{i,x} & 0 & 0 \\ 0 & N_{i,y} & 0 \\ 0 & 0 & N_{i,z} \\ 0 & N_{i,z} & N_{i,y} \\ N_{i,z} & 0 & N_{i,x} \\ N_{i,y} & N_{i,x} & 0 \end{bmatrix} \quad \ldots\ldots\ldots\ldots\ldots\ldots \quad 5\text{-}6$$

$$B_a = \begin{bmatrix} (N_i \Psi_i^\alpha)_{,x} & 0 & 0 \\ 0 & (N_i \Psi_i^\alpha)_{,y} & 0 \\ 0 & 0 & (N_i \Psi_i^\alpha)_{,z} \\ 0 & (N_i \Psi_i^\alpha)_{,z} & (N_i \Psi_i^\alpha)_{,y} \\ (N_i \Psi_i^\alpha)_{,z} & 0 & N_{i,x} \\ (N_i \Psi_i^\alpha)_{,y} & (N_i \Psi_i^\alpha)_{,x} & 0 \end{bmatrix} \quad \ldots\ldots\ldots\ldots\ldots\ldots\ldots\ldots \quad 5\text{-}7$$

$$N_{i,k} = \frac{\partial (N_i(x))}{\partial x_k}$$

$$(N_i \Psi_i^\alpha)_{,k} = \frac{\partial (N_i(x) \Psi_i^\alpha)}{\partial x_k}$$

$(N_i \Psi_i^\alpha)_{,k}$ — Can be calculated using:

$$\frac{\partial (N_i(x) \Psi_i^\alpha)}{\partial x_k} = \frac{\partial (N_i(x))}{\partial x_k} \Psi_i^\alpha(x) + N_i(x) \frac{\partial (\Psi_i^\alpha(x))}{\partial x_k} \quad \ldots\ldots\ldots\ldots\ldots\ldots \quad 5\text{-}8$$

q and f matrixes can be expressed as follows:

$$q^T = (u \quad a)^T \quad \ldots\ldots\ldots\ldots\ldots\ldots \quad 5\text{-}9$$

$$f^T = (f_u^T \quad f_a^T) \quad \ldots\ldots\ldots\ldots\ldots\ldots \quad 5\text{-}10$$

Where f_u and f_α are classical applied force and improved displacement vectors.

It is now simple task to define strain and stress vectors:

$$\varepsilon = [\ B_u \quad B_a](u \quad a)^T \quad \ldots\ldots\ldots\ldots\ldots\ldots \quad 5\text{-}11$$

$$\sigma = C \,.\, \varepsilon \quad \ldots\ldots\ldots\ldots\ldots\ldots\ldots\ldots\ldots\ldots\ldots\ldots \quad 5\text{-}12$$

5.3 XFEM Implementation in Code-Aster

XFEM is included in the multi-purpose commercial FEM program as there are some of the huge advancements that XFEM has to offer. The lack of commercial programming evidence for practicing a method like XFEM is due to the fact that it

was created and exploited in the late last century. Code-Aster is a finite element analysis engine, due to its convenient data files, it will produce a batch of result files. The Code- Aster with Morfeo programs are highly capable programs among other programs [94]. The first components of X-FEM are available as of Code-Aster version 7, and with its development, version 8 was obtained that allows for mechanical calculation with two- or three-dimensional linear flexibility, with boundary conditions far from crack, represented by levels groups. It is possible to consider contact on crack lips. Version 9 featured many advanced features like (multiplicity of cracking, plasticity ...). In version 10 powerful automated publishing algorithms are suggested. As for version 11, the X-FEM method has been extended to a heat linear actuator in order to take into account the problem of crack heat the initial specific mechanical problem [95].

Finite element X-FEM can be produced from 3D, C_PLAN, D_PLAN or AXIS models. Oppose, X-FEM elements (* _SI forms) are not available. The X-FEM method theoretically makes it possible to represent a strong break (cracks or interface) or a low cut (an interface between suspended binary materials). It all depends on the fertilization function being introduced into the displacement or temperature approximation.

In Code-Aster only a strong discontinuity is possible (field of displacements, constraints, or of temperature discontinuous).

5.3.1 Modeling Approach

To model moving fracture in Abaqus, arrangement with phantom node technique, cohesive segment method and VCCT technique are used [98]. It is assumed that a crack extension of $\Delta\alpha$ from $\alpha + \Delta\alpha$ (node i) to $\alpha + 2\Delta\alpha$ node (k) does not significantly alter the stresses and strains at the crack tip, Fig. 5.3. For a crack modeled with two-dimensional, 4-noded elements, the work $\Delta \mathrm{E}$ can be calculated as

$$\Delta E = \frac{1}{2}[X_i \Delta u_i + Z_i \Delta w_i] \qquad \ldots\ldots\ldots\ldots\ldots\ldots \qquad 5\text{-}13$$

where X_i and Z_i are opening and shear forces, respectively, at node i and Δu_i and Δw_i, are opening and shear displacements at node j. The expression of the work w based on this two-steps Virtual Crack Closure Technique is given by:

$$W = \frac{1}{2}\left(\int_0^{\Delta a} \sigma_{yy}^{(a)}(x)\,\delta u_y^{(b)}(x)\,dx + \int_0^{\Delta a} \sigma_{yx}^{(a)}(x)\,\delta u_x^{(b)}(x)\,dx + \int_0^{\Delta a} \sigma_{yz}^{(a)}(x)\,\delta u_z^{(b)}(x)\,dx \right) \qquad 5\text{-}14$$

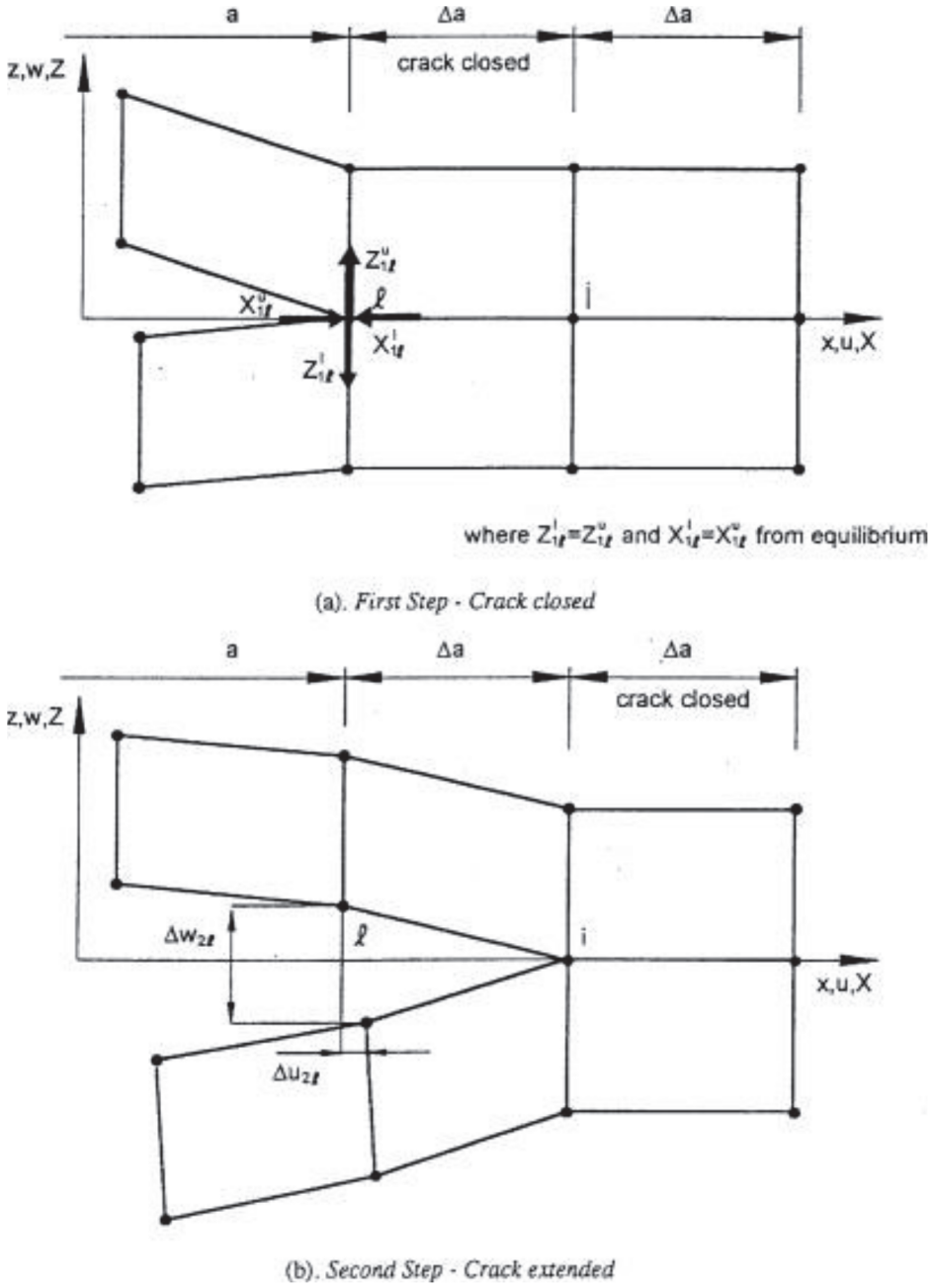

Figure 5.3 Crack closure two-step method

Another approach is the one step Virtual Crack Closure Technique, where the the work W is defined as:

$$W = \frac{1}{2}\left(\int_0^{\Delta a} \sigma_{yy}^{(a)}(x)\,\delta u_y^{(b)}(x-\Delta a)\,dx + \int_0^{\Delta a} \sigma_{yx}^{(a)}(x)\,\delta u_x^{(b)}(x-\Delta a)\,dx + \int_0^{\Delta a} \sigma_{yz}^{(a)}(x)\,\delta u_z^{(b)}(x-\Delta a)\,dx \right) \qquad 5\text{-}15$$

Finally, the Energy Release Rate is defined as:

$$G = \lim_{\Delta a \to 0} \frac{W}{\Delta a} \qquad 5\text{-}16$$

5.4. Crack Growth Criteria in stress corrosion cracking

For a reliable test, different types of specimens are used to evaluate fracture toughness [98]. One of the most used criteria is the power law defined as follows:

$$\left(\frac{G_I}{G_{IC}}\right)^{\alpha} + \left(\frac{G_{II}}{G_{IIC}}\right)^{\alpha\beta} + \left(\frac{G_{III}}{G_{IIIC}}\right)^{\gamma} = 1 \qquad 5\text{-}17$$

Another option is the B-K criterion [100]:

$$\frac{G_T}{G_{IC} + \left[(G_{IIC} - G_{IC})\frac{G_{II}}{G_T} + (G_{IIIC} - G_{IC})\frac{G_{III}}{G_T}\left(\frac{G_{II} + G_{III}}{G_T}\right)^{\eta-1}\right]} = 1 \qquad 5\text{-}18$$

5.4.1 Evaluation of the stress intensity factors

Conversion of the contour collaboration energy integral is defined as:

$$I = \int_{\Gamma} (\sigma_{ik}\, \varepsilon_{ik}^{aux} \delta_{1j} - \sigma_{ij} u_{i,1}^{aux} - \sigma_{ij}^{aux} u_{i,1}) n_j \, d\Gamma \qquad 5\text{-}19$$

where $u_{i,1}^{aux}, \varepsilon_{ik}^{aux}, \sigma_{ij}^{akx}$ are auxiliary displacement, strain, and stress fields respectively. The domain form of this integral is:

$$I = \int_{A} (\sigma_{ik}\, \varepsilon_{ik}^{aux} \delta_{1j} - \sigma_{ij} u_{i,1}^{aux} - \sigma_{ij}^{aux} u_{i,1}) q_j \, dA \qquad 5\text{-}20$$

5.4.2 Difficulties with the XFEM

Although XFEM is a robust method, there are few associated difficulties:

• Singular and discontinuous integrands

• Blending the different partitions of unity

• Poor convergence rate

• Stress intensity factor computation

• ILL-conditioning

• Additional unknowns

CHAPTER 6 - RESULTS

6.1. Finite elements formulation

Geometry of tensile test specimen is shown in Figure 6.1. In order to trim the size of the file and processing time, the 'heads' of the specimen were shortened. It was supposed that it would not affect stress concentration at the crack tip. Structured grid was generated on the one half of specimen, Figure 6.2, with fine mesh in the mid-section of the specimen. Detailed mesh refinement can be seen on Figure 6.3. Extended Finite Elements Method (X-FEM) was used with provision of Fracture Mechanics module in Code-Aster. The crack itself was not drawn but it was defined as a simple function within the Code-Aster environment. A series of calculations were performed with crack size, as a lateral notch, a=3 -10mm. Applies stress was σ=1/3 of the yield stress (σ_y= 450 MPa). External Python procedure was written to enhance some automation. Stored K and crack size values were used to estimate dK/da

$$\frac{dK}{da} = \frac{\Delta K}{\Delta a} \tag{23}$$

The result of XFEM calculation is shown in Figure 6.4 and zoomed crack region in Figure 6.5. It was a test, benchmark case, since the calculated values should be, and they were, close to the analytical solution of Equation 20.

Another set of computations, based on elsto-plastic fracture mechanics, were performed on the compact tension (CT) specimen, Figure 6.6. The mesh and detailed mesh refinement are shown in Figures 6.7 and 6.8. Boundary condition was set as a displacement in y-direction, Δy=1-5 mm. Plastic behaviour of the material was governed by Ramberg-Osgood equation, n=8 case in the Equation 14 and Figure 6.4. Simo-Miehe algorithm was used, which is supposed to be accurate up to 5% of plastic deformation. Calculated K and dK/da values were used for crack tip

strain rate evaluation. Von-Mises output of XFEM calculations are shown in Figures 6.9 and 6.10. This particular case was for a crack size a=5mm, and y-axis displacement Δy=5 mm.

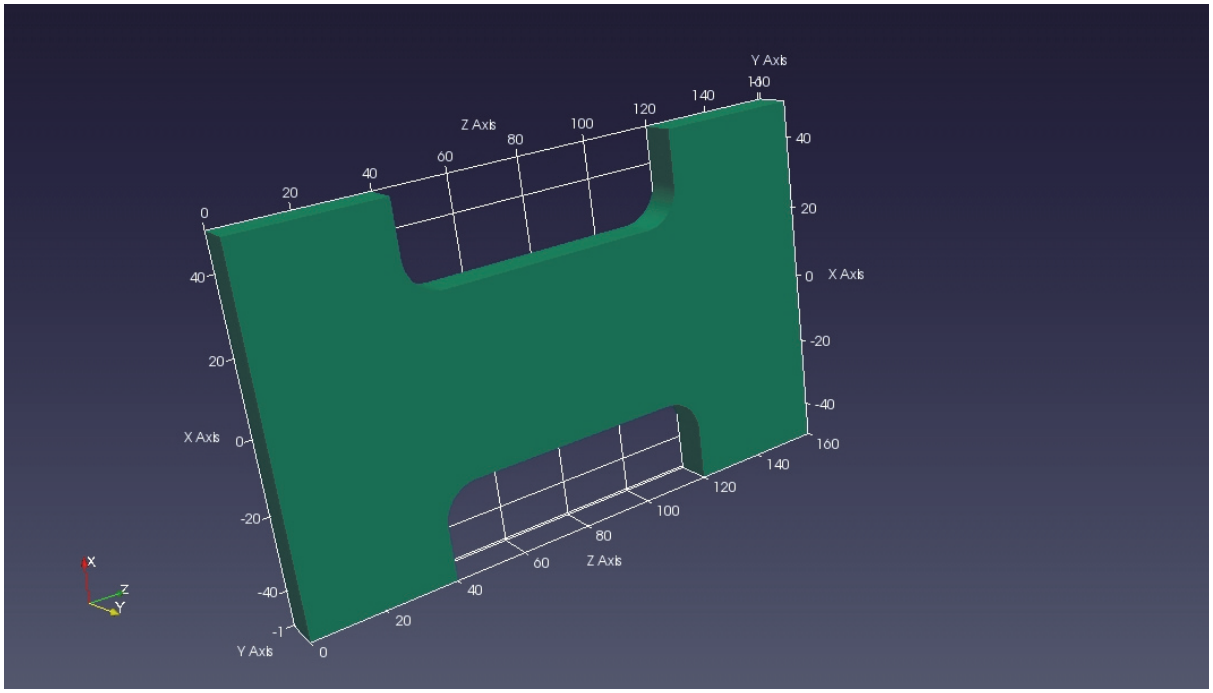

Fig. 6.1. Geometry of tensile test specimen. (Dimensions are in mm.)

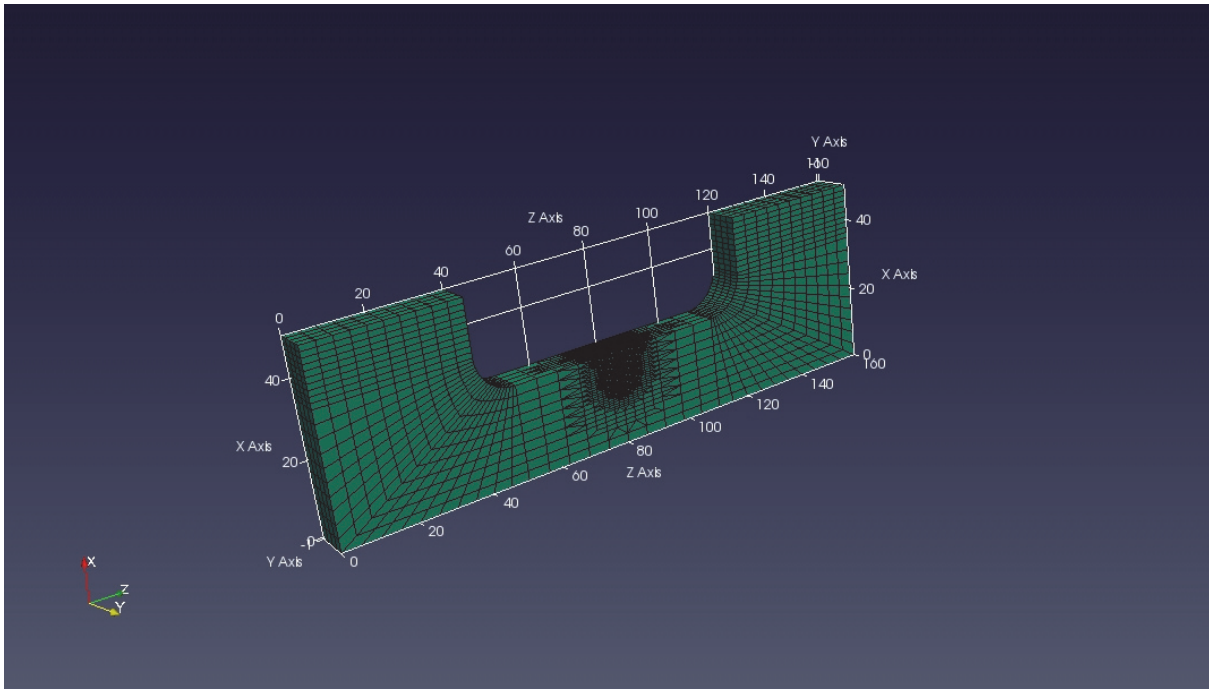

Fig. 6.2. Structured mesh on the half of the tensile test specimen.

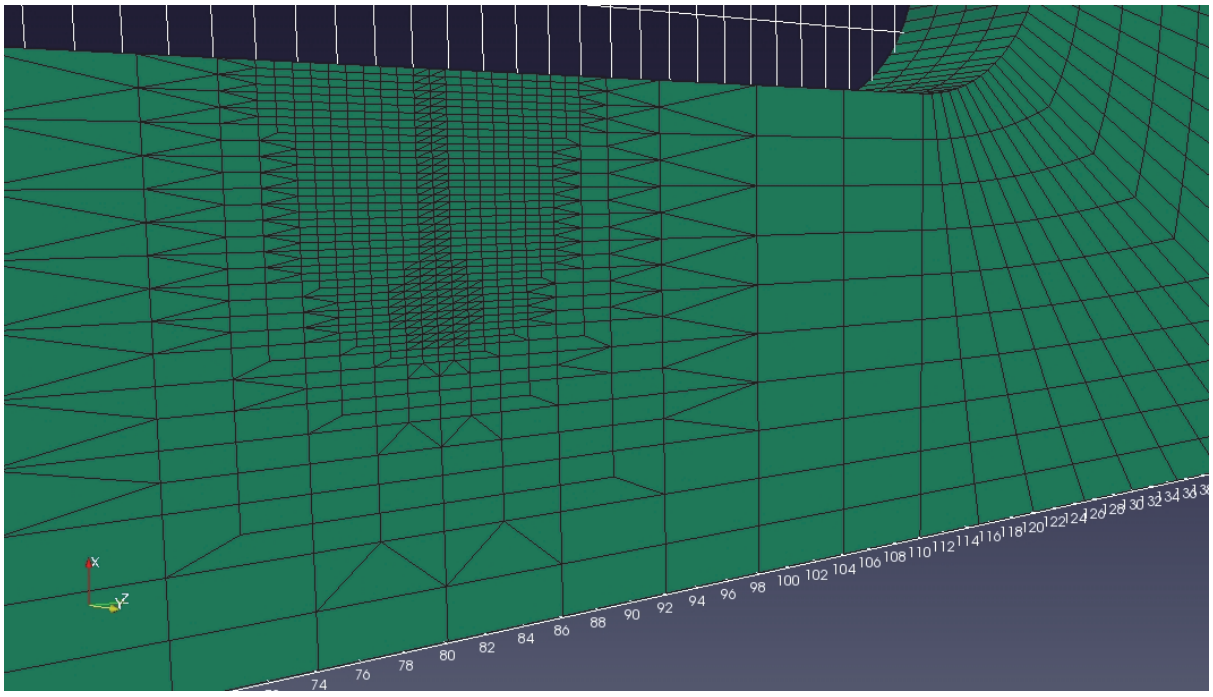

Fig. 6.3. Refined mesh in the crack section of the tensile test specimen.

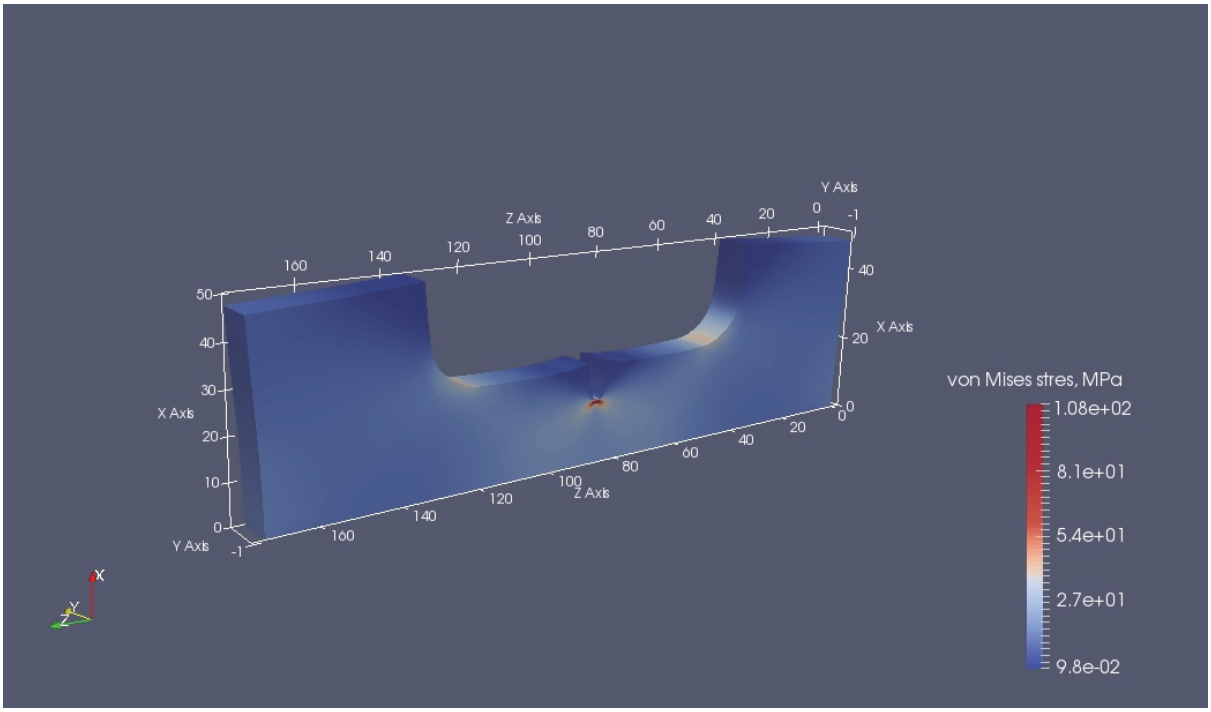

Fig. 6.4. Von-Mises stress distribution.

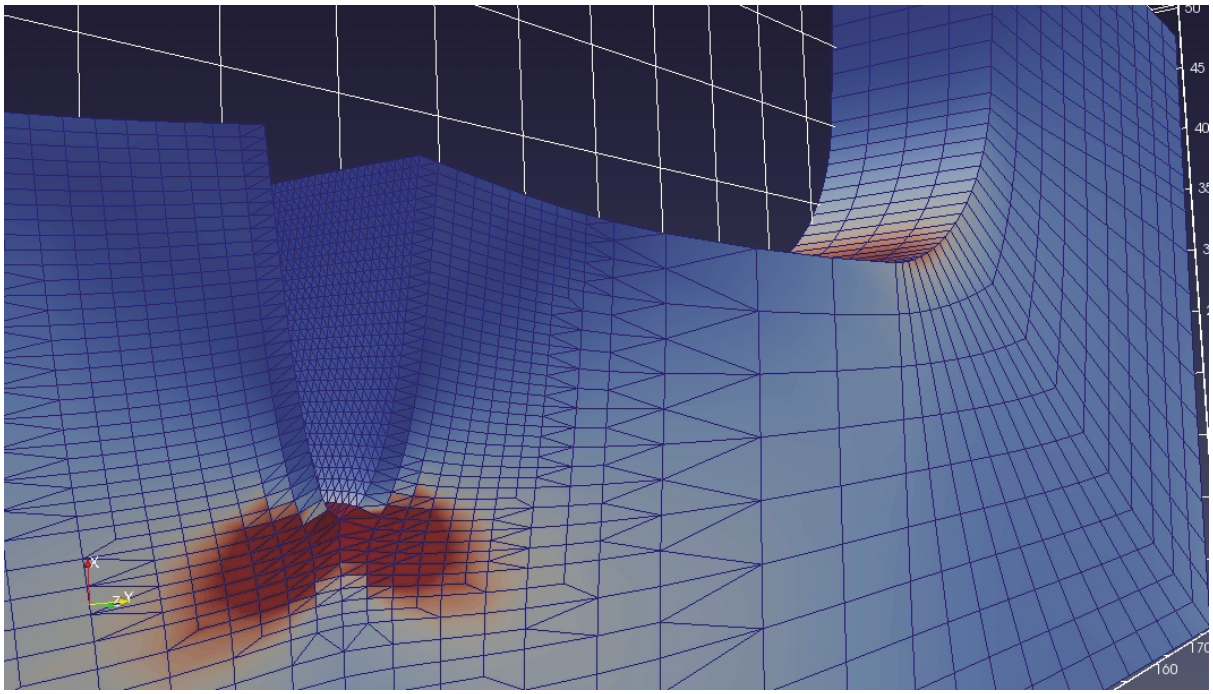

Fig. 6.5. Enlarged section of the crack zone.

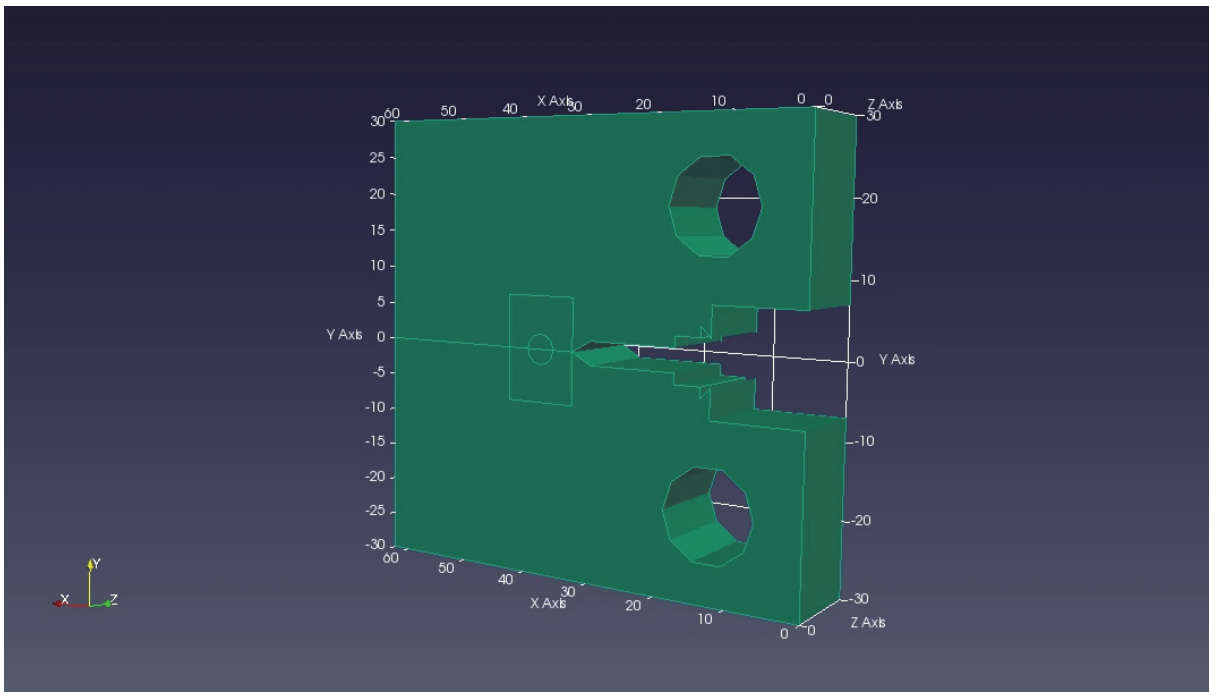

Fig. 6.6. Compact tension (CT) specimen. Dimensions in mm.

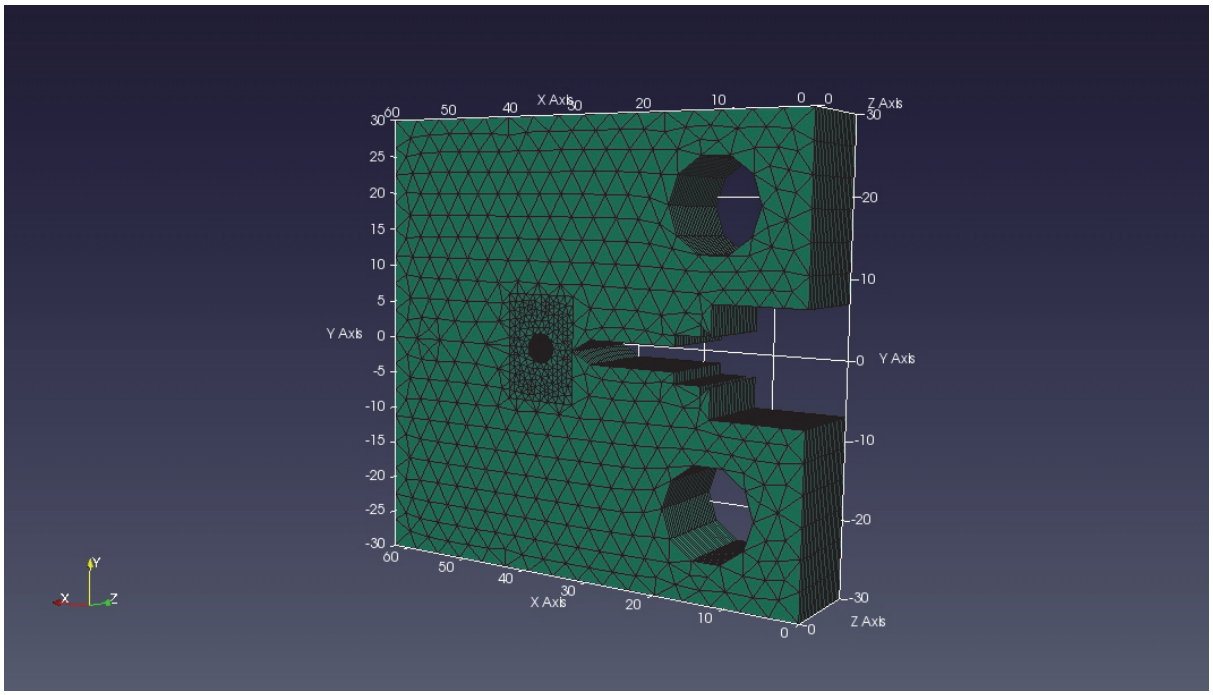

Fig. 6.7. Mesh of the CT specime

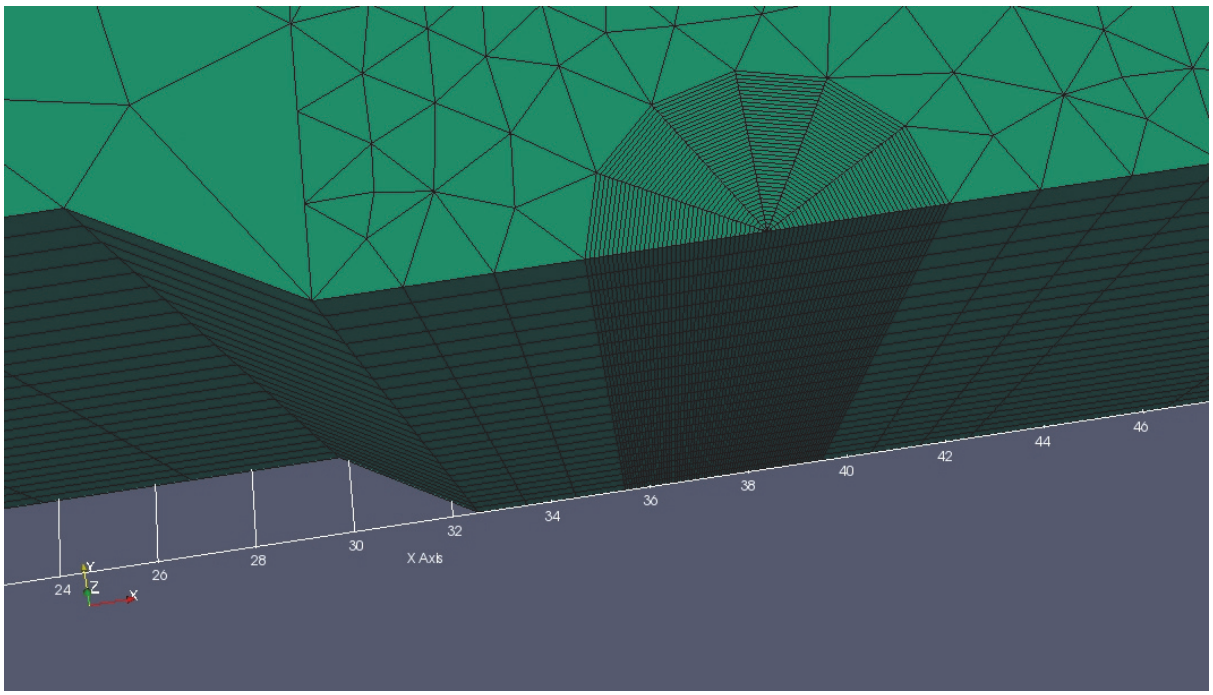

Fig. 6.8. Locally refined mesh of the CT specimen in the crack zone.

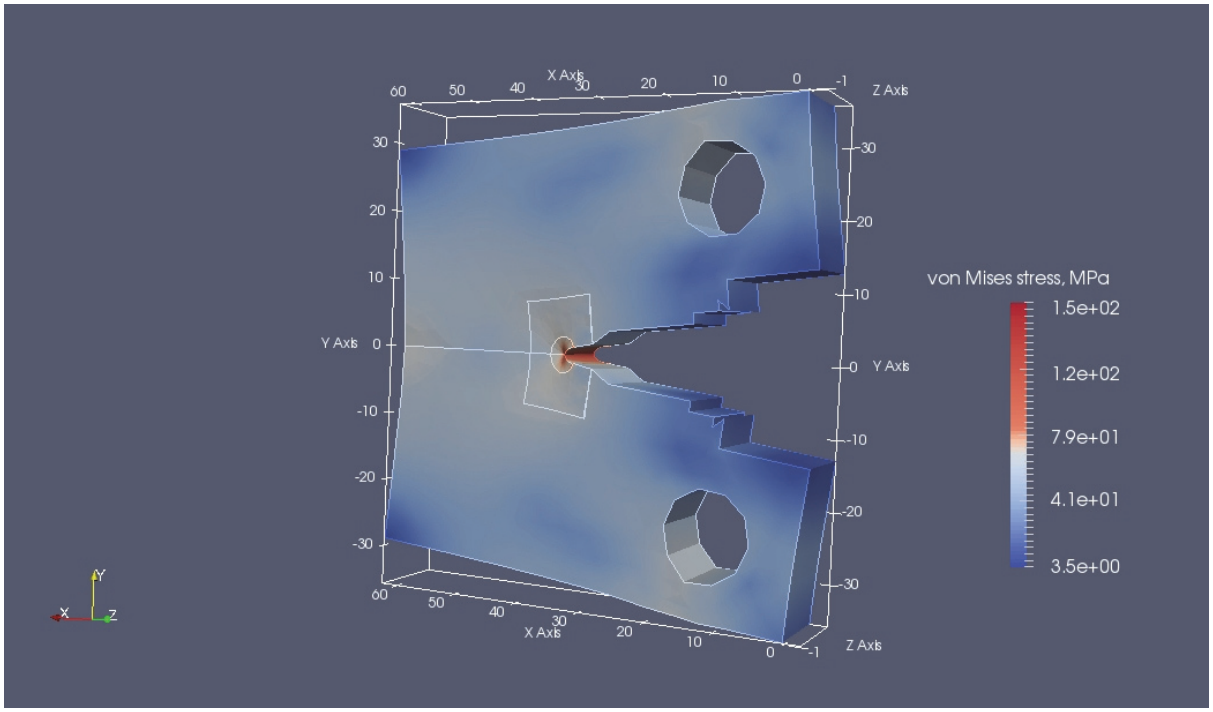

Fig. 6.9. Von-Misess stresses in CT specimen.

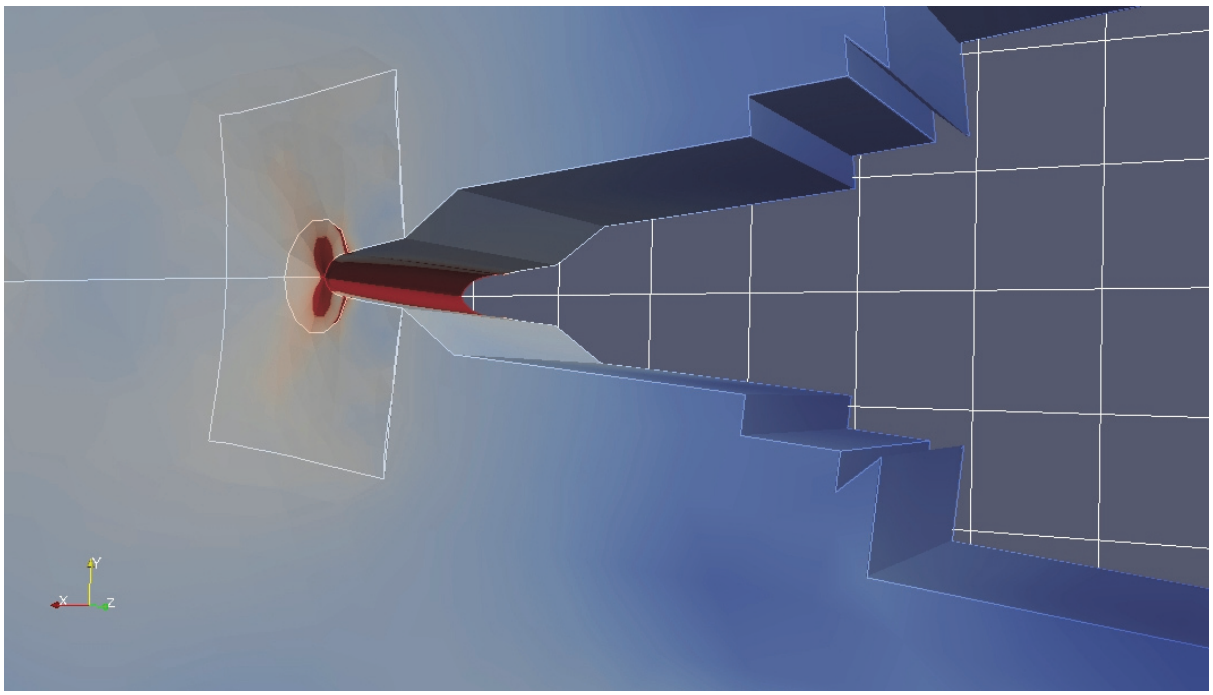

Fig. 6.10. Stress concentration on the tip of the crack.

6.2. Experimental validation

Numerical investigations were validated on experimentally published results for three different materials - stainless steel, mild steel and aluminum-copper alloy 2014. The predicted crack growth rate for stainless steel is depicted in Figure 6.11. Material data typical for stainless steel were taken. The experimental results reported for sentisized 304 stainless steel in oxygenated water at $t=288^0C$ are shown for comparison [29]. As well, empirical equation, so called EPRI2007 equation, is included [30]. Crack growth rate calculation for mild steel, with the experimentally reported data, are shown in Figure 6.12, [31]. Here the current density was calculated assuming corrosion potential E_{corr}=-0.725 V at $t=75^0C$. Finally, the crack propagation rate for a Al-Cu alloy is shown in Figure 6.13, [32]. These examples demonstrate that the model can provide reasonable prediction for SCC crack growth rate of various materials. Necessary prerequisites are determination the physical (M, ρ), electrochemical (polarization curve) and mechanical (σ_y and Ramberg-Osgood exponent) parameters of the particular material.

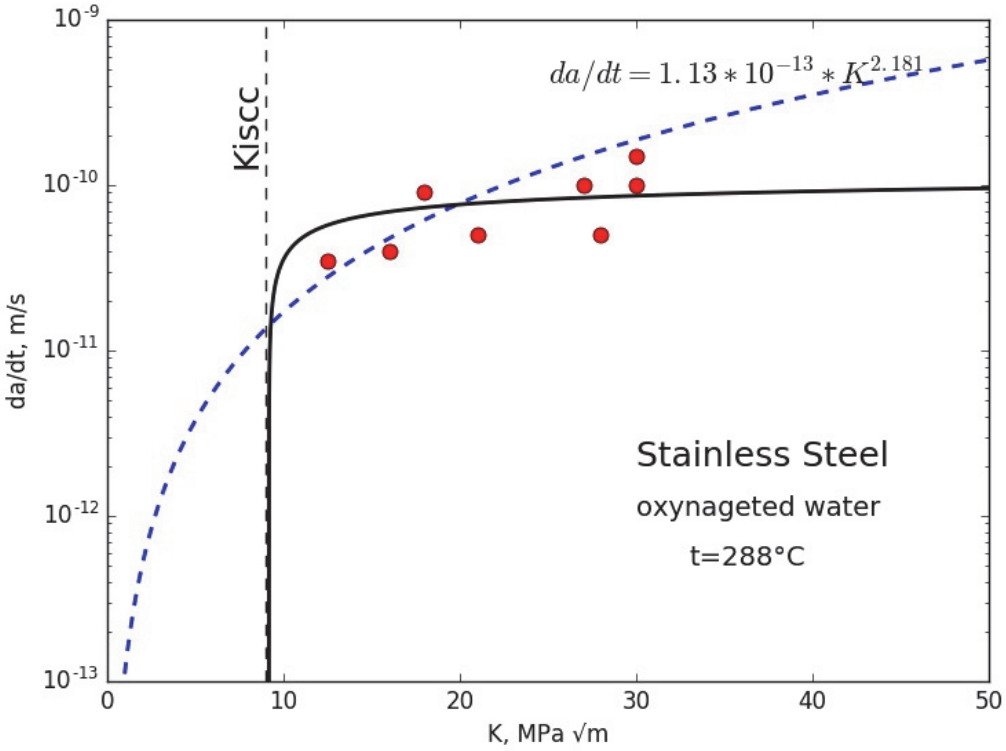

Fig. 6.11. Stainless steel calculated crack growth rate and experimental data from [29].

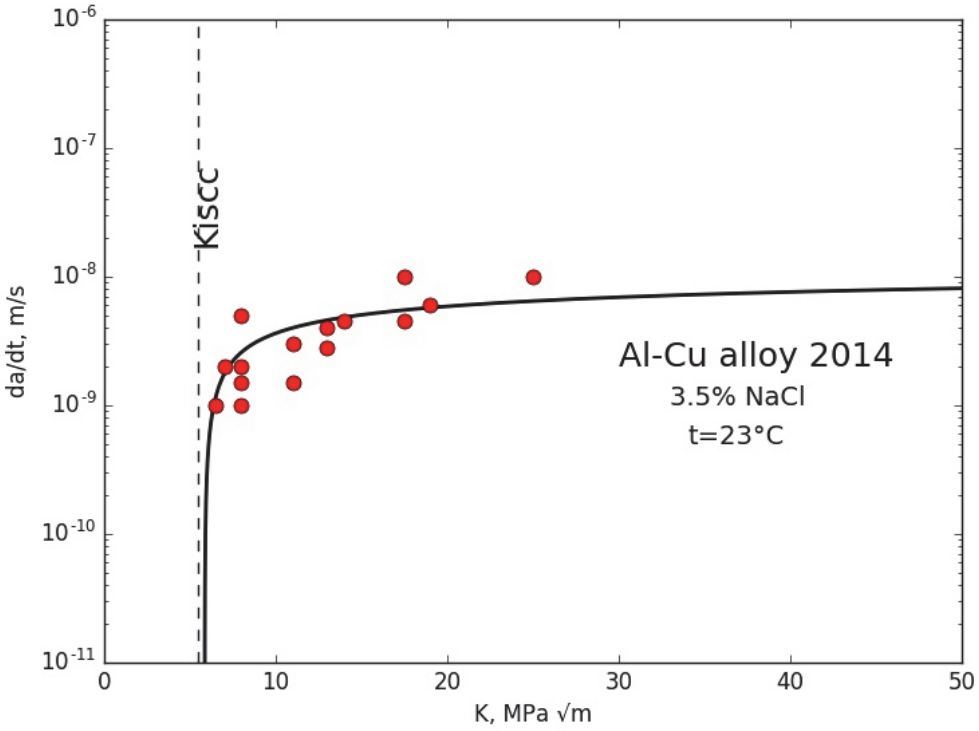

Fig. 6.12. Mild steel crack growth rate simulation and experimental data [31].

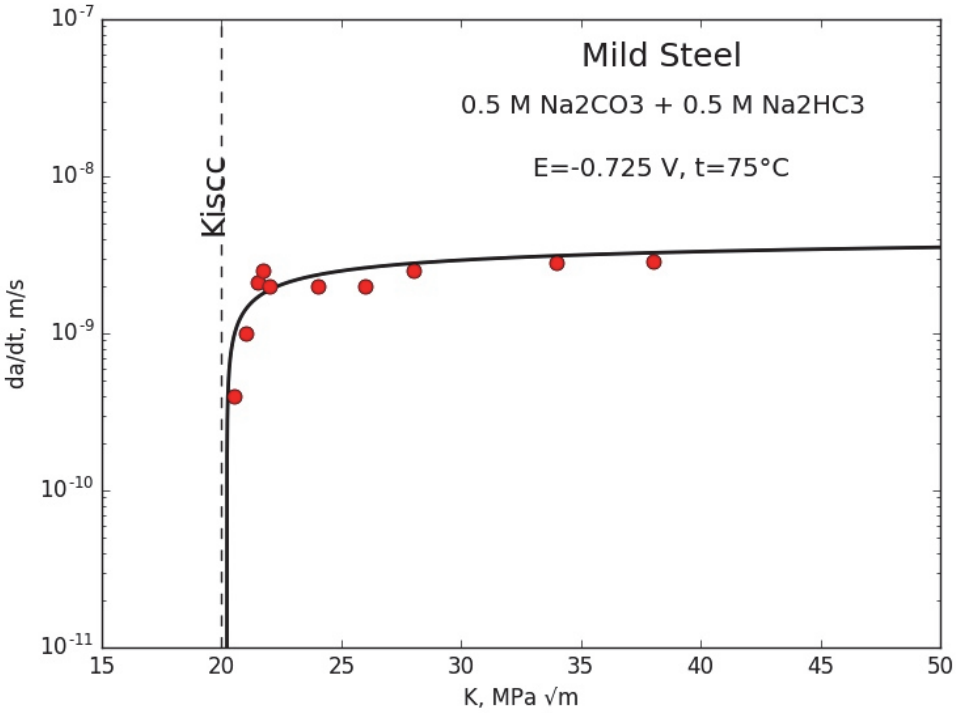

Fig. 6.13. Aluminium-coper simulation, experimental data from [32].

6.3. Detailed calculation of fracture mechanics parameters

In the follow text (Figs. 6.14-6.23) results for tensile specimen are shown for every 2 mm of crack length growth.

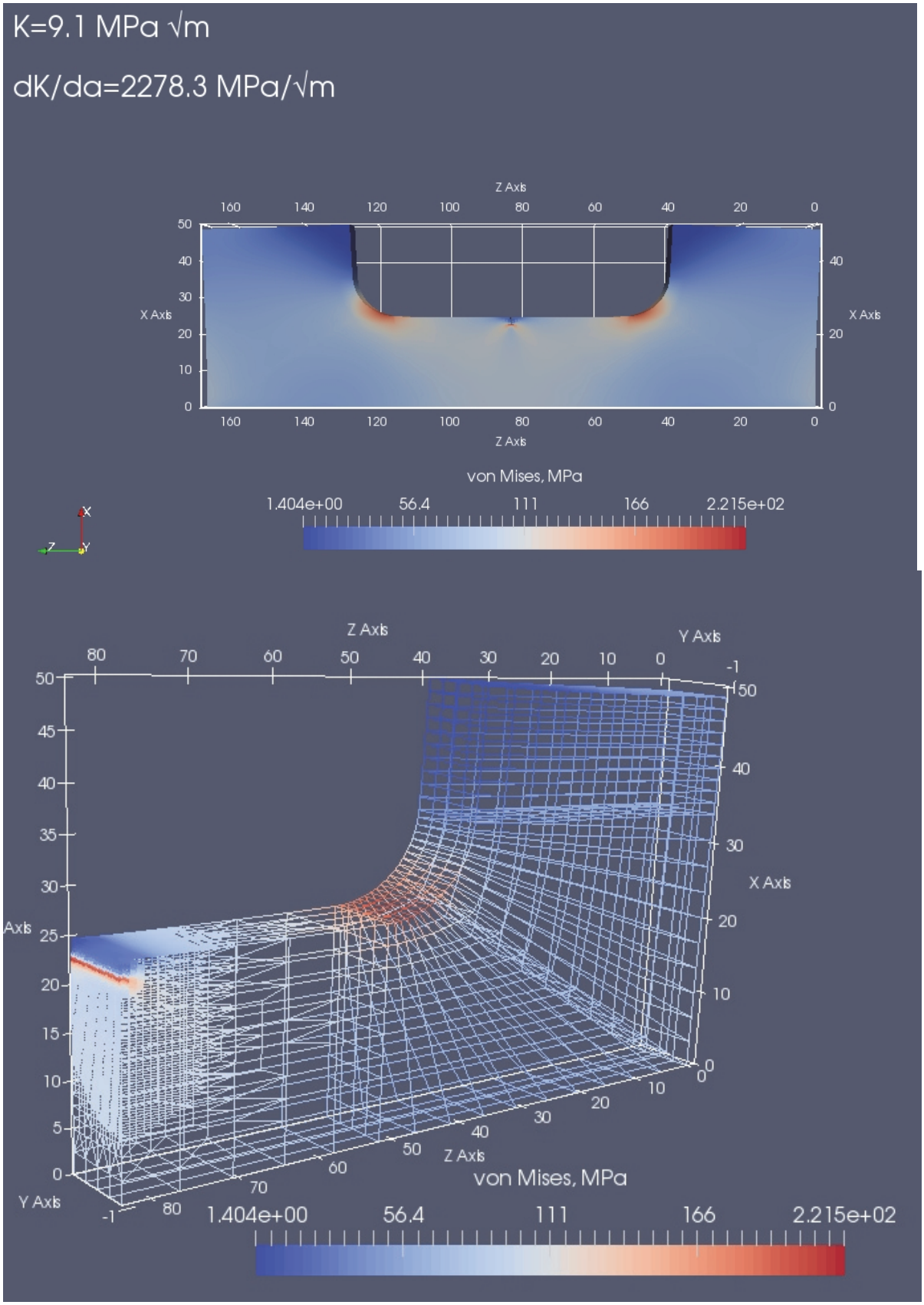

Fig. 6.14. Data for a=2 mm

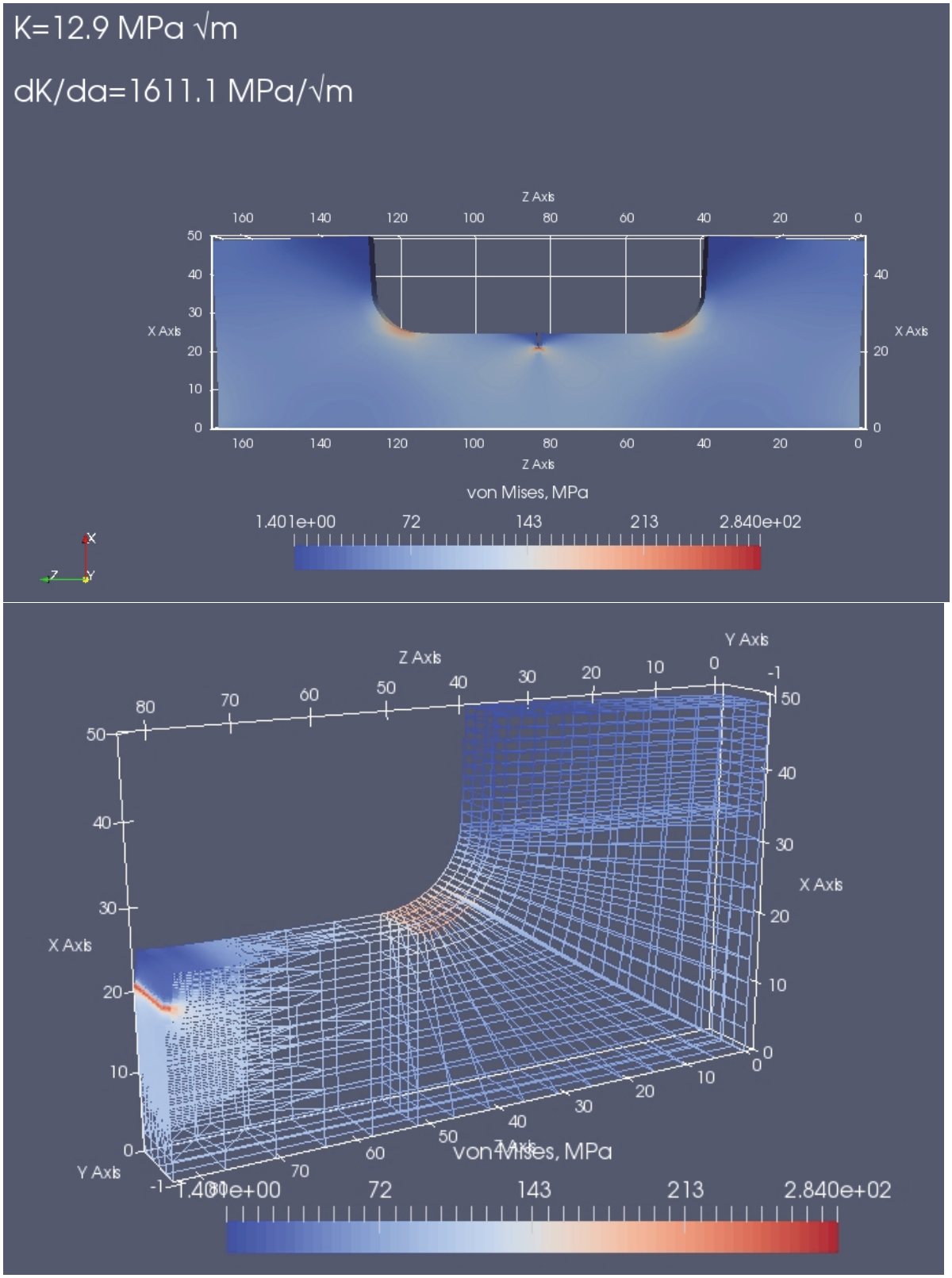

Fig. 6.15. Data for a=4 mm

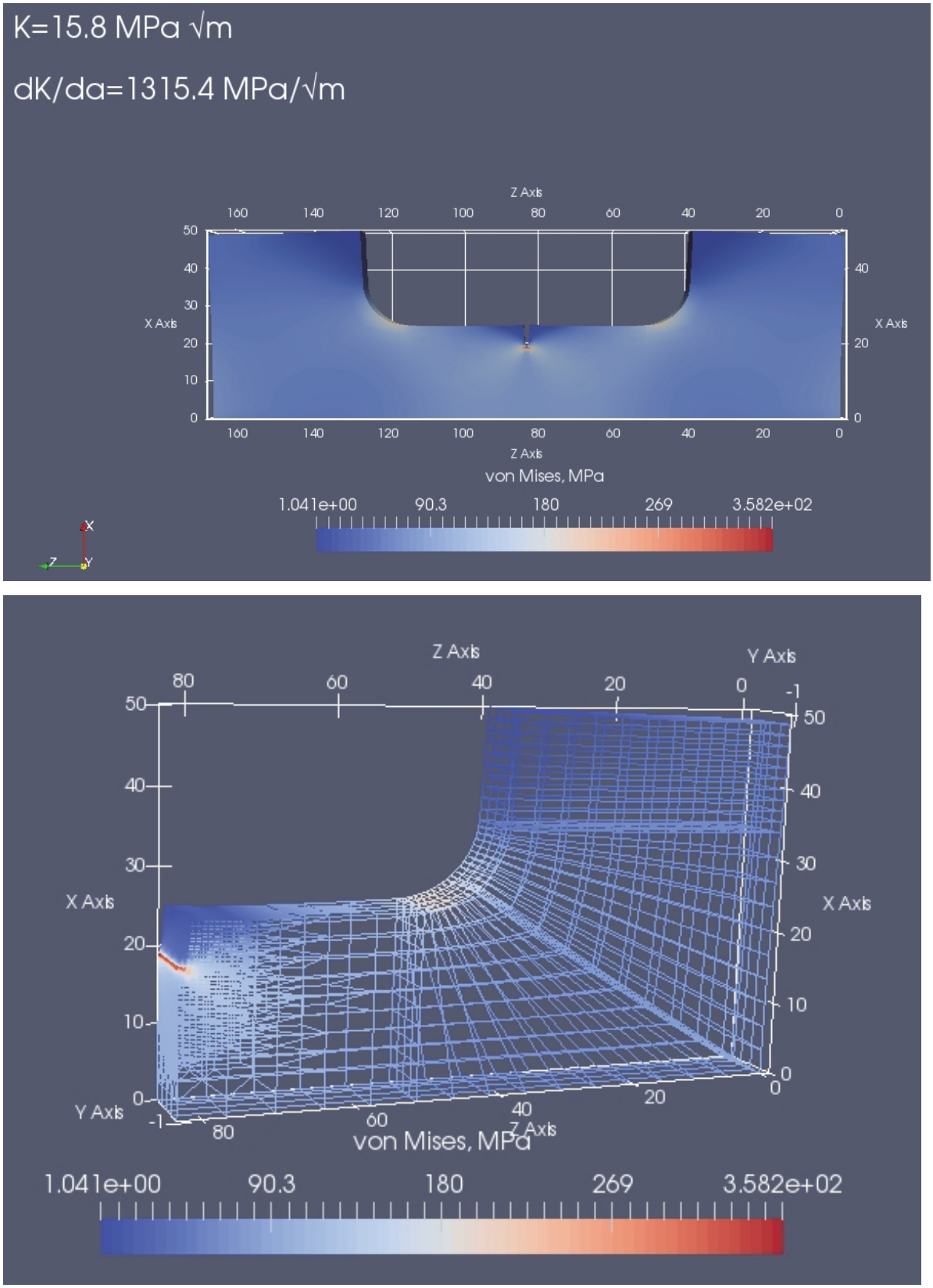

Fig. 6.16. Data for a=6 mm

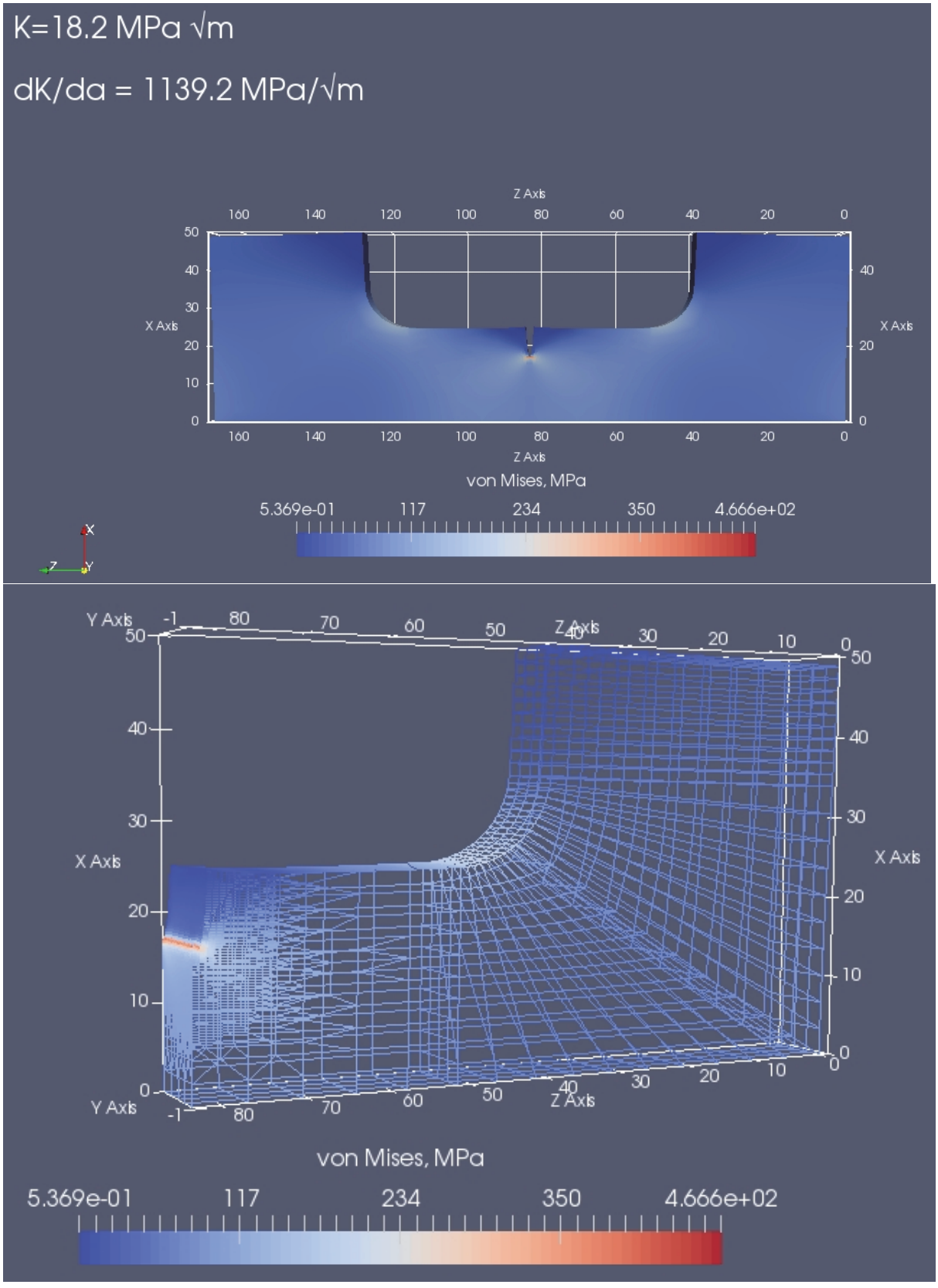

Fig. 6.17. Data for a=8 mm

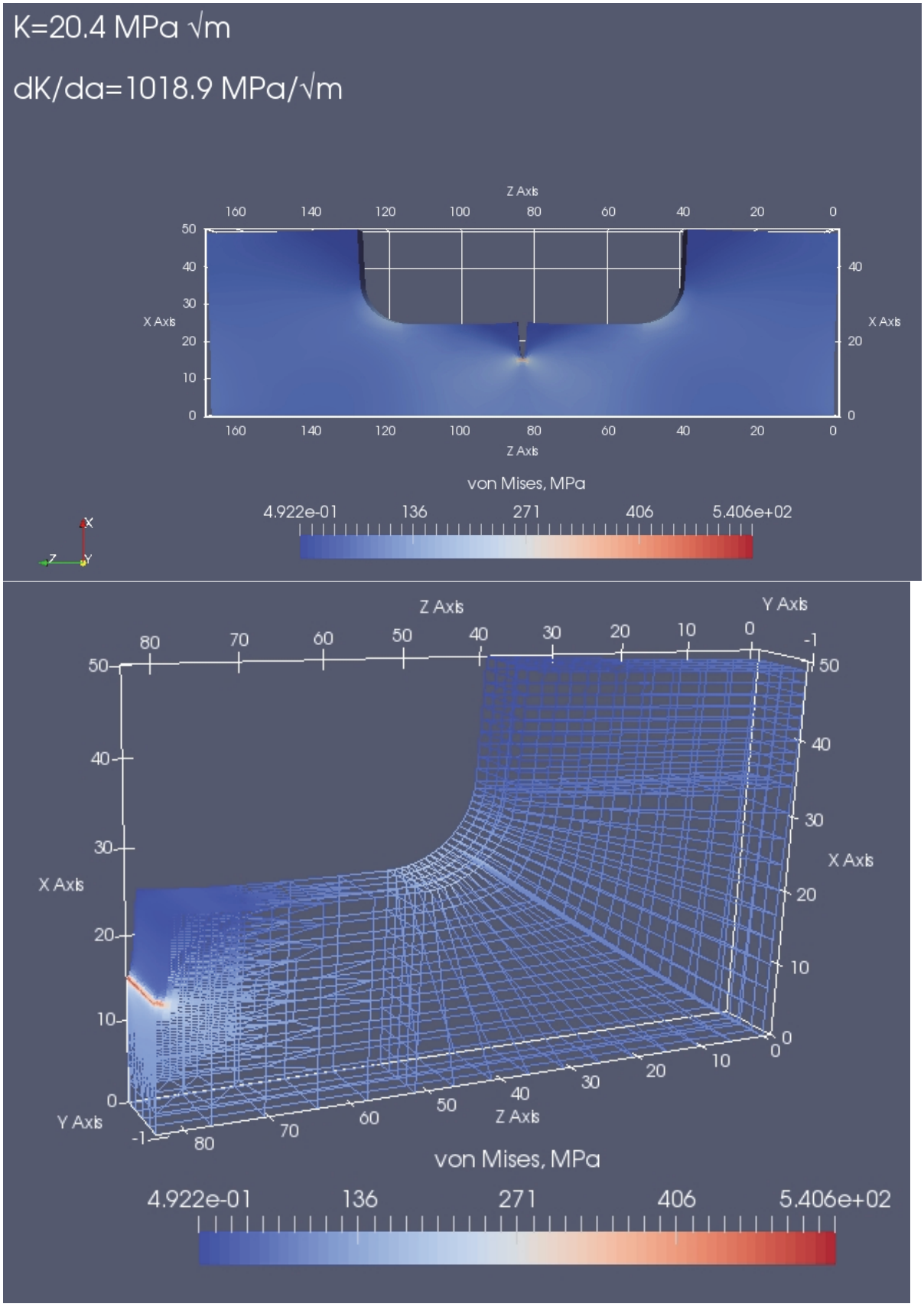

Fig. 6.18. Data for a=10 mm

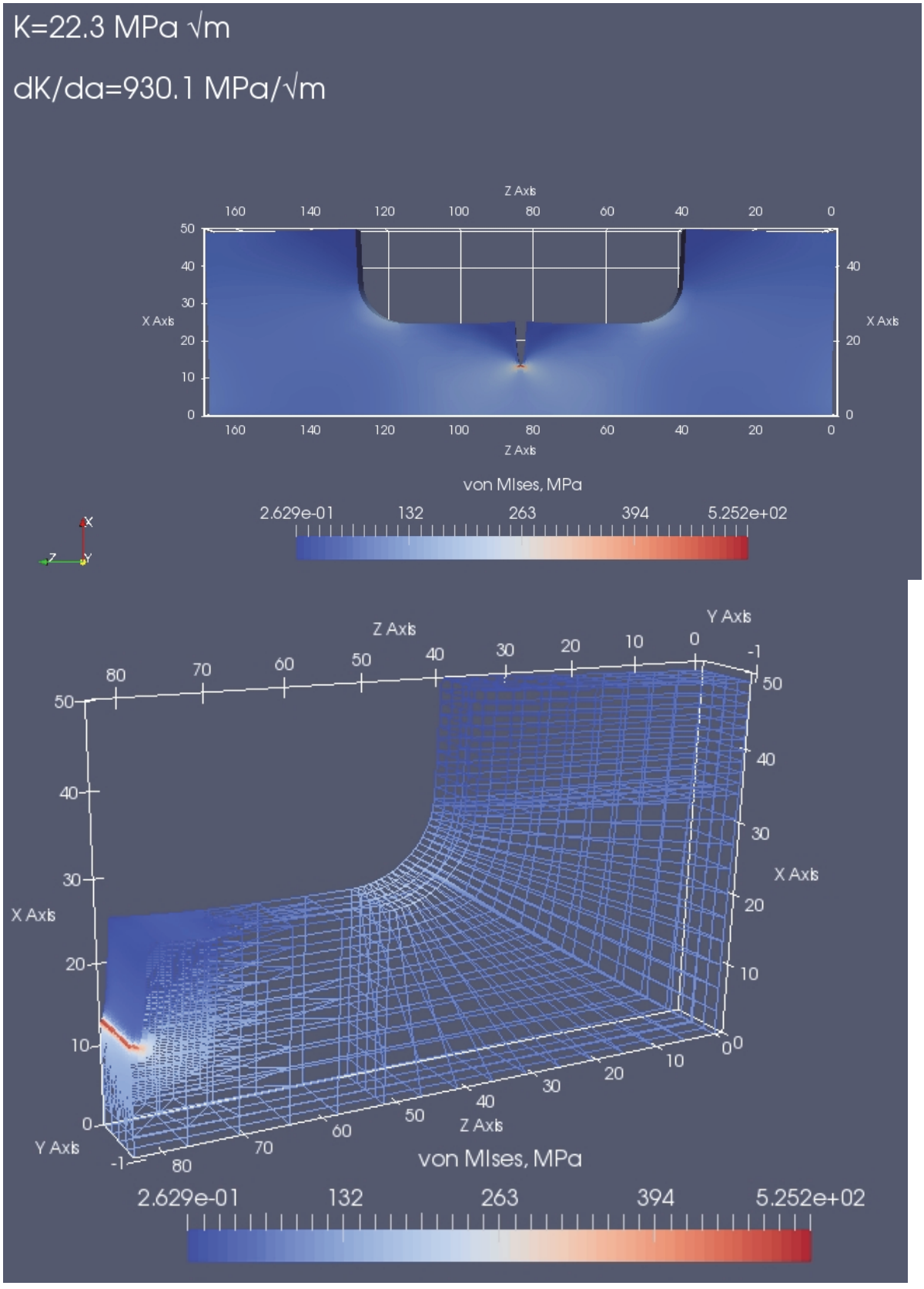

Fig. 6.19. Data for a=12 mm

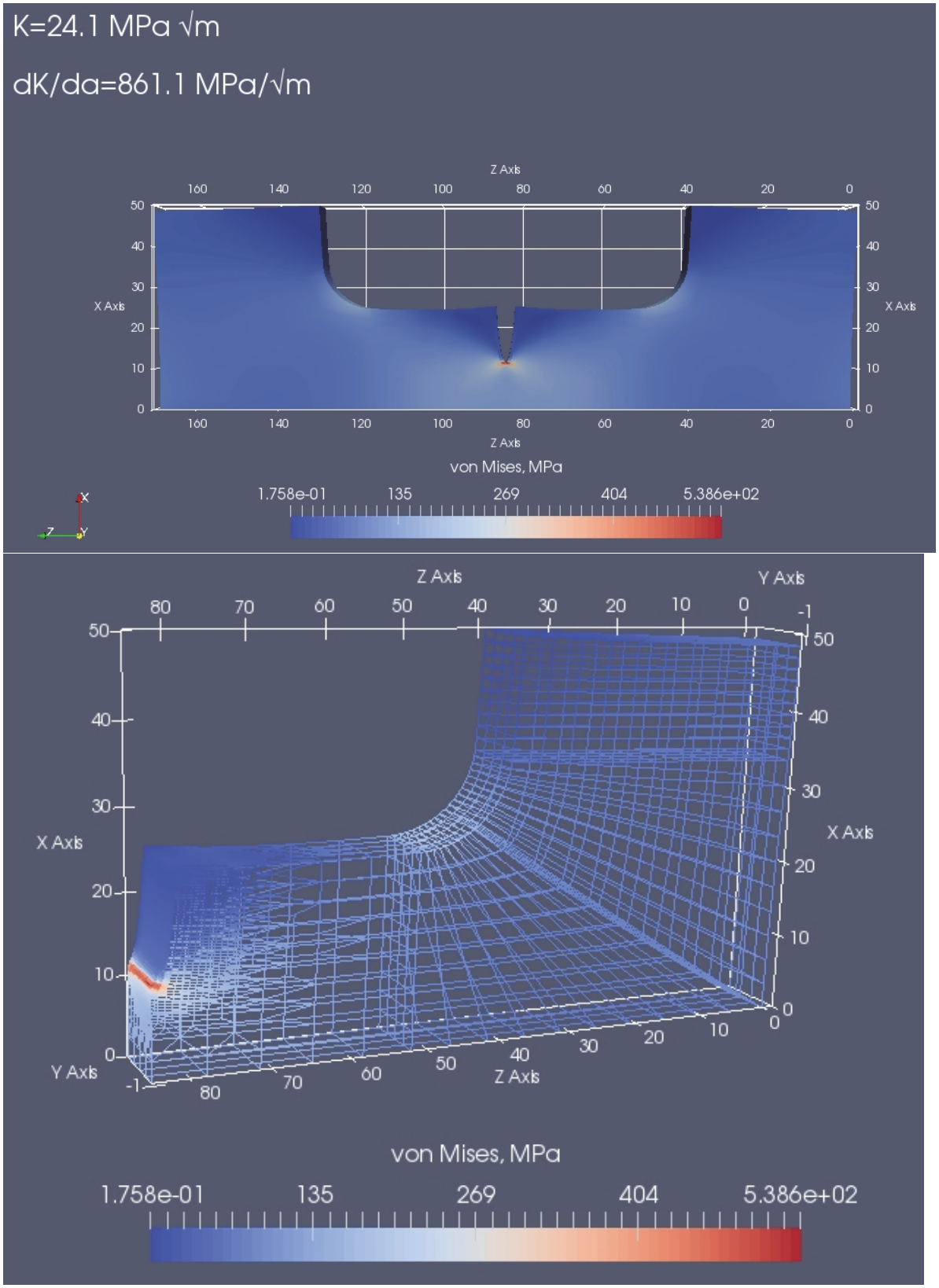

Fig. 6.20. Data for a=14 mm

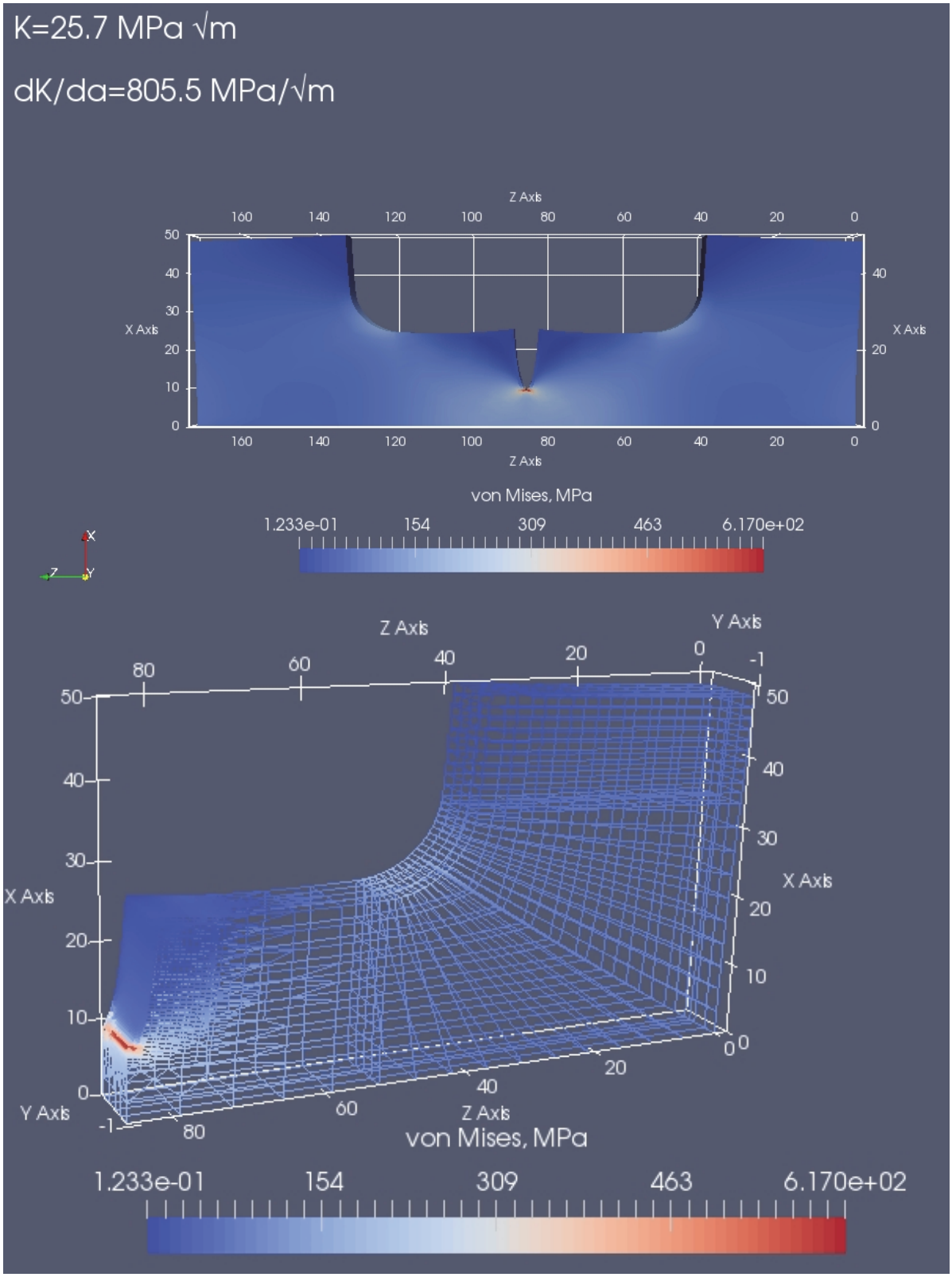

Fig. 6.21. Data a=16 mm

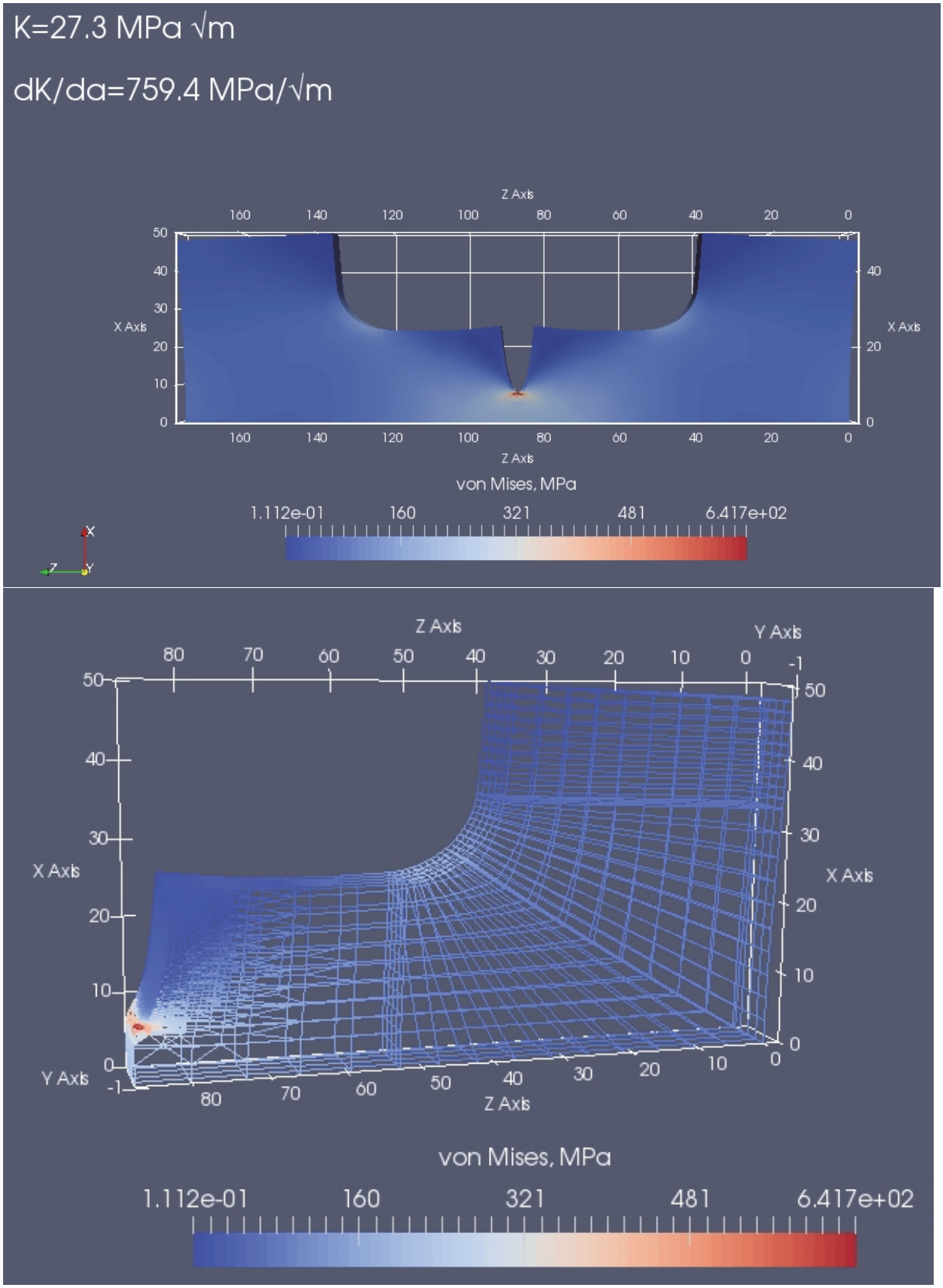

Fig. 6.22. Data for a=18 mm

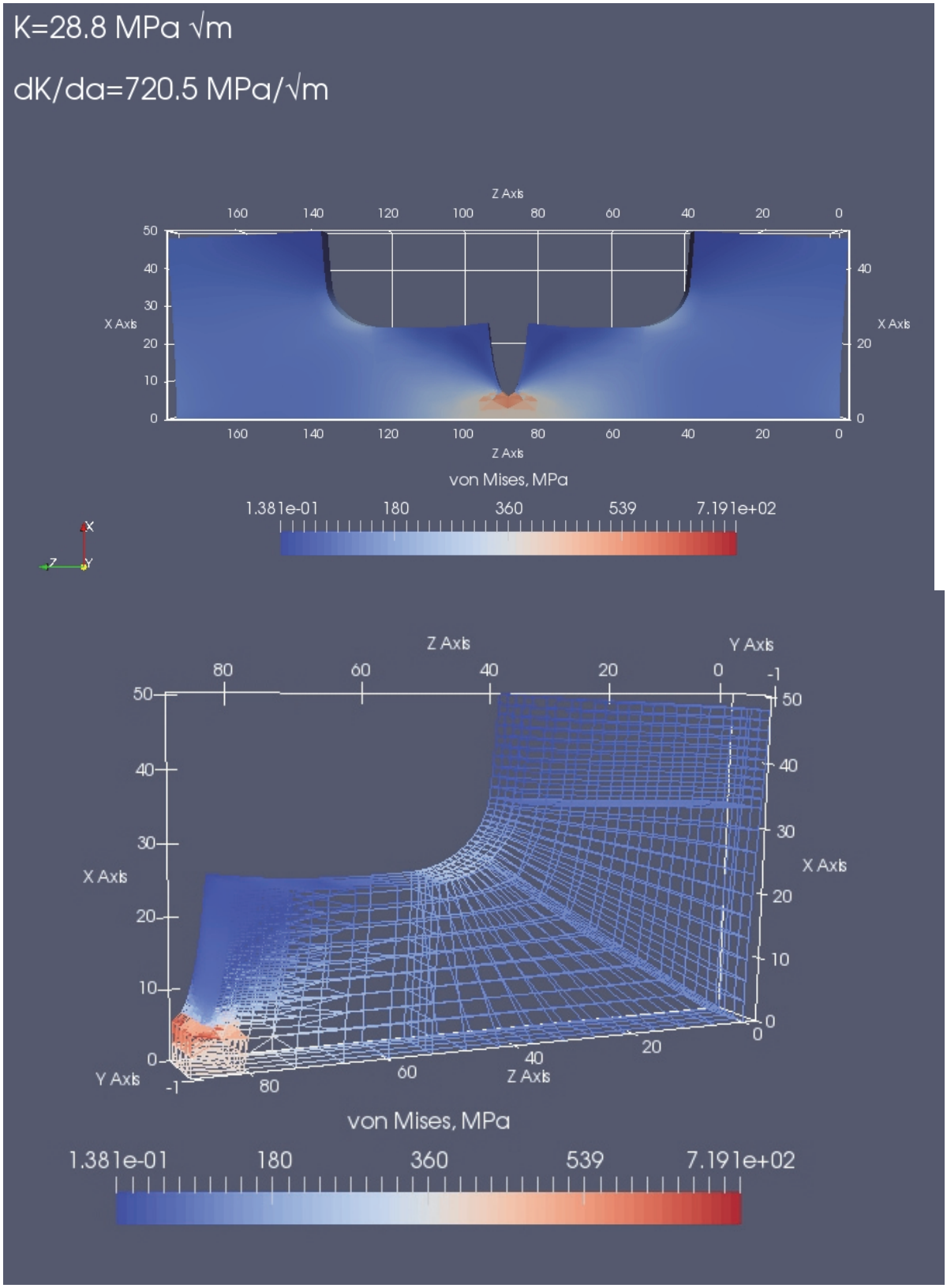

Fig. 6.23. Data a=20 mm

Figures 6.24 – 6.26 show K, dK/da and max. stress vs. as diagrammes.

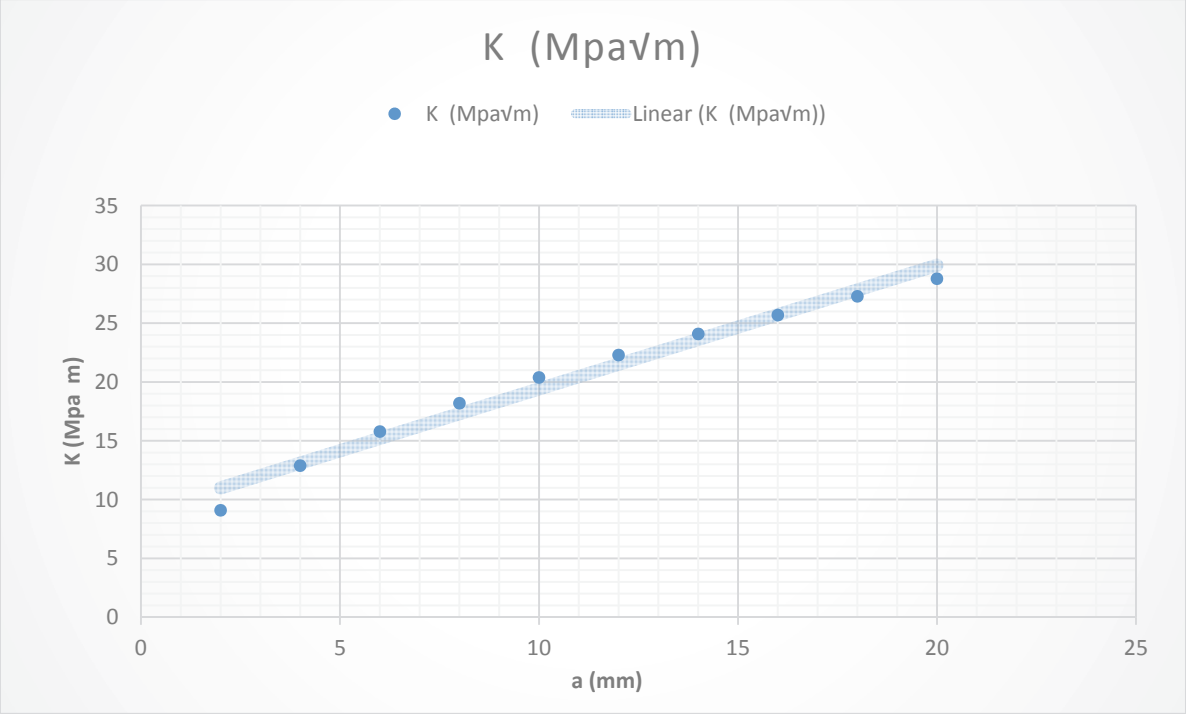

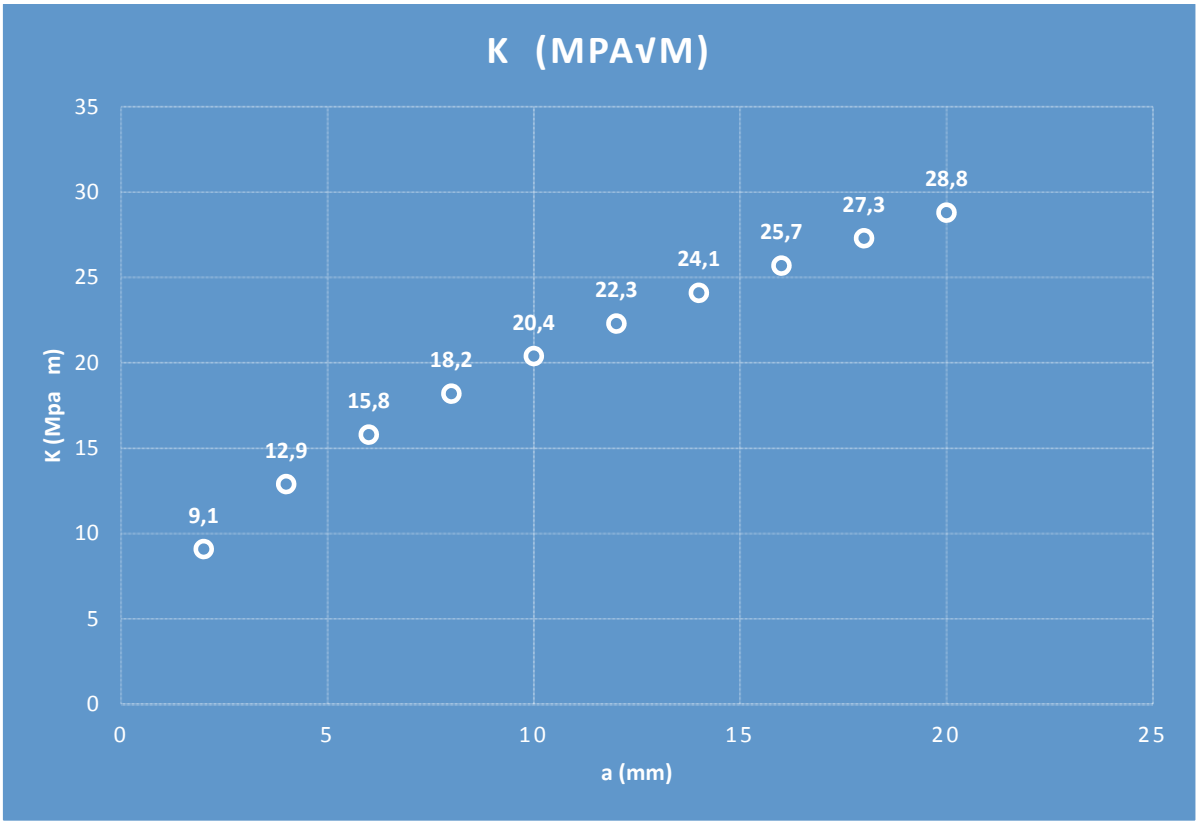

Fig. 6.24. K vs. a

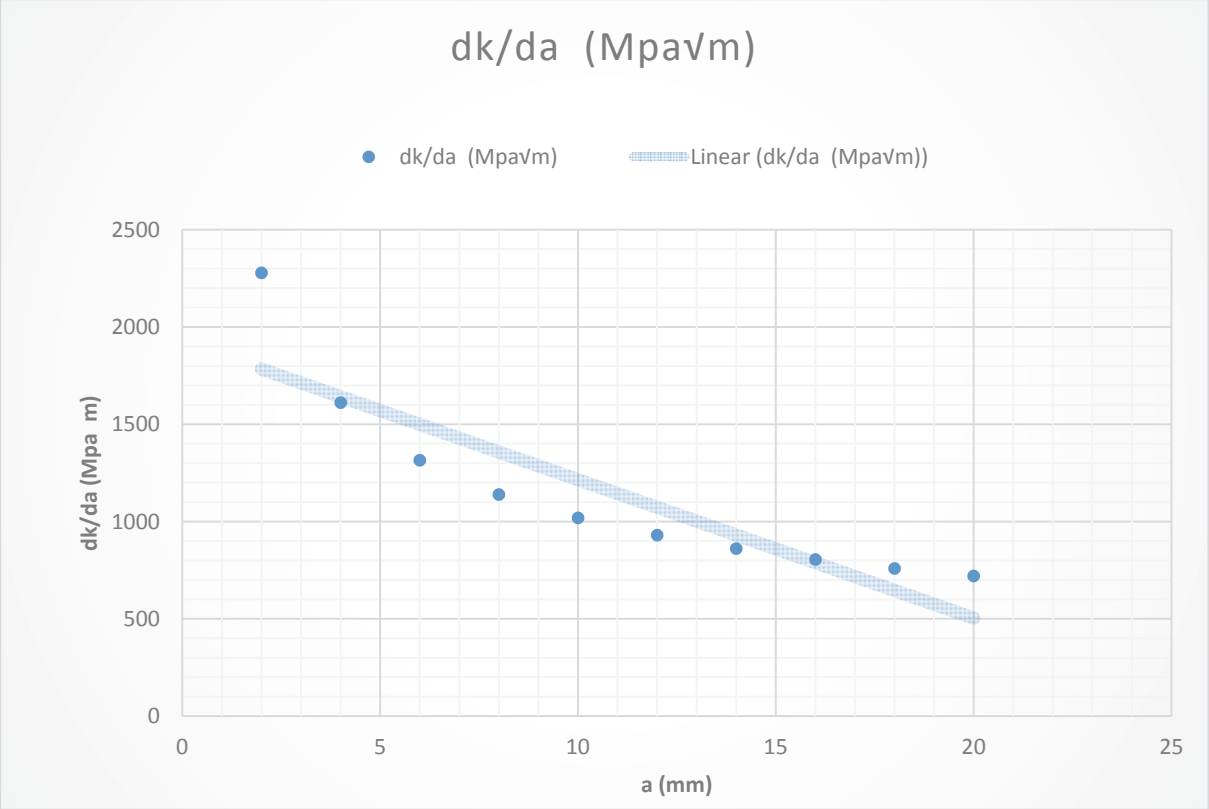

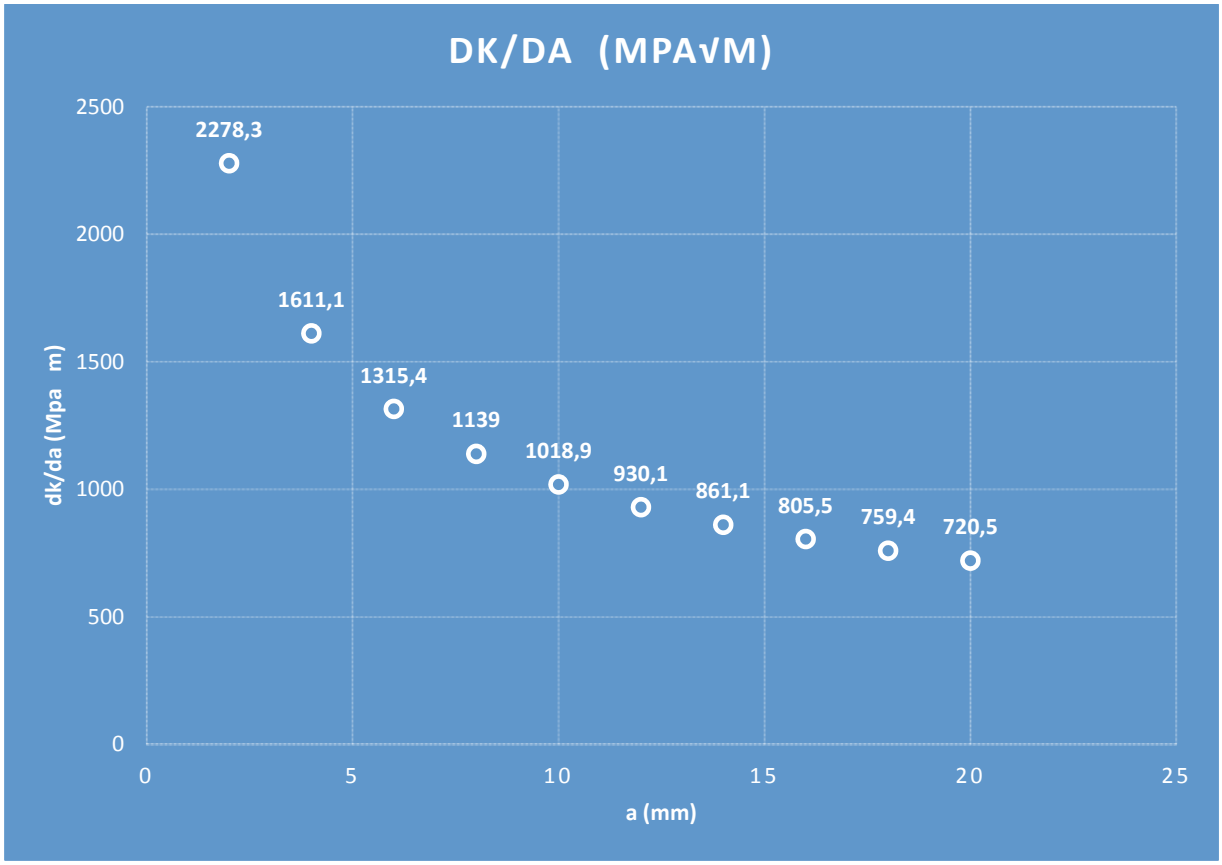

Fig. 6.25. dK/da vs a

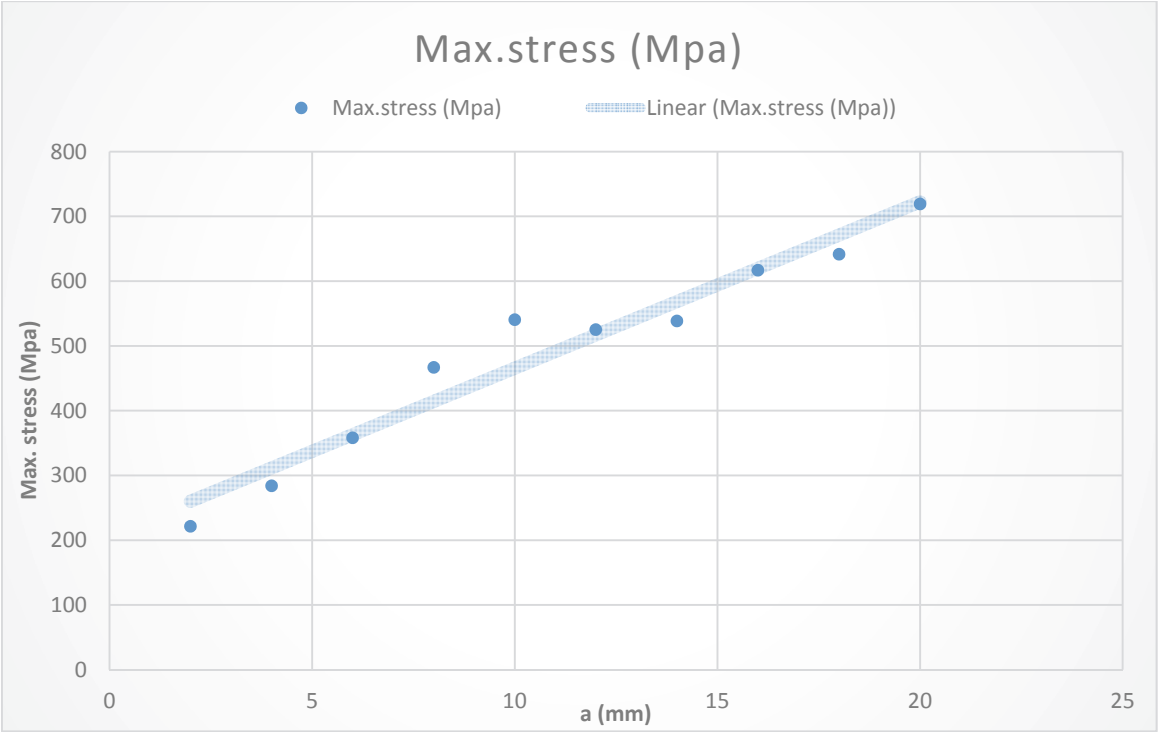

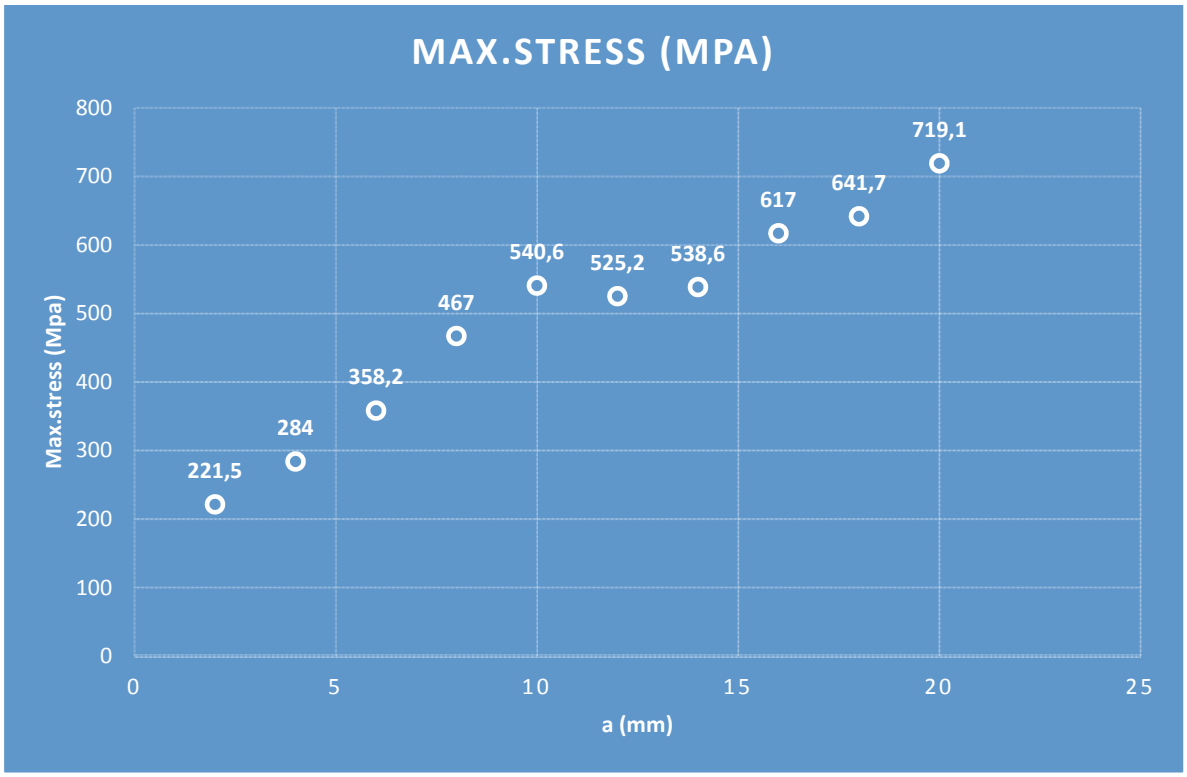

Fig. 6.26. max.stress vs. a

The same data as in Figs. 6.24-6.26 is presented in Table 6.1, just for convenience.

Table 6.1. Data for K, dK/da and max stress vs. crack length a

a (mm)	K (MPa√m)	dK/da (MPa√m)	Max.stress (MPa)
2	9.1	2278.3	221.5
4	12.9	1611.1	284
6	15.8	1315.4	358.2
8	18.2	1139	467
10	20.4	1018.9	540.6
12	22.3	930.1	525.2
14	24.1	861.1	538.6
16	25.7	805.5	617
18	27.3	759.4	641.7
20	28.8	720.5	719.1

Through the obtained results shown in Table (6.1), to assess crack growth using FEM. Several relationships between the variables can be obtained to know the stages of crack growth and its effect on the mechanical factors causing SCC.

Many factors influence the growth of SCC, which makes the SCC assessment of substances a complex issue. It is also difficult to separate the influence of different factors and variables on SCC.

The tensile sample is subjected to a constant applied load, thus determining the sample stress for the SCC under which it does not spread but rather grows a crack in the sample. The stress applied to the specimen is a factor affecting either the resistance or growth of SCC. Therefore, in some cases, the crack may have a beneficial effect on the SCC resistance of the material.

It has been shown that SCC always begins from corrosion pits or localized erosion areas. Erosion drilling provides increased stresses that warn drilling and also there are electrochemical stimuli, favourable to SCC. A different mechanism of SCC has been observed for steels in different environments.

Mechanism factors are important for discussing the behavior of crack growth and propagation, and such factors as crack mouth fatigue, stress intensity factor.

Different SCC behaviour must be taken into account by providing information on the metal.

SCC propagation mechanisms are varied and range from electrochemical to mechanical. Several factors influence these mechanisms, and they can be mechanical, thermal, chemical, or environmental.

Looking at Figure 6.24, one finds that it represents the correlation of K (MPa√m) and a (mm), under the conditions causing SCC, and a constant load. The K was measured along the sample length and the crack length ranged between 2-20 mm.

The K is shifted along with the crack interface in the plastic region of the sample, along the crack a. It was found that, under conditions of constant loading of the sample, the K equivalent before the crack front and with the crack length increases, leads to an increase in the crack length, so that as the crack length increases, the value of the K increases, starting from the value of (2mm) for the crack corresponding to the value of the stress intensity factor K (9.1 MPa√m), down to the crack length of (20 mm), up to the amount of (28.8 MPa√m) from the value of K.

Figure (6.25) describes the relationship between the rate of change of the stress intensity factor concerning the rate of change of the amount of crack length (Mpa√m) dk/da, with crack length a (mm), for the same previous conditions, when a constant load is applied. One can see that dk/da has an inverse relationship with a. We find that the relationship decreases over the length of the sample, where the value of dK/da (2278.3 MPa√m) when the length of the crack a at its beginning was equal to (2 mm), then it decreased with increasing the length of the crack until it reached (20 mm), this length corresponds to dk / da with a value of (720.5 MPa√m). This decrease indicates that the SCC process occurs slowly in the accompanying environmental conditions, which is consistent with what was previously assumed and studied.

Figure (6.26) shows the relationship between traction length a, with maximum stress σ Max. It has been observed that this relationship is direct, i.e., with increasing crack length, the maximum stress value σ_{max}.

An increase in crack length, accompanied by increased maximum stress until the length of 10 mm, a quasi-stability of the maximum stress was observed at the values (540.6, 525.2, 538.6) MPa, which accompanies an increase in the crack length for the values of (10, 12, 14) mm, this stability, which is considered to be instantaneous, does not wish to have a direct effect on the process, but rather shows the extent of the process being affected by the surrounding conditions. Then σ max increased a, until it reached the last point with a value (719.1 MPa), corresponding to the crack length of 20 mm. By noting the stress applied to the sample, the length and depth of the crack affects the stress at the front of the crack and is considered more dramatic on the maximum stress.

From the above, this part can be investigated by observing the parameters on the sample, the K and the maximum stress σ_{max}, through the plastic strain at the crack front.

The stress in the sample is distributed by applying tensile stress to it, where the front of the crack is affected when the crack length is 2 mm, and by the stress applied to the sample, the opening stress of the crack frontage increases, which is associated with the growth of the crack.

This positive increase between the variables of K and maximum stress σ_{max} with crack length a is an increase similar to what was obtained in many previous studies when investigating this phenomenon with several analytical and practical methods as well as by FEM method. Once the crack is initiated, the growth of the crack is determined by the K and it is found that in the range of maximum stress σ_{max} corresponds to the region dominated by SCC.

As one can see from Table 6.1 and Figures. 6.24, 6.25, 6.26, stress intensity factor increases with increasing slit length, decreases dK/da and σ_{max} increases. This means that as the crack grows, in spite of K and σ Max, the stress increases, and the K rate decreases. This corresponds to what was obtained mathematically and analytically in Chapter Four, as is evident in Figure 4.13, which links these variables with increasing and decreasing relationships.

Thus, the process slows down, at least from this point of view, leading to the conclusion that stress corrosion cracking is a slow and stable process.

Chapter 7 - Conclusions

Stress corrosion cracking is a kind of environmentally assisted failure of engineering materials. Gradual crack propagation and eventual final failure, are a result of simultaneous response of chemical reactions and mechanical forces at the crack tip [1]. The SCC is caused by three main factors: 1) material susceptibility to cracking, 2) environmental corrosive conditions, 3) applied tensile stress, possibly of the low level or even only residual stress. If the applied loading is cyclic, “corrosion fatigue” (CF) is considered as a particular case of SCC. In addition, depending on the rate of chemical reactions in the crack tip, “hydrogen induced cracking” (HIC) is also considered as a specific mechanism of the SCC [3].

The SCC mechanisms are classified into anodic and cathodic SCC, the first one governed by anodic metal dissolution at the crack tip, whereas the later one, dominantly occurring in welded joints, is governed by hydrogen diffusion, causing hydrogen embrittlement and/or HIC. However, during corrosion, both anodic and cathodic reactions occur simultaneously and the governing mechanism is determined by the rate of the particular reaction [4].

During the SCC crack growth, three regions can be observed: (1) low K values, when crack propagation rate increases rapidly, (2) intermediate stress-intensity levels, when the crack growth rate approaches almost constant plateau and, finally, (3) when the K value approaches K_{Ic}, rapid crack growth and the onset of final failure [5].

This doctoral dissertation presents a brief introduction to slip dissolution model, (electro)chemical and mechanical aspects of the model, two finite element models for to different geometries (with applied stress and variable displacement as a boundary conditions) and, finally, verifications with experimentally published results for two different materials, stainless steel and mild steel SCC. The model was calculated in Python programming language, while the Code-Aster was used for

finite element analysis. Pre- and post-processing were performed in a Salome-Meca environment. All of them are open-source, free software, under the Linux OS, successfully used in other applications [19].

The Stress Corrosion Cracking model for crack growth rate was examined by using analytical and XFEM model, based on open-source software. These results are also compared with the experimental ones, providing the following conclusions:

- Good predictions by XFEM were obtained for the crack growth rate for two different materials, better in the case of the mild steel.
- Analytical model is also in relatively good agreement with experimental results, and with numerical ones, at least in certain range of K values.
- The analysis crucially depends on (i) the crack tip strain rate (which is a function of mechanical properties and loading conditions) and, (ii) the anodic current density (which was revealed from electrochemical polarisation curves).
- Loading conditions don’t affect significantly the stress state.

As another aspect of this research, one can conclude that the stress intensity factor increases with crack length increase, dK/da decreases and max. stress increases. This means that as crack grows, although K and max. stress increase, the rate of K decreases, so the process decelerate, at least from that point of view, leading to the conclusion that stress corrosion cracking is a slow and stable process.

References:

[1] G. R. Lobley, “Stress corrosion cracking,” Environ. Crack. Mater., pp. 401–410, 2008.

[2] R. H. Jones and R. E. Ricker, “Mechanisms of stress-corrosion cracking,” RH Jones, ASM Int., 1992.

[3] S. Ramamurthy and A. Atrens, “Stress corrosion cracking of high-strength steels,” Corros. Rev., vol. 31, no. 1, pp. 1–31, 2013.

[4] A. Khalifeh, “Stress Corrosion Cracking Damages,” Fail. Anal., no. October, 2019.

[5] C. A. Loto, “Stress corrosion cracking : characteristics , mechanisms and experimental study,” pp. 3567–3582, 2017.

[6] Y. Hirose and T. Mura, “Growth mechanism of stress corrosion cracking in high strength steel,” Eng. Fract. Mech., vol. 19, no. 6, pp. 1057–1067, 1984.

[7] S. Mohanty, S. Majumdar, and K. Natesan, “A Review of Stress Corrosion Cracking / Fatigue Modeling for Light Water Reactor Cooling System Components Nuclear Engineering Division Argonne National Laboratory,” no. June, 2012.

[8] T. Shoji, Z. Lu, and H. Murakami, “Formulating stress corrosion cracking growth rates by combination of crack tip mechanics and crack tip oxidation kinetics,” Corros. Sci., vol. 52, no. 3, pp. 769–779, 2010.

[9] T. T. Nguyen, J. Bolivar, J. Réthoré, M. C. Baietto, and M. Fregonese, “A phase field method for modeling stress corrosion crack propagation in a nickel base alloy,” Int. J. Solids Struct., vol. 112, pp. 65–82, 2017.

[10] W. Wang, Z. Zhang, X. Ren, Y. Guan, and Y. Su, “Corrosion Product Film-Induced Stress Facilitates Stress Corrosion Cracking,” Nat. Publ. Gr., pp. 1–11, 2015.

[11] J. V Sharp, J. Billingham, and A. Stacey, “Performance of high strength steels used in jack-ups,” Mar. Struct., vol. 12, no. 4–5, pp. 349–370, 1999.

[12] A. D. Batte, P. J. Boothby, and A. B. Rothwell, “Understanding the weldability of niobium-bearing HSLA steels,” in Proceedings of the International Symposium Niobium, Orlando, Florida, USA, 2001, pp. 931–958.

[13] D. A. Skobir, “High-strength low-alloy (HSLA) steels: Visokotrdna malolegirana (HSLA) konstrukcijska jekla,” Mater. Tehnol., vol. 45, no. 4, pp. 295–301, 2011.

[14] L.-A. Steels, “High-Strength Low-Alloy Steels,” 2001.

[15] Y. Sun, H. Fujii, H. Imai, and K. Kondoh, “Suppression of hydrogen-induced damage in friction stir welded low carbon steel joints,” Corros. Sci., vol. 94, pp. 88–98, 2015.

[16] J. Ćwiek, “Hydrogen assisted cracking of high-strength weldable steels in sea-water,” J. Mater. Process. Technol., vol. 164, pp. 1007–1013, 2005.

[17] J. J. Li et al., “Large-scale synthesis of nearly monodisperse CdSe/CdS core/shell nanocrystals using air-stable reagents via successive ion layer adsorption and reaction,” J. Am. Chem. Soc., vol. 125, no. 41, pp. 12567–12575, 2003.

[18] H. Zhang, X. Wang, R. Jia, J. Hou, and W. Guo, “Investigation on stress corrosion cracking behavior of welded high strength low alloy steel in seawater containing various dissolved oxygen concentrations,” Int. J. Electrochem. Sci., vol. 8, no. 1, pp. 1262–1273, 2013.

[19] “Mechanistic Studies on Stress Corrosion Cracking of Pipeline in NNPH-PhD thesis.pdf.” .

[20] R. Phillips, “Modelling and Simulation in Materials Science and Engineering,” Model. Simul. Mater. Sci. Eng., no. November 2009, pp. 2009–2009, 2010.

[21] R. Capriotti, M. Colavita, F. De Paolis, and P. Silvestri, “Hydrogen embrittlement detection on high-strength steel by means of XRD residual stress determination technique,” in 15th World Conference on Nondestructive Testing, Roma (Italy), 2000, pp. 15–21.

[22] M. Wu, X. Chen, C. He, and J. Xiao, “Effect of CO 2 partial pressure on SCC behavior of welded X80 pipeline in simulated soil solution,” vol. 24, no. 1, pp. 65–74, 2011.

[23] E. Ghali, V. S. Sastri, and M. Elboujdaini, Corrosion prevention and protection: practical solutions. John Wiley & Sons, 2007.

[24] N. Eliaz, A. Shachar, B. Tal, and D. Eliezer, “Characteristics of hydrogen embrittlement, stress corrosion cracking and tempered martensite embrittlement in high-strength steels,” Eng. Fail. Anal., vol. 9, no. 2, pp. 167–184, 2002.

[25] J. Billingham, J. V Sharp, J. Spurrier, and P. J. Kilgallon, “Review of the performance of high strength steels used offshore,” Heal. Saf. Exec, vol. 111, 2003.

[26] T. Shibasaki, K. Takemura, and T. Mohri, “Stress Corrosion Cracking of Nb-Corrtaining,” pp. 206–212, 1998.

[27] S. A. Shipilov, “Stress corrosion cracking and corrosion fatigue " a record of progress , 1873-1973,” 1973.

[28] S. Ramamurthy, W. M. L. Lau, and A. Atrens, “Influence of the applied stress rate on the stress corrosion cracking of 4340 and 3.5NiCrMoV steels under conditions of cathodic hydrogen charging,” Corros. Sci., vol. 53, no. 7, pp. 2419–2429, 2011.

[29] V. Kramar, V. Dushko, A. Rodkina, and A. Zaiets, “Influence of stress-corrosion fractures on potential of shipbuilding metals in the sea water,” Procedia Eng., vol. 100, no. January, pp. 1068–1074, 2015.

[30] H. C. Ma et al., “Stress corrosion cracking of E690 steel as a welded joint in a simulated marine atmosphere containing sulphur dioxide,” Corros. Sci., vol. 100, pp. 627–641, 2015.

[31] J.-P. Tinnes, D. Delafosse, C. Bosch, O. Raquet, and G. Santarini, “Micro-mechanical study of the Stress Corrosion Cracking of the 316L austenitic stainless steel in chloride medium,” Proc. Eurocorr 2004, 2004.

[32] Y. Shintaku, F. Iwamatsu, K. Suga, Y. Wada, and M. Kikuchi, “Simulation of Stress Corrosion Cracking in In-Core Monitor Housing of Nuclear Power Plant,” vol. 137, no. August 2015, pp. 1–13, 2017.

[33] J. Gao and D. J. Quesnel, “Enhancement of the stress corrosion sensitivity of AA5083 by heat treatment,” Metall. Mater. Trans. A, vol. 42, no. 2, pp. 356–364, 2011.

[34] J. Gao and D. J. Quesnel, “Stress Corrosion Cracking of Sensitized AA5083 in NaCl Solution,” in CORROSION 2011, 2011.

[35] S. P. Lynch, “1-Mechanistic and Fractographic Aspects of Stress-Corrosion Cracking (Scc), eds. VS Raja, T. Shoji.” Woodhead Publishing, Cambridge, United Kingdom, 2011.

[36] A. Turnbull, D. A. Horner, and B. J. Connolly, “Challenges in modelling the evolution of stress corrosion cracks from pits,” Eng. Fract. Mech., vol. 76, no. 5, pp. 633–640, 2009.

[37] R. N. Parkins, “Significance of pits, crevices, and cracks in environment-sensitive crack growth,” Mater. Sci. Technol., vol. 1, no. 6, pp. 480–486, 1985.

[38] C. Lei, “TECHNICAL REPORT,” no. September, 2012.

[39] D. D. Cv, “CO ARPA Coupling Program on Stress-Corrosion Cracking Final Technical Report : Second Edition,” 1971.

[40] F. P. Ford and P. L. Andresen, “Development and use of a predictive model of crack propagation in 304/316L, A533B/A508 and Inconel 600/182 alloys in 288 0 C water,” in Proceedings of the third international symposium on environmental degradation of materials in nuclear power systems, 1988.

[41] R. A. Vadlamani, S. T. Revankar, and J. R. Riznic, “Stress Corrosion Cracking Models and Mechanisms for Inconel 600 , Part 2 : Crack Growth Stress Corrosion Cracking Models and Mechanisms for Inconel 600 , Part 2 : Crack Growth,” no. January, 2012.

[42] V. N. Shah et al., “Assessment of primary water stress corrosion cracking of PWR steam generator tubes,” Nucl. Eng. Des., vol. 134, no. 2–3, pp. 199–215, 1992.

[43] T. Shoji, “Evaluation of the Fracture Research Institute Theoretical Stress Corrosion Cracking Model,” no. December, 2014.

[44] P. M. Scott, “An overview of internal oxidation as a possible explanation of intergranular stress corrosion cracking of alloy 600 in PWRs,” in Proc. 9^< th> Int. Symp. on Environmental Degradation of Materials in Nuclear Power Systems-Water Reactors, 1999, 1999, vol. 3.

[45] J. Billingham, J. Healy, and J. Spurrier, Current and potential use of high strength steels in offshore structures. Marine Technology Directorate Limited London, 1995.

[46] A. Contreras, A. Albiter, I. Mexicano, and D. F, “Mechanical and microstructural effects on the stress corrosion cracking of weld beads of X-52 and X-70 pipeline steels,” pp. 49–53, 2004.

[47] J. W. Kennedy and J. A. Whittaker, “STRESS-CORROSION CRACKING OF HIGH STRENGTH STEELS *,” vol. 8, no. September 1967, pp. 359–375, 1968.

[48] J. Gao and D. J. Quesnel, “The Effect of Sensitization on Stress Corrosion Cracking of AA5083,” in CORROSION 2010, 2010.

[49] J. R. Davis, Corrosion of Weldments Edited by. .

[50] S. Structures, “Osaka University Knowledge Archive : OUKA,” 1973.

[51] P. Boothby, B. Rothwell, and B. Rothwell, “UNDERSTANDING THE WELDABILITY OF NIOBIUM-BEARING HSLA STEELS,” no. April, 2015.

[52] M. Fleming, “Accuracy Control and Welding Distortion Prediction in a Deck Plate,” 2009.

[53] J. R. Davis, Alloying: understanding the basics. ASM international, 2001.

[54] J. Adamczyk, “Development of the microalloyed constructional steels,” vol. 14, no. 1, pp. 9–20, 2006.

[55] J. R. Davis, “ASM Specialty Handbook: Carbon and alloy steels,” ASM Int. Met. Park. OH, vol. 731, 1996.

[56] W. Hu, “Data-driven metallurgical design for high strength low alloy (HSLA) steel,” 2008.

[57] A. Gaikwad, “DEVELOPMENT OF DUAL PHASE STEEL AND DETERMINATION IT ’ S OF,” no. August, 2014.

[58] Z. Xiaodong, M. Zhaohui, and W. Li, “Current Status of Advanced High Strength Steel for Auto-making and its Development in Baosteel,” pp. 1–8.

[59] W. A. Steel, “Transformation Induced Plasticity (TRIP),” pp. 2–6, 2014.

[60] A. K. Lis and B. Gajda, “Modelling of the DP and TRIP micro- structure in the CMnAlSi automotive steel,” vol. 15, no. 1, pp. 127–134, 2006.

[61] J. N. Hall, “Evolution of advanced high strength steels in automotive applications,” Gen. Mot. Co. Chair, Jt. Policy Counc. Auto/Steel Partnersh. May, vol. 18, 2011.

[62] B. K. Zuidema, S. G. Denner, B. Engl, and J.-O. Sperle, “New high strength steels applied to the body structure of ULSAB-AVC,” SAE Technical Paper, 2001.

[63] W. B. Morrison, “Overview of Microalloying in Steel,” 1988.

[64] R. W. Revie, Corrosion and corrosion control: an introduction to corrosion science and engineering. John Wiley & Sons, 2008.

[65] D. A. Jones, “Principles and Prevention of Corrosion Prentice Hall,” Saddle River, 1996.

[66] M. L. Bauccio and R. Williams, “Corrosion in the aircraft industry,” ASM Int. ASM Handbook., vol. 13, pp. 1019–1057, 1987.

[67] J. Gao, “Experiments to Explore the Mechanisms of Stress Corrosion Cracking,” ProQuest Diss. Theses Glob., 2011.

[68] M. B. Whiteman and A. R. Troiano, “Hydrogen embrittlement of austenitic stainless steel,” Corrosion, vol. 21, no. 2, pp. 53–56, 1965.

[69] L. Christodoulou and H. M. Flower, “Hydrogen embrittlement and trapping in Al6% Zn-3% Mg,” Acta Metall., vol. 28, no. 4, pp. 481–487, 1980.

[70] S. P. Lynch, “Mechanisms of stress-corrosion cracking and liquid-metal embrittlement in Al-Zn-Mg bicrystals,” J. Mater. Sci., vol. 20, no. 9, pp. 3329–3338, 1985.

[71] M. Puiggali, A. Zielinski, J. M. Olive, E. Renauld, D. Desjardins, and M. Cid, “Effect of microstructure on stress corrosion cracking of an Al-Zn-Mg-Cu alloy,” Corros. Sci., vol. 40, no. 4–5, pp. 805–819, 1998.

[72] D. R. Baer, C. F. Windisch Jr, M. H. Engelhard, M. J. Danielson, R. H. Jones, and J. S. Vetrano, “Influence of Mg on the corrosion of Al,” J. Vac. Sci. Technol. A Vacuum, Surfaces, Film., vol. 18, no. 1, pp. 131–136, 2000.

[73] K. R. Cooper and R. G. Kelly, “Crack tip chemistry and electrochemistry of environmental cracks in AA 7050,” Corros. Sci., vol. 49, no. 6, pp. 2636–2662, 2007.

[74] C. A. Zapffe and C. E. Sims, “Hydrogen embrittlement, internal stress and defects in steel,” Trans. AIME, vol. 145, no. 1941, pp. 225–271, 1941.

[75] N. J. Petch and P. Stables, “Delayed fracture of metals under static load,” Nature, vol. 169, no. 4307, pp. 842–843, 1952.

[76] R. A. Oriani, “A mechanistic theory of hydrogen embrittlement of steels,” Berichte der Bunsengesellschaft für Phys. Chemie, vol. 76, no. 8, pp. 848–857, 1972.

[77] C. D. Beachem, “A new model for hydrogen-assisted cracking (hydrogen ‘embrittlement’),” Metall. Mater. Trans. B, vol. 3, no. 2, pp. 441–455, 1972.

[78] G. M. Pressouyre and I. M. Bernstein, “A quantitative analysis of hydrogen trapping,” Metall. Trans. A, vol. 9, no. 11, pp. 1571–1580, 1978.

[79] P. L. Andresen and F. P. Ford, “Life prediction by mechanistic modeling and system monitoring of environmental cracking of iron and nickel alloys in aqueous systems,” Mater. Sci. Eng. A, vol. 103, no. 1, pp. 167–184, 1988.

[80] R. W. Staehle, “Predictions and experimental verification of the slip dissolution model for stress corrosion cracking of low strength alloys,” Stress Corros. Crack. Hydrog. Embrittlement Iron Base Alloy., pp. 180–205, 1973.

[81] D. Lee, Y. Huang, and J. D. Achenbach, “A comprehensive analysis of the growth rate of stress corrosion cracks,” Proc. R. Soc. A Math. Phys. Eng. Sci., vol. 471, no. 2178, 2015.

[82] G. T. Burstein, L. L. Shreir, and R. A. Jarman, “Corrosion, Vol. 1.” Butterworth-Heinemann, Linacre House, Oxford, UK, 1994.

[83] M. G. Fontana, Corrosion engineering. Tata McGraw-Hill Education, 2005.

[84] J. W. Hutchinson, “Plastic stress and strain fields at a crack tip,” J. Mech. Phys. Solids, vol. 16, no. 5, pp. 337–342, 1968.

[85] Jr. Rice and G. F. Rosengren, “Plane strain deformation near a crack tip in a power-law hardening material,” J. Mech. Phys. Solids, vol. 16, no. 1, pp. 1–12, 1968.

[86] Y. C. Gao, X. T. Zhang, and K. C. Hwang, “The asymptotic near-tip solution for mode-III crack in steady growth in power hardening media,” Int. J. Fract., vol. 21, no. 4, pp. 301–317, 1983.

[87] K. Chen, J. Wang, D. Du, P. L. Andresen, and L. Zhang, “dK/da effects on the SCC growth rates of nickel base alloys in high-temperature water,” J. Nucl. Mater., vol. 503, pp. 13–21, 2018.

[88] F. F. Ling, Mechanical Engineering Series. 2006.

[89] A. Sedmak, S. Sedmak, L. Milovic, “Pressure equipment integrity assessment by elastic-plastic fracture mechanics methods,” Monography, Society Structural Integrity and Life (DIVK), Belgrade, 2011.

[90] D. M. Kulkarni and R. Prakash, “Experimental analysis of fracture criterion in general yielding fracture mechanics,” J. Inst. Eng. Mech. Eng. Div., vol. 84, no. 1, apr, pp. 18–21, 2003.

[91] B. L. Karihaloo and Q. Z. Xiao, “Modelling of stationary and growing cracks in FE framework without remeshing: a state-of-the-art review,” vol. 81, pp. 119–129, 2003.

[92] D. Datta, “Introduction to eXtended Finite Element (XFEM) Method,” 2013.

[93] J. E. Dolbow, “An extended finite element method with discontinuous enrichment for applied mechanics.,” 2000.

[94] J. Aubry, Jean-Pierre Aubry Beginning with code_aster. 2013.

[95] R. G. Samuel and R. G. Samuel, “Note of use of method GTP Code _ Aster,” pp. 2–4, 2017.

[96] D. Systemes, “Abaqus 6.9 Overview,” Last Modif., 2009.

[97] H. H. Abass, S. Hedayati, and D. L. Meadows, “Nonplanar fracture propagation from a horizontal wellbore: experimental study,” SPE Prod. Facil., vol. 11, no. 03, pp. 133–137, 1996.

[98] P. Elisa, “Virtual crack closure technique and finite element method for predicting the delamination growth initiation in composite structures,” Adv. Compos. Mater. Nat. man-made Mater., pp. 463–480, 2011.

[99] J. R. Reeder and J. R. C. Jr, “Mixed-Mode Bending Method for Delamination Testing,” vol. 28, no. 7, 1990.

[100] H. P. Klotz, G. Outzekovsky, H. Elmaleh, “Etude De La Fonction Parathyrouidienne Dans Un Cas De Scl’Erodermie. Effets Th’Erapeutiques De La Parathormone.,” Ann. Endocrinol. (Paris)., vol. 24, pp. 859–865, 1963.

ПРИЛОЗИ

Општи биографски подаци

Мохамед Алкатеб рођен је 10.8.1967 у месту Сабратха у Либији. Ожењен је и држављанин је Либије.

Образовање

Основну и средњу школу је завршио у месту Сабратха, 1988-2000, у Либији. Дипломирао је 1993. године на Факултету Техничких Наука Сабратха, Либија. Мастер студије завршио је 2008. на Факултету Техничких Наука, Либија

Радио као машински инжењер у Бродоградилишту, Триполи, Либија, 2005-2008. Од 2012. Шеф одељења за материјале у Бродоградилишту, Триполи.

Школеске 2015/16 године уписао је докторске студије на Универзитету у Београду, Машински факултет.

Prilog 1

Izjava o autorstvu

Potpisan

Mohamed Mabrouk Al Kateb

broj indeksa: D26/2015

Izjavljujem:

da je doktorska disertacija pod naslovom: EXPERIMENTAL AND NUMERICAL INVESTIGATION OF CORROSION CRACK GROWTH IN MILD STRUCTURAL STEEL

- rezultat sopstvenog istraživačkog rada,
- da predložena disertacija u celini ni u delovima nije bila predložena za dobijanje bilo koje diplome prema studijskim programima drugih visokoškolskih ustanova,
- da su rezultati korektno navedeni
- da nisam kršio autorska prava i koristio intelektualnu svojinu drugih lica.

Potpis

Beograd, 12.03.2021.

Prilog 2

Izjava o istovetnosti štampane i elektronske verzije doktorskog rada

Ime i prezime autora: Mohamed Mabrouk Al Kateb

Broj indeksa: D26/2015

Studijski program: Doktorske akademske studije

Naslov rada: "EXPERIMENTAL AND NUMERICAL INVESTIGATION OF CORROSION CRACK GROWTH IN MILD STRUCTURAL STEEL"

Mentor : Prof. dr Aleksandar Sedmak

Izjavljujem da je štampana verzija mog doktorskog rada istovetna elektronskoj verziji koju sam predao za objavljivanje na portal **Digitalnog repozitorijuma Univerziteta u Beogradu.**

Dozvoljavam da se objave moji lični podaci vezani za dobijanje akademskog zvanja doktora nauka, kao što su ime i prezime, godina i mesto rođenja i datum odbrane rada.

Navedeni lični podaci mogu se objaviti na mrežnim stranicama digitalne biblioteke, u elektronskom katalogu i u publikacijama Univerziteta u Beogradu.

Potpis

Beograd, 12.03.2021.

Prilog 3

Izjava o korišćenju

Ovlašćujem Univerzitetsku biblioteku „Svetozar Marković“ da u Digitalni repozitorijum Univerziteta u Beogradu unese moju doktorsku disertaciju pod naslovom: “EXPERIMENTAL AND NUMERICAL INVESTIGATION OF CORROSION CRACK GROWTH IN MILD STRUCTURAL STEEL”

koja je moje autorsko delo.

Disertaciju sa svim prilozima predao sam u elektronskom formatu pogodnom za trajno arhiviranje.

Moju doktorsku disertaciju pohranjenu u Digitalni repozitorijum Univerziteta u Beogradu mogu da koriste svi koji poštuju odredbe sadržane u odabranom tipu licence Kreativne zajednice (Creative Commons) za koju sam se odlučio.

1. Autorstvo
2. Autorstvo - nekomercijalno
3. Autorstvo – nekomercijalno – bez prerade
4. Autorstvo – nekomercijalno – deliti pod istim uslovima
5. Autorstvo – bez prerade
6. Autorstvo – deliti pod istim uslovima

(Molimo da zaokružite samo jednu od šest ponuđenih licenci, kratak opis

licenci dat je na poleđini lista).

Potpis

Beograd, 12.03.2021.

1. Autorstvo - Dozvoljavate umnožavanje, distribuciju i javno saopštavanje dela, i prerade, ako se navede ime autora na način određen od strane autora ili davaoca licence, čak i u komercijalne svrhe. Ovo je najslobodnija od svih licenci.

2. Autorstvo – nekomercijalno. Dozvoljavate umnožavanje, distribuciju i javno saopštavanje dela, i prerade, ako se navede ime autora na način određen od strane autora ili davaoca licence. Ova licenca ne dozvoljava komercijalnu upotrebu dela.

3. Autorstvo - nekomercijalno – bez prerade. Dozvoljavate umnožavanje, distribuciju i javno saopštavanje dela, bez promena, preoblikovanja ili upotrebe dela u svom delu, ako se navede ime autora na način određen od strane autora ili davaoca licence. Ova licenca ne dozvoljava komercijalnu upotrebu dela. U odnosu na sve ostale licence, ovom licencom se ograničava najveći obim prava korišćenja dela.

4. Autorstvo - nekomercijalno – deliti pod istim uslovima. Dozvoljavate umnožavanje, distribuciju i javno saopštavanje dela, i prerade, ako se navede ime autora na način određen od strane autora ili davaoca licence i ako se prerada distribuira pod istom ili sličnom licencom. Ova licenca ne dozvoljava komercijalnu upotrebu dela i prerada.

5. Autorstvo – bez prerade. Dozvoljavate umnožavanje, distribuciju i javno saopštavanje dela, bez promena, preoblikovanja ili upotrebe dela u svom delu, ako se navede ime autora na način određen od strane autora ili davaoca licence. Ova licenca dozvoljava komercijalnu upotrebu dela.

6. Autorstvo - deliti pod istim uslovima. Dozvoljavate umnožavanje, distribuciju i javno saopštavanje dela, i prerade, ako se navede ime autora na način određen od strane autora ili davaoca licence i ako se prerada distribuira pod istom ili sličnom licencom. Ova licenca dozvoljava komercijalnu upotrebu dela i prerada. Slična je softverskim licencama, odnosno licencama otvorenog koda.